5-2016

Interaction of Fibrinogen with Fibronectin: Purification and Characterization of a Room Temperature-Stable Fibrinogen-Fibronectin Complex from Normal Human Plasma

Ayman E. Ismail
University of Nebraska-Lincoln, ismailo80@yahoo.com

Interaction of Fibrinogen with Fibronectin: Purification and Characterization of a Room Temperature-Stable Fibrinogen-Fibronectin Complex from Normal Human Plasma

by

Ayman Ismail

A DISSERTATION

Presented to the Faculty of

The Graduate College at the University of Nebraska

In Partial Fulfillment of Requirements

For the Degree of Doctor of Philosophy

Major: Chemical and Biomolecular Engineering

Under the Supervision of Professor William H. Velander

Lincoln, Nebraska

May, 2016

Interaction of Fibrinogen with Fibronectin: Purification and Characterization of a Room Temperature-Stable Fibrinogen-Fibronectin Complex from Normal Human Plasma

Ayman E. Ismail, Ph.D.
University of Nebraska, 2016

Advisor: William H. Velander

A fibrinogen-fibronectin complex (γγ'pdFI-pdFN) was purified from normal human plasma using a sequence of cryoprecipitation, ammonium sulfate fractionation, and DEAE Sepharose chromatography. Sodium dodecyl sulfate polyacrylamide gel electrophoresis (SDS-PAGE) under reducing condition showed both a 1:1 stoichiometric ratio of fibrinogen (FI) to fibronectin (FN) as well as a stoichiometric ratio of 1:1 of γγ to γγ'. The γγ'pdFI-pdFN complex was non-covalent in nature as it was disrupted by affinity adsorption to Gelatin Sepharose where pdFN bound strongly and the disrupted γγ'pdFI fell through the chromatographic column. Surprisingly, the purified γγ'pdFI-pdFN complex was more broadly thermally stable than plasma FI (pdFI) preparations not containing plasma FN (pdFN) and was stable at physiologic pH, ionic strength and temperature.

The complex appeared as a compact species that was distinctly larger than pdFN alone when analyzed by high pressure size exclusion chromatography (HPSEC). Dynamic light scattering (DLS) showed that the native γγ'pdFI-pdFN complex is a more compact form at low ionic strength but adopt and extended conformation in high salt and denaturing conditions. DLS

also showed that FN decreased the degree of polydispersity and hydrodynamic radius of both γγ and γγ' FI, indicating that FN interact with both subspecies.

The clottability of the native γγ'pdFI-pdFN complex and mixtures of FN with unfractionated FI and FI subspecies was evaluated by Thromboelastography (TEG) assay. The γγ'pdFI-pdFN complex had appreciably enhanced clotting strength than comparable mixtures of FI and FN. FN had not effect on the polymerization rates of fibrin clots. FN, however, showed greater influence on the shear strength of fibrin clots even in the absence of factor FXIII mediated crosslinking. The maximal amplitude and shear strength increased over the entire range of FN concentrations for clots made from unfractionated FI and γγ'FI. FN had mixed effect on the rigidity of clots made from γγFI. While high concentrations of FN enhanced the maximal amplitude and shear modulus, low concentrations decreased both factors.

The fibrin clots made from γγ'pdFI-pdFN showed a biological activity of human fibroblast and human umbilical vein endothelial cells (HUVEC) recruitment and adhesion *in vitro* exceeding that of fibrin made from equimolar concentration of pdFI and pdFN.

DEDICATION

This work is dedicated with gratitude to my amazing wife Isra and to my daughter Haneen.

Acknowledgements

I would like to thank my advisor, Dr. William H. Velander, for his guidance and encouragement throughout the project. Special thanks also to my committee members, Dr. Gustavo Larsen, Dr. Srivatsan Kidambi, Dr. Yuguo Lei, and Dr. Mark Carlson for their advice and support of this project.

I would like to gratefully acknowledge the generous encouragement of the late Dr. Bill Burgess, his technical advice and invaluable contribution to the success of this project. I would like to acknowledge Mostafa Fatemi, Jennifer Calcaterra, Weijie Xu, Nicholas Vanderslice, and Frank Fabian for their support, encouragement and guidance. I wish to thank Weijie Xu for reviewing and proofreading the document.

I am grateful to Dr. Mark Carlson for his gifts of human fibroblasts foreskin and human umbilical vein endothelial cells. I am indebted to Dr. Donald Becker for performing the analytical ultracentrifugation experiments and for his insightful discussions during the course of these experiments. Finally, I would like to thank Tiffany Peña for helping us with the cell adhesion studies.

Table of Contents

List of Tables

List of Figures

Chapter 1 INTRODUCTION

Fibrinogen

Fibrinogen (FI), the main component of the hemostatic system, is transformed by thrombin into fibrin monomers which spontaneously polymerizes forming a clot that fills the wound and prevent the loss of blood. In addition to preserving the integrity of the vascular system, the clot also initiates the wound healing process by functioning as a provisional matrix for cell adhesion and migration into the injured tissue [4]. Furthermore, because it has multiple binding sites that can react with other proteins, FI plays important roles in many physiological and pathological processes including fibrinolysis, cell adhesion, inflammation, angiogenesis, atherogenesis, tumorigenesis, and wound healing.

Fibrinogen is a 340 kDa glycoprotein containing two identical subunits, each is made of three different polypeptide chains termed Aα, Bβ, and γ [5, 6] (Figure 1.1). A series of disulfide bonds link fibrinogen polypeptide chains forming elongated 45 nm tri-nodular structures with several distinct domains. These domains are arranged into three main structural regions: a central E, two distal D and the αC regions. The central E nodule is formed by the N-terminal portions of the six polypeptide chains. The distal D nodules, formed by the C-terminal portions of the Bβ and γ as well as a fraction of the Aα chains, are separated from the E region by coiled-coil regions [7, 8]. The C-termini of the two Aα-chain, known as the αC domains, have been shown to extends freely into solution or associate noncovalently with the central nodule [9]. The properties of the fibrinogen molecule are listed in Table 1.1.

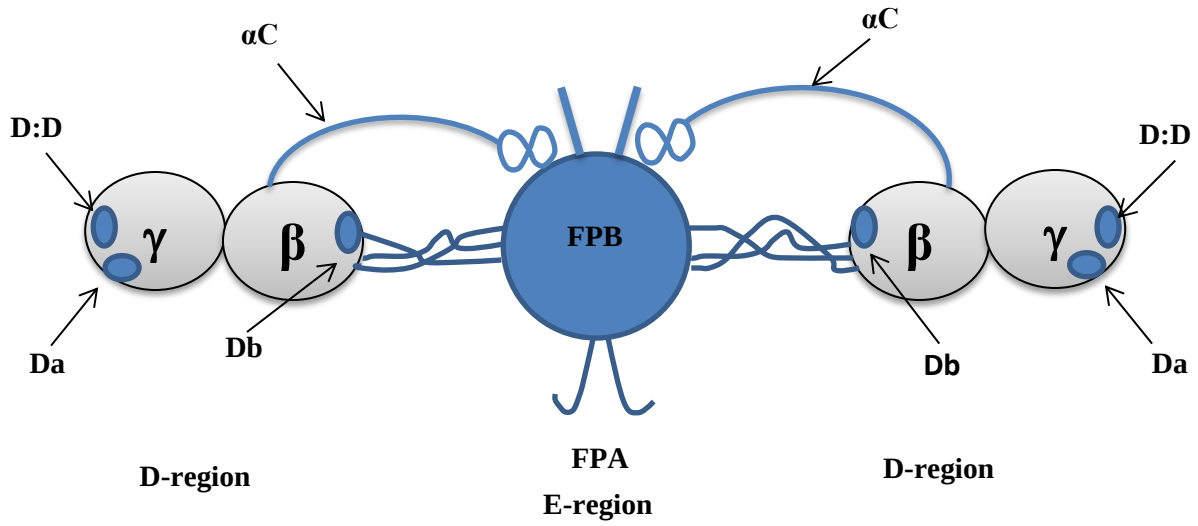

Figure 1.1 Schematic diagram of the structure of human fibrinogen. The domains and subunits are shown. The figure is adopted from reference [1]

Table 1.1 Properties of fibrinogen

Molecular weight [10]	340 kDa
Subunits	Two Aα, two Bβ, and two γ
Amino acids [11]	610 Aα, 461 Bβ, 411 γ
Synthesized by	Primarily hepatocytes and secondarily platelets
Plasma concentration	2-4 mg/ml
Carbohydrate [12]	3% of total weight, consist of Sia, Gal, Man, and GlcNAc sugars
Isoelectric point [13]	5.8
Diffusion coefficient [14]	2×10^{-7} cm^2 s^{-1} in ionic strength of 0.15 M and pH 7.35

The Aα, Bβ, and γ polypeptide chains of human fibrinogen are encoded by three separate genes [15]. The three genes are closely linked as a cluster in a region of 50-kilobase on

chromosome 4q31.3. The Aα gene is in the middle and surrounded by the Bβ gene from one side and the γ-gene on the other. The Aα and Bβ genes are produced by simple transcription events, whereas plasma γ gene is generated by complex transcriptional event that involve differential RNA splicing and polyadenylation [16, 17].

Human FI heterogeneity results from variant splicing, phosphorylation or glycosylation, and a number of genetic polymorphisms [18]. The heterogeneity occurs naturally when FI is partially degraded during circulation to low molecular weight species with 305 kDa and 270 kDa with one or two of Aα-chains partially degraded at the c-terminus, respectively [19-21]. The heterogeneity is also due in part to the presence of a minor variant form of the γ-chain, known as γ'. The γ'-chain accounts for about 5-15% [22, 23] of normal human plasma fibrinogen and is formed by the alternative processing of the primary mRNA transcript [24, 25]. Amino acid sequence analysis has demonstrated the replacement of 4 amino acids (AGDV) in the C-terminal of the γ-chain with a unique 20 amino acid sequence [26] that contains two sulfated tyrosines and several Asp and Glu residues. Therefore, the γ′-chain is longer, contains more anion groups, and has higher molecular weight than the γ-chain. It has been reported that the γ′-chain bind to the B subunit of factor XIII (FXIII) and serves as a carrier for FXIII in plasma [27].

Fibrinogen has the ability to interact with numerous substances with important physiological consequences. For example, The C-terminal of the Aα-chain (αC domains) of fibrinogen has binding sites for α_2-AP, plasminogen, tissue-type plasminogen activator (tPA), and PAI-2. Table 1.2 lists binding sites and physiological roles of some fibrinogen-protein interactions.

Table 1.2 list of some molecules that interact with fibrinogen and their physiological roles

Ligands	Binding site	Function
Fibronectin [28]	Aα-chain	Cell adhesion
Lipoprotein (a) [29]	-	Proliferation of endothelial cells
Thrombin [30]	γ′-chain	Inhibit fibrinolysis
Plasminogen [31, 32]	Aα-chain	Enhance fibrinolysis
FXIII [27]	γ′-chain	Clot stabilization
α_2-AP [33]	Aα-chain	Fibrinolysis resistance
Integrin [34]	Aα-chain	Cellular interactions
Calcium	Bβ and γ-chains	Promote polymerization
Heparin [35-37]	Bβ-chain	Cell-matrix interactions

During coagulation, thrombin converts soluble fibrinogen into fibrin monomers, which then polymerize to form a network of fibrin fibers. This network is stabilized by thrombin activated FXIII to form an insoluble fibrin clot. Formation of fibrin begins when thrombin binds to a substrate site in fibrinogen and cleaves fibrinopeptides A (FpA) and B (FpB) from the amino termini of the Aα and Bβ chains, respectively. The removal of FpA exposes the polymerization site "A" that contains the N-terminal sequence Gly-Pro-Arg-Val of the Aα-chain, while the removal of FpB exposes the polymerization site "B" that contains the N-terminal sequence Gly-His-Arg-Pro of the Bβ-chain [38]. The polymerization site "A" interacts with the complementary binding site of the γ-chain, whereas the polymerization site "B" interacts with the complementary binding site of the β chain. These interactions lead to the formation of half-staggered, double-stranded protofibrils that undergo lateral aggregation to form fibrils [39-42].

The resulting fibrils also undergo lateral aggregation forming three-dimensional fiber matrix [43, 44]. Thrombin simultaneously converts FXIII to the active form (FXIIIa) which catalyzes the formation of covalent ε-(γ-glutamyl) lysine bonds between adjacent fibrin molecules. The cross-linking occurs rapidly between Lys-406 of one γ-chain and Gln-398 of another γ-chain to form γ-dimers [45-47]. FXIIIa also catalyzes the formation of slowly developing ε-(γ-glutamyl) lysine linkages between amine donor and lysine acceptor in the α-chains [48, 49] resulting in oligomers and larger polymers [50-52]. In addition, ε-(γ-glutamyl) lysine bonds also occur between α and γ chains [43, 53] as well as γ and γ chains leading to formation of hetero-dimers cross-linked α-γ [54], γ trimmers, and γ tetramers [43, 51, 53, 55].

Purification of fibrinogen from human plasma

Different techniques have been developed for the purification of fibrinogen from plasma materials. Cryoprecipitation is the most common method for isolating fibrinogen, which reduces the solubility of fibrinogen at lower temperature to prevent its denaturation. Compared to fresh frozen plasma, cryoprecipitate contains an increased percentage of fibrinogen. Cryoprecipitation involves freezing the citrated plasma at lower temperature, usually -20 °C or less for at least 12 hours. The frozen plasma is slowly thawed at 4 °C followed by centrifugation to isolate the fibrinogen precipitate. The concentration of fibrinogen produced by cryoprecipitation is between 8 to 30 mg/ml and can be increased to 40 to 60 mg/ml using repeated freeze/thaw cycles. An ultrafiltration procedure has been used to purify fibrinogen where platelet rich plasma is separated using an ultrafiltration chamber with a molecular weight cutoff of 30 kDa. Fibrinogen obtained using this method has a final concentration of 6 mg/ml and lower clottability due to large amount of fibrinogen being denatured. Fibrinogen has also been isolated from human

plasma by using chemical precipitation methods in which chemical agents such as ethanol, glycine, β-alanine, ether, or ammonium sulfate are used to precipitate fibrinogen from plasma.

The clinical use of fibrinogen from pooled human plasma has been previously associated with a high risk of transmission of plasma–borne infectious species such as HIV, HBV, and HCV. The improvements in viral testing and screening have reduced, but not eliminated this risk. Therefore, different techniques have been developed in order to inactivate pathogenic viruses in fibrinogen derived from human plasma. Dry heat treatment at 60-68 °C of plasma cryoprecipitate inactivates HIV but it does not prevent the transmission of HCV. Plasma pathogens have been inactivated by treating fresh plasma with methylene blue followed by exposure to visible light. This approach is less effective versus non-enveloped viruses and results in approximately 20% fibrinogen loss. Solvent detergent treatment is the most effective procedure for inactivating blood-borne lipid-enveloped viruses. Solvent detergent treatment inactivates viruses by dissolving their lipid envelope but it does not inactivate non-lipid enveloped viruses such as parvovirus or hepatitis A virus. The treatment of cryoprecipitate with a combination of organic solvent, tri (n-butyl) phosphate (TNBP), and detergent (sodium cholate, Tween 80, or Triton X-100) has been shown to inactivate very large quantities of HBV, HCV, and HIV while preserving the activity of the purified protein. Radosevich et al showed that treating cryoprecipitate with a mixture of 0.3% TNBP and 1% tween 80 at 25 °C for 6 hours inactivated ≥ 5.5 $\log_{10}$ of HIV, ≥ 5 $\log_{10}$ of VSV virus, and ≥ 6.5 $\log_{10}$ of sindbis virus [56]. Horowitz and coworkers revealed that subjecting pooled plasma to a mixture of 1% TNPB and 1% Triton X-100 for 4 hours at 30 °C inactivates $\geq 10^6$ CID_{50} of HBV, 10^5 CID_{50} of HCV, and $10^{6.2}$ $TCID_{50}$ of HIV.

Fibronectin

Fibronectin (FN) is a large, multifunctional, adhesive glycoprotein that is present in a soluble form in plasma or as insoluble filaments deposited on the extracellular matrix (ECM) [57]. It regulates cellular processes and deposited by cells into a provisional ECM where it functions as a scaffold to maintain and direct tissue organization [58]. FN incorporated into fibrin by FXIIII mediates interaction of fibrin with cells or platelets during clot formation. Bound fibronectin forms a three-dimensional matrix at the wound site that attracts different cell types and ECM proteins.

FN is secreted as a dimer composed of two nearly identical polypeptides chains each with a molecular weight of ~220-250 kDa [59-61] that are linked together by two disulfide bonds located close to the C-terminal region [62, 63]. Each polypeptide chain is made of three types of repeating modular consensus amino acid sequences known as types I, II, and III (F1, F2, and F3) [64]. FN properties are listed in Table 1.3. There are 12 type I modules, two type II modules, and 15-17 type III modules, which together accounts for ~90% of the fibronectin sequence. Type I modules contain ~45 amino acids held together by two disulfide bonds and located in the amino and carboxyl termini regions of each subunit. Type II modules are composed of ~60 amino acids linked by two disulfide bonds and localized in the gelatin binding domain of the subunit. Type III modules consists of ~90 amino acids that are clustered together in the middle of the subunit and does not contain disulfide bonds. The N-terminal region of fibronectin consist of five type I modules whereas the C-terminal contains three type I modules. These modules are organized into well-defined functional domains that include the 70 kDa N-terminal domain, the 120 kDa central binding domain, and the heparin binding domain. Fibronectin domains are shown in Figure 1.2.

These domains interact with a variety of molecules that include other ECM components and cell-surface receptors [65].

Table 1.3 Properties of fibronectin

Molecular weight	440-450 kDa
Subunits	Two subunits of 200 and 220 kDa
Carbohydrate content [66, 67]	~5% oligosaccharides
Concentration in normal plasma [68, 69]	300-400 µg/ml
Concentration in serum [70, 71]	3 µg FN/3×10^8 platelets in 1 ml of blood
Isoelectric point	5.5-6.2
No of cysteine residues	1.6 free cysteine/220 kDa subunit
Hydrodynamic properties $S_{20,w}$	12-14 S
Synthesized by [72]	Hepatocytes is the major source of pdFN
Half-life [73]	24-72 hours

Plasma fibronectin (pdFN), also known as cold insoluble globulin, is synthesized by hepatocytes and secreted into plasma where it circulates at a concentration of approximately 300-400 µg/ml [68, 69]. Soluble pdFN is present as a semi compact structure that is stabilized by intramolecular ionic interactions between specific modules that include the 1F1–5F1, the 2F3–3F3, and 12F3–14F3 segments. Electron microscopy of pdFN deposited on surface revealed an extended V-shaped structure [74-76] or compact globular molecules with dimensions varying from 16 × 9 nm to 51 × 32 nm [77-79]. The V region contains the binding site for $\alpha_4\beta_1$ and is essential for the secretion of FN dimer.

Cellular fibronectin (cFN) is secreted by different resident cells in tissues including fibroblasts, osteoblasts, endothelial cells, chondrocytes, macrophages, and certain epithelial cells [58]. In the ECM, cFN exists in a more extended conformation forming multimeric fibrous strands. Many cFN subunits contain the V region but only one pdFN dimer subunit contains that region.

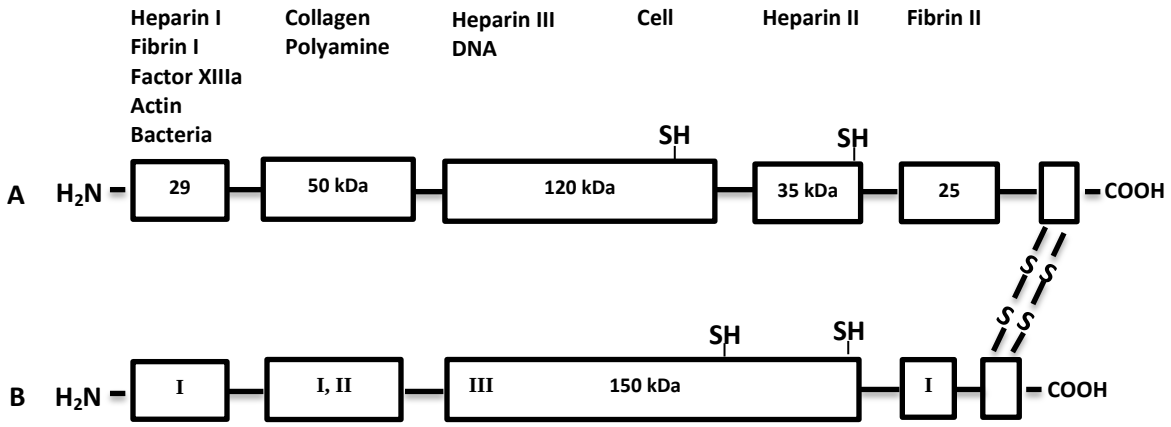

Figure 1.2 Schematic representation of the structure of human fibronectin. The structure and location of domains and subunits is shown. Fibronectin is composed of two subunits (A and B) that are linked by disulfide bridges at their C-terminal region. The binding sites are illustrated. The location of functional domains derived from partial proteolytic fragmentation of fibronectin. The diagram is reproduced from a previous model structure developed by Gene [2]

Fibronectin, the second most abundant protein within the ECM, interacts with other ECM components and integrin receptors on the cell surface [80-82]. FN contains binding sites for different molecules that are localized along the length of the monomer enabling FN to play an important role in many physiological processes (Table 1.4). For example, FN plays a critical role in regulating cellular adhesion, spreading, migration, growth, proliferation, and differentiation

[66, 83-85]. These processes are mediated through interactions of FN with a variety of ECM and cellular receptors, primarily of the integrin family. Integrins represent a family of dimeric cell surface receptors that recognize specific ECM and cell bound ligands. The cell-binding domain and the alternatively spliced V region are the two main sites in fibronectin that mediate cell adhesion. Integrins α3β1, α5β1, α8β1, αvβ1, αIIbβ3, αvβ3, αvβ5, and αvβ6 interact with the Arg-Gly-Asp sequence in the central cell-binding domain, whereas integrins α4β1 and α4β7 interact with the peptide Leu-Asp-Val in the V region. These cellular functions in turn play significant roles in a variety of biological processes such as wound healing, homeostasis, embryonic development, and ECM assembly [66, 84, 86].

Table 1.4 molecules that interact with FN and their physiological functions

Substrate	Function
Fibrinogen, Fibrin [87, 88]	Hemostasis and thrombosis
Heparin [64]	Enhance binding of FN to collagen, stabilize FN-collagen Complex [89]
Hyaluronic acid [90]	Affects interaction of hyaluronic acid with cells and ECM Molecules [90-92]
Bacteria [93, 94]	Phagocytosis
FXIII [87, 88]	Hemostasis and thrombosis
Cells	Promote adhesion, migration, proliferation
Proteoglycans	Platelets aggregation [95, 96]
DNA [97]	
Actin [98]	Promote phagocytosis
Thrombospondin [99]	
Collagen [88]	Mediate cells binding [100, 101]

FN is encoded by a single gene that is alternatively spliced at three different regions forming the different forms of fibronectin [102]. The alternatively spliced domains include type III A domain (EIIIA), type III B domain (EIIIB), and type III connecting segment (IIICS) domain. Exons EIIIA and EIIIB are independently excluded in most adult tissues and included during tissue rearrangements processes such as embryogenesis and wound healing. Domain IIICS contain about five distinct spliced variant and undergoes complex splicing of mRNA transcribed from a single exon. Domains EIIIA and EIIIB are found in a proportion in cFN subunits but not in pdFN, whereas domain IIICS is present in the majority of cFN subunits and one subunit of each pdFN dimer. While IIICS domain is essential for the secretion of FN dimer and provides the binding site for $\alpha_4\beta_1$, domains EIIIA and EIIIB functional roles have been difficult to determine.

The conformation of pdFN is affected readily by the solution and surface conditions such as pH and ionic environment. Studies using sedimentation velocity show that FN can undertake reversible transition forming a compact to a more extended form [59, 76, 103]. At lower ionic strength, physiological pH and salt concentration, pdFN is present in a compact structure. The compact form is stabilized by salt bridges between acidic and basic residues [104]. However, exposing pdFN to extreme pH or high salt concentration induce a reversible expansion of the pdFN forming an extended structure. The compact conformation of FN contains a number of cryptic sites which suppresses its biological activity. However, studies have shown that conformational changes of compact FN expose these cryptic binding sites and enable the protein to play important biological roles.

Interaction of fibronectin with fibrinogen and fibrin

The reaction of fibrinogen with fibronectin has been proposed to occur through a tow step mechanism. The first step is a noncovalent interaction in which fibronectin binds reversibly to fibrinogen. In the second step, FXIIIa stabilize the noncovalent interaction by mediating the covalent cross-linking between the two proteins. FXIIIa catalyzes the formation of an isopeptide bond between ε-NH_2 groups of lysine residue on one protein and γ-carbamoyl groups of specific glutamine residues on the other protein [105]. Studies have shown that the FXIIIa catalyzed fibrin-fibronectin covalent cross-linking occurs specifically between the lysyl residues in fibrin and glutaminyl residues in fibronectin. Figure 1.3 depicts the noncovalent and covalent interactions between the αC domain of fibrin/fibrinogen and NH_2-terminal Fib-1 region of fibronectin.

Enzymatic degradation of FN followed by affinity chromatography and amino acid sequencing of eluted fragments have allowed the identification of different FI binding sites in FN. Using this approach, each fibronectin subunit was shown to contains two fibrin binding regions known as Fib-1 and Fib-2. Fib-1 binding region consists of the 29 kDa N-terminal fragments formed by the first five finger modules of fibronectin (F1-F5) while Fib-2 region contains the 19 kDa C-terminal formed by the three finger modules of fibronectin (F10-F12) [106, 107]. Matsuka and colleagues have shown that FN fragments including the 29 kDa Fib-1 fragment, the 19 kDa Fib-2 fragment, and the 42 kDa gelatin-binding fragment all bound to fibrin-Sepharose at 4℃ [108]. However, only the Fib-1 and Fib-2 binding fragments exhibited binding when temperature was raised to physiological level. By studying the binding of individual recombinant fingers (rF1-rF5) to fibrin-Sepharose, the same group have further localized fibrin recognition site within fingers 4 and 5.

In a separate investigation, Seidl and Hormann isolated two fibrin recognition sites from a chymotryptic digest of pdFN followed by fractionation on fibrin-Sepharose [106]. The first fragment has a molecular weight of 30 kDa and correlate to the well-established N-terminal Fib-1 binding domain. The second fragment with a molecular weight of 60 kDa also exhibited affinity towards denatured collagen and can further be degraded with cathepsin D to 18 kDa and 40 kDa fragments. The idea of a fibrin binding site within the gelatin binding domain was suggested by earlier studies that showed gelatin inhibits the binding of fibronectin to a fibrin clot [109]. These studies also showed that the gelatin binding domain is located in close proximity to fibrin binding domain. The presence of the gelatin and fibrin binding domains in close proximity may leads to the steric interference of the two domains and help explains the affinity of 60 kDa gelatin domains towards fibrin [106].

Studies were also carried out to localize FN binding sites in FI. Using ELISA and Surface Plasmon resonance, Medved and colleagues studied the interaction of recombinant αC-domain of FI with FN [3]. They found that the amino terminal half of FI αC-domain contains FN binding sites and is the only region in FI that interacts with FN. The fibrin C-terminal portion of the Aα-chain appears to be the major recognition site for FN. This peptide is highly susceptible to proteolysis [110] indicating the rapid release of FN form the clot during plasmin degradation. The same recognition site is implicated to play a key role in the cryoprecipitation of FN and FI or fibrin in the cold.

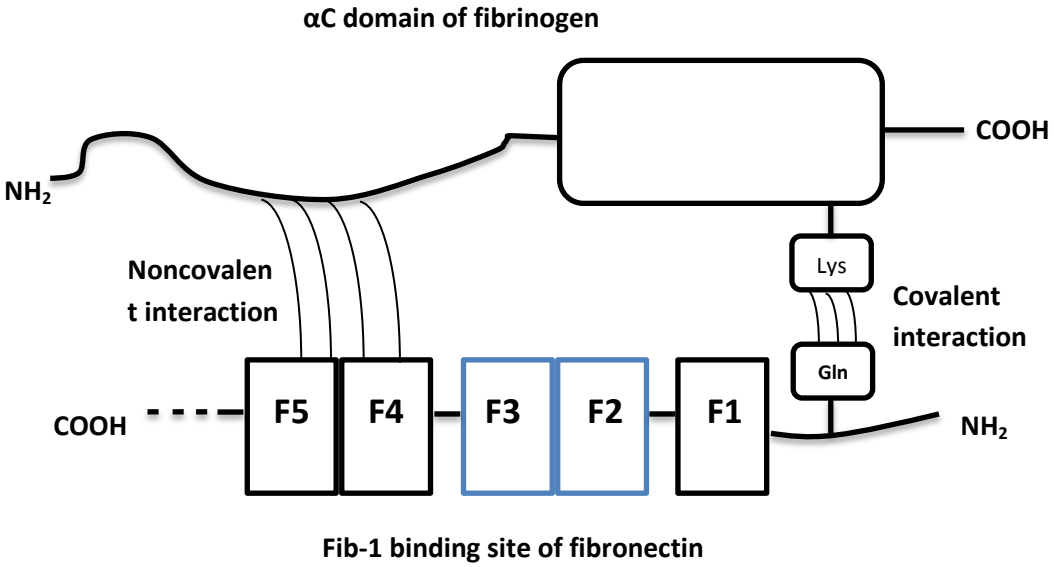

Figure 1.3 Schematic representation of the interaction of the N-terminal Fib-1 region with the αC domain. The numbered boxes represent the five FN fingers. This figure is reproduced from reference [3].

Dissertation objectives

Studies have shown that fibrinogen-fibronectin complexes only exist in the plasma of patients with various inflammatory diseases. Few of these studies have described the properties of these complexes. Furthermore, although some studies have examined the interaction of FN with FI, the interactions of FN with γγ and γγ' FI subspecies was not investigated. Therefore, the specific goals of this dissertation were to:

a) Characterize the properties of a fibrinogen-fibronectin complex purified from human plasma of healthy individuals.
b) Characterize the size distributions and hydrodynamic properties of the isolated complex and comparable mixtures of FI and FN.

c) Characterize the kinetics and mechanical properties of fibrin clots derived from the isolated complex and comparable mixtures of FI and FN.

d) Characterize the biological activities of the isolated complex with an *in vitro* cell adhesion model.

References

1. M. COLAFRANCESCHI, A.G.A.A.C. and *PRIMARY STRUCTURES OF PROTEINS AS SPACE-DEPENDENT SIGNALS.* Biophys. & Bioengin., 2008. **1**.
2. Homandberg, G.A. and J.W. Erickson, *Model of fibronectin tertiary structure based on studies of interactions between fragments.* Biochemistry, 1986. **25**(22): p. 6917-25.
3. Makogonenko, E., et al., *Interaction of fibrin(ogen) with fibronectin: further characterization and localization of the fibronectin-binding site.* Biochemistry, 2002. **41**(25): p. 7907-13.
4. Clark, R.A., et al., *Fibronectin and fibrin provide a provisional matrix for epidermal cell migration during wound reepithelialization.* J Invest Dermatol, 1982. **79**(5): p. 264-9.
5. Mosesson, M.W., K.R. Siebenlist, and D.A. Meh, *The structure and biological features of fibrinogen and fibrin.* Ann N Y Acad Sci, 2001. **936**: p. 11-30.
6. Herrick, S., et al., *Fibrinogen.* Int J Biochem Cell Biol, 1999. **31**(7): p. 741-6.
7. Doolittle, R.F., *Fibrinogen and fibrin.* Annu Rev Biochem, 1984. **53**: p. 195-229.
8. Brown, J.H., et al., *The crystal structure of modified bovine fibrinogen.* Proc Natl Acad Sci U S A, 2000. **97**(1): p. 85-90.
9. Weisel, J.W., et al., *A model for fibrinogen: domains and sequence.* Science, 1985. **230**(4732): p. 1388-91.
10. McKee, P.A., et al., *The subunit polypeptides of human fibrinogen.* Arch Biochem Biophys, 1966. **116**(1): p. 271-9.
11. Henschen, A., et al., *Covalent structure of fibrinogen.* Ann N Y Acad Sci, 1983. **408**: p. 28-43.
12. G, B.B.E., *In: Gottschalk A, ed. Glycoproteins*. Vol. 5, Part B. 1972, New York: Elsevier/North Holland.
13. Wasilewska, M., Z. Adamczyk, and B. Jachimska, *Structure of fibrinogen in electrolyte solutions derived from dynamic light scattering (DLS) and viscosity measurements.* Langmuir, 2009. **25**(6): p. 3698-704.
14. Aptel, J.D., J.C. Voegel, and A. Schmitt, *Adsorption kinetics of proteins onto solid surfaces in the limit of the interfacial interaction control.* Colloids Surf., 1988. **29**(4): p. 359-71.
15. Kant, J.A., et al., *Evolution and organization of the fibrinogen locus on chromosome 4: gene duplication accompanied by transposition and inversion.* Proc Natl Acad Sci U S A, 1985. **82**(8): p. 2344-8.

16. Crabtree, G.R. and J.A. Kant, *Organization of the rat gamma-fibrinogen gene: alternative mRNA splice patterns produce the gamma A and gamma B (gamma ') chains of fibrinogen.* Cell, 1982. **31**(1): p. 159-66.
17. Chung, D.W. and E.W. Davie, *γ and γ' chains of human fibrinogen are produced by alternative mRNA processing.* Biochemistry, 1984. **23**(18): p. 4232-6.
18. de Maat, M.P. and M. Verschuur, *Fibrinogen heterogeneity: inherited and noninherited.* Curr Opin Hematol, 2005. **12**(5): p. 377-83.
19. Holm, B., et al., *Purification and characterization of 3 fibrinogens with different molecular weights obtained from normal human plasma.* Thromb Res, 1985. **37**(1): p. 165-76.
20. Holm, B., et al., *Polymerization properties of two normally circulating fibrinogens, HMW and LMW. Evidence that the COOH-terminal end of the a-chain is of importance for fibrin polymerization.* Thromb Res, 1985. **39**(5): p. 595-606.
21. Holm, B., D.W. Nilsen, and H.C. Godal, *Evidence that low molecular fibrinogen (LMW) is formed in man by degradation of high molecular weight fibrinogen (HMW).* Thromb Res, 1986. **41**(6): p. 879-84.
22. Francis, C.W., V.J. Marder, and S.E. Martin, *Plasmic degradation of crosslinked fibrin. I. Structural analysis of the particulate clot and identification of new macromolecular-soluble complexes.* Blood, 1980. **56**(3): p. 456-64.
23. Wolfenstein-Todel, C. and M.W. Mosesson, *Human plasma fibrinogen heterogeneity: evidence for an extended carboxyl-terminal sequence in a normal gamma chain variant (gamma').* Proc Natl Acad Sci U S A, 1980. **77**(9): p. 5069-73.
24. Chung, D.W. and E.W. Davie, *gamma and gamma' chains of human fibrinogen are produced by alternative mRNA processing.* Biochemistry, 1984. **23**(18): p. 4232-6.
25. Fornace, A.J., Jr., et al., *Single-copy inverted repeats associated with regional genetic duplications in gamma fibrinogen and immunoglobulin genes.* Science, 1984. **224**(4645): p. 161-4.
26. Wolfenstein-Todel, C. and M.W. Mosesson, *Carboxy-terminal amino acid sequence of a human fibrinogen gamma-chain variant (gamma').* Biochemistry, 1981. **20**(21): p. 6146-9.
27. Siebenlist, K.R., D.A. Meh, and M.W. Mosesson, *Plasma factor XIII binds specifically to fibrinogen molecules containing gamma chains.* Biochemistry, 1996. **35**(32): p. 10448-53.
28. Stathakis, N.E. and M.W. Mosesson, *Interactions among heparin, cold-insoluble globulin, and fibrinogen in formation of the heparin-precipitable fraction of plasma.* J Clin Invest, 1977. **60**(4): p. 855-65.
29. Romanic, A.M., et al., *Factor XIIIa cross-links lipoprotein(a) with fibrinogen and is present in human atherosclerotic lesions.* Circ Res, 1998. **83**(3): p. 264-9.
30. Meh, D.A., et al., *The amino acid sequence in fibrin responsible for high affinity thrombin binding.* Thromb Haemost, 2001. **85**(3): p. 470-4.
31. Kimura, S. and N. Aoki, *Cross-linking site in fibrinogen for alpha 2-plasmin inhibitor.* J Biol Chem, 1986. **261**(33): p. 15591-5.
32. Ritchie, H., et al., *Cross-linking of plasminogen activator inhibitor 2 and alpha 2-antiplasmin to fibrin(ogen).* J Biol Chem, 2000. **275**(32): p. 24915-20.

33. Siebenlist, K.R., et al., *Coexisting dysfibrinogenemia (γR275C) and factor V Leiden deficiency associated with thromboembolic disease (fibrinogen Cedar Rapids).* Blood Coagulation Fibrinolysis, 2000. **11**(3): p. 293-304.
34. Doolittle, R.F., et al., *The amino acid sequence of the α-chain of human fibrinogen.* Nature (London), 1979. **280**(5722): p. 464-8.
35. Odrljin, T.M., et al., *Thrombin cleavage enhances exposure of a heparin binding domain in the N-terminus of the fibrin beta chain.* Blood, 1996. **88**(6): p. 2050-61.
36. Odrljin, T.M., et al., *Heparin-binding domain of fibrin mediates its binding to endothelial cells.* Arterioscler Thromb Vasc Biol, 1996. **16**(12): p. 1544-51.
37. Yakovlev, S., et al., *Interaction of fibrin(ogen) with heparin: further characterization and localization of the heparin-binding site.* Biochemistry, 2003. **42**(25): p. 7709-16.
38. Olexa, S.A. and A.Z. Budzynski, *Evidence for four different polymerization sites involved in human fibrin formation.* Proc. Natl. Acad. Sci. U. S. A., 1980. **77**(3): p. 1374-8.
39. Ferry, J.D., *The mechanism of polymerization of fibrinogen.* Proc. Natl. Acad. Sci. U. S. A., 1952. **38**: p. 566-9.
40. Krakow, W., et al., *Electron microscopic investigation of the polymerization of bovine fibrin monomer.* J. Mol. Biol., 1972. **71**(1): p. 95-103.
41. Fowler, W.E., et al., *Structure of the fibrin protofibril.* Proc. Natl. Acad. Sci. U. S. A., 1981. **78**(8): p. 4872-6.
42. Muller, M.F., H. Ris, and J.D. Ferry, *Electron microscopy of fine fibrin clots and fine and coarse fibrin films. Observations of fibers in cross-section and in deformed states.* J Mol Biol, 1984. **174**(2): p. 369-84.
43. Mosesson, M.W., et al., *Identification of covalently linked trimeric and tetrameric D domains in crosslinked fibrin.* Proc Natl Acad Sci U S A, 1989. **86**(4): p. 1113-7.
44. Hewat, E.A., L. Tranqui, and R.H. Wade, *Electron microscope structural study of modified fibrin and a related modified fibrinogen aggregate.* J. Mol. Biol., 1983. **170**(1): p. 203-22.
45. Doolittle, R.F., R. Chen, and F. Lau, *Hybrid fibrin: proof of the intermolecular nature of - crosslinking units.* Biochem Biophys Res Commun, 1971. **44**(1): p. 94-100.
46. Chen, R. and R.F. Doolittle, *γ-γ Cross-linking sites in human and bovine fibrin.* Biochemistry, 1971. **10**(24): p. 4486-91.
47. Purves, L., M. Purves, and W. Brandt, *Cleavage of fibrin-derived D-dimer into monomers by endopeptidase from puff adder venom (Bitis arietans) acting at cross-linked sites of the gamma-chain. Sequence of carboxy-terminal cyanogen bromide gamma-chain fragments.* Biochemistry, 1987. **26**(15): p. 4640-6.
48. Sobel, J.H. and M.A. Gawinowicz, *Identification of the alpha chain lysine donor sites involved in factor XIIIa fibrin cross-linking.* J Biol Chem, 1996. **271**(32): p. 19288-97.
49. Matsuka, Y.V., et al., *Factor XIIIa-catalyzed cross-linking of recombinant alpha C fragments of human fibrinogen.* Biochemistry, 1996. **35**(18): p. 5810-6.
50. Siebenlist, K.R., D.A. Meh, and M.W. Mosesson, *Protransglutaminase (factor XIII) mediated crosslinking of fibrinogen and fibrin.* Thromb Haemost, 2001. **86**(5): p. 1221-8.
51. McKee, P.A., P. Mattock, and R.L. Hill, *Subunit structure of human fibrinogen, soluble fibrin, and cross-linked insoluble fibrin.* Proc. Nat. Acad. Sci. U. S., 1970. **66**(3): p. 738-44.

52. Folk, J.E. and J.S. Finlayson, *The epsilon-(gamma-glutamyl)lysine crosslink and the catalytic role of transglutaminases.* Adv Protein Chem, 1977. **31**: p. 1-133.
53. Shainoff, J.R., D.A. Urbanic, and P.M. DiBello, *Immunoelectrophoretic characterizations of the cross-linking of fibrinogen and fibrin by factor XIIIa and tissue transglutaminase. Identification of a rapid mode of hybrid alpha-/gamma-chain cross-linking that is promoted by the gamma-chain cross-linking.* J Biol Chem, 1991. **266**(10): p. 6429-37.
54. Siebenlist, K.R. and M.W. Mosesson, *Evidence of intramolecular cross-linked A alpha.gamma chain heterodimers in plasma fibrinogen.* Biochemistry, 1996. **35**(18): p. 5817-21.
55. Siebenlist, K.R. and M.W. Mosesson, *Factors affecting gamma-chain multimer formation in cross-linked fibrin.* Biochemistry, 1992. **31**(3): p. 936-41.
56. Burnouf-Radosevich, M., T. Burnouf, and J.J. Huart, *Biochemical and physical properties of a solvent-detergent-treated fibrin glue.* Vox Sang, 1990. **58**(2): p. 77-84.
57. Abe, Y., et al., *Extra domain A and type III connecting segment of fibronectin in assembly and cleavage.* Biochem Biophys Res Commun, 2005. **338**(3): p. 1640-7.
58. Peters, D.M.P.a.M., DP. In: Yurchenco PD, Birk DE, and M.R. (eds), *Extracellular Matrix Assembly and Structure*. 1989, San Diego, CA: Academic Press.
59. Mosesson, M.W., A.B. Chen, and R.M. Huseby, *The cold-insoluble globulin of human plasma: studies of its essential structural features.* Biochim Biophys Acta, 1975. **386**(2): p. 509-24.
60. Mosher, D.F., *Fibronectin.* J. Biol. Chem., 1985. **260**: p. 6614-6621.
61. Kurkinen, M., T. Vartio, and A. Vaheri, *Polypeptides of human plasma fibronectin are similar but not identical.* Biochim Biophys Acta, 1980. **624**(2): p. 490-8.
62. Furie, M.B., A.B. Frey, and D.B. Rifkin, *Location of a gelatin-binding region of human plasma fibronectin.* J Biol Chem, 1980. **255**(10): p. 4391-4.
63. Skorstengaard, K., et al., *Purification of twelve cyanogen bromide fragments from bovine plasma fibronectin and the amino acid sequence of eight of them. Overlap evidence aligning two plasmic fragments, internal homology in gelatin-binding region and phosphorylation site near C terminus.* Eur J Biochem, 1982. **128**(2-3): p. 605-23.
64. Petersen, T.E., et al., *Partial primary structure of bovine plasma fibronectin: three types of internal homology.* Proc Natl Acad Sci U S A, 1983. **80**(1): p. 137-41.
65. Pickford, A.R. and I.D. Campbell, *NMR studies of modular protein structures and their interactions.* Chem Rev, 2004. **104**(8): p. 3557-66.
66. Mosher, D., *Fibronectin*. 1989, New York: Academic Press.
67. Ruoslahti, E., et al., *Comparative studies on amniotic fluid and plasma fibronectins.* Biochem. J., 1981. **193**(1): p. 295-9.
68. Matsuda, M., et al., *Distribution of cold-insoluble globulin in plasma and tissues.* Ann N Y Acad Sci, 1978. **312**: p. 74-92.
69. Mosher, D.F. and E.M. Williams, *Fibronectin concentration is decreased in plasma of severely ill patients with disseminated intravascular coagulation.* J Lab Clin Med, 1978. **91**(5): p. 729-35.
70. Plow, E.F., C. Birdwell, and M.H. Ginsberg, *Identification and quantitation of platelet-associated fibronectin antigen.* J Clin Invest, 1979. **63**(3): p. 540-3.

71. Zucker, M.B., et al., *Release of platelet fibronectin (cold-insoluble globulin) from alpha granules induced by thrombin or collagen; lack of requirement for plasma fibronectin in ADP-induced platelet aggregation.* Blood, 1979. **54**(1): p. 8-12.
72. Voss, B., et al., *Primary cultures of rat hepatocytes synthesize fibronectin.* Biochem Biophys Res Commun, 1979. **90**(4): p. 1348-54.
73. Mosher, D.F., *Physiology of fibronectin.* Annu Rev Med, 1984. **35**: p. 561-75.
74. Engel, J., et al., *Shapes, domain organizations and flexibility of laminin and fibronectin, two multifunctional proteins of the extracellular matrix.* J Mol Biol, 1981. **150**(1): p. 97-120.
75. Erickson, H.P., N. Carrell, and J. McDonagh, *Fibronectin molecule visualized in electron microscopy: a long, thin, flexible strand.* J Cell Biol, 1981. **91**(3 Pt 1): p. 673-78.
76. Erickson, H.P. and N.A. Carrell, *Fibronectin in extended and compact conformations. Electron microscopy and sedimentation analysis.* J Biol Chem, 1983. **258**(23): p. 14539-44.
77. Koteliansky, V.E., M.V. Bejanian, and V.N. Smirnov, *Electron microscopy study of fibronectin structure.* FEBS Lett, 1980. **120**(2): p. 283-6.
78. Price, T.M., et al., *Structure of fibronectin and its fragments in electron microscopy.* Eur J Biochem, 1982. **129**(2): p. 359-63.
79. Tooney, N.M., et al., *Solution and surface effects on plasma fibronectin structure.* J Cell Biol, 1983. **97**(6): p. 1686-92.
80. Hynes, R.O., *Integrins: versatility, modulation, and signaling in cell adhesion.* Cell, 1992. **69**(1): p. 11-25.
81. Haas, T.A. and E.F. Plow, *Integrin-ligand interactions: a year in review*. Curr Opin Cell Biol, 1994. **6**(5): p. 656-62.
82. Ruoslahti, E., *Integrin signaling and matrix assembly.* Tumour Biol, 1996. **17**(2): p. 117-24.
83. Carsons, S.E., *Fibronectin in Health and Disease*. 1989, Florida: CRC Press, Inc.
84. Hynes, R.O., *Fibronectins*. 1990, New York: Springer-Verlag.
85. RAF, Y.K.a.C., *Provisional matrix. In: The Molecular and Cellular Biology of Wound Repair* 1996, New York: Plenum Press.
86. Ruoslahti, E., *Fibronectin and its receptors.* Annu Rev Biochem, 1988. **57**: p. 375-413.
87. Mosher, D.F., *Action of fibrin-stabilizing factor on cold-insoluble globulin and α2-macroglobulin in clotting plasma.* J. Biol. Chem., 1976. **251**(6): p. 1639-45.
88. Mosher, D.F. and P.E. Schad, *Cross-linking of fibronectin to collagen by blood coagulation Factor XIIIa.* J Clin Invest, 1979. **64**(3): p. 781-7.
89. Johansson, S. and M. Hook, *Heparin enhances the rate of binding of fibronectin to collagen.* Biochem J, 1980. **187**(2): p. 521-4.
90. Yamada, K.M., et al., *Characterization of fibronectin interactions with glycosaminoglycans and identification of active proteolytic fragments.* J Biol Chem, 1980. **255**(13): p. 6055-63.
91. Jilek, F. and H. Hormann, *Fibronectin (cold-insoluble globulin), VI. Influence of heparin and hyaluronic acid on the binding of native collagen.* Hoppe Seylers Z Physiol Chem, 1979. **360**(4): p. 597-603.
92. Hormann, H. and V. Jelinic, *Regulation by heparin and hyaluronic acid of the fibronectin-dependent association of collagen, Type III, with macrophages.* Hoppe Seylers Z Physiol Chem, 1981. **362**(1): p. 87-94.

93. Kuusela, P., *Fibronectin binds to Staphylococcus aureus.* Nature, 1978. **276**(5689): p. 718-20.
94. Mosher, D.F. and R.A. Proctor, *Binding and factor XIIIa-mediated cross-linking of a 27-kilodalton fragment of fibronectin to Staphylococcus aureus.* Science, 1980. **209**(4459): p. 927-9.
95. Gartner, T.K., et al., *Thrombin-induced platelet aggregation is mediated by a platelet plasma membrane-bound lectin.* Science, 1978. **200**(4347): p. 1281-3.
96. Jaffe, E.A., et al., *Thrombospondin is the endogenous lectin of human platelets.* Nature (London), 1982. **295**(5846): p. 246-8.
97. Zardi, L., et al., *Fibronectin: a chromatin-associated protein?* Cell, 1979. **18**(3): p. 649-57.
98. Keski-Oja, J. and K.M. Yamada, *Isolation of an actin-binding fragment of fibronectin.* Biochem. J., 1981. **193**(2): p. 615-20.
99. Lahav, J., M.A. Schwartz, and R.O. Hynes, *Analysis of platelet adhesion with a radioactive chemical crosslinking reagent: interaction of thrombospondin with fibronectin and collagen.* Cell, 1982. **31**(1): p. 253-62.
100. Klebe, R.J., *Isolation of a collagen-dependent cell attachment factor.* Nature, 1974. **250**(463): p. 248-51.
101. Pearlstein, E. and L.I. Gold, *High-molecular-weight glycorprotein as a mediator of cellular adhesion.* Ann N Y Acad Sci, 1978. **312**: p. 278-92.
102. Hynes, R., *Molecular biology of fibronectin.* Annu Rev Cell Biol, 1985. **1**: p. 67-90.
103. Alexander, S.S., Jr., G. Colonna, and H. Edelhoch, *The structure and stability of human plasma cold-insoluble globulin.* J Biol Chem, 1979. **254**(5): p. 1501-5.
104. Hormann, H., *Fibronectin--mediator between cells and connective tissue.* Klin Wochenschr, 1982. **60**(20): p. 1265-77.
105. Henschen, A. and J. McDonagh, *Fibrinogen, fibrin and factor XIII.* New Compr. Biochem., 1986. **13**(Blood Coagulation): p. 171-241.
106. Seidl, M. and H. Hormann, *Affinity chromatography on immobilized fibrin monomer, IV. Two fibrin-binding peptides of a chymotryptic digest of human plasma fibronectin.* Hoppe Seylers Z Physiol Chem, 1983. **364**(1): p. 83-92.
107. Sekiguchi, K. and S. Hakomori, *Domain structure of human plasma fibronectin. Differences and similarities between human and hamster fibronectins.* J Biol Chem, 1983. **258**(6): p. 3967-73.
108. Matsuka, Y.V., et al., *The NH2-terminal fibrin-binding site of fibronectin is formed by interacting fourth and fifth finger domains. Studies with recombinant finger fragments expressed in Escherichia coli.* J Biol Chem, 1994. **269**(13): p. 9539-46.
109. Engvall, E., E. Ruoslahti, and E.J. Miller, *Affinity of fibronectin to collagens of different genetic types and to fibrinogen.* J Exp Med, 1978. **147**(6): p. 1584-95.
110. Doolittle, R.F., *Structural aspects of the fibrinogen to fibrin conversion.* Adv Protein Chem, 1973. **27**: p. 1-109.

Chapter 2 Purification and characterization of fibrinogen-fibronectin complex

Abstract

We have developed a method for isolating a 1:1 fibrinogen-fibronectin complex from normal human plasma using a sequence of cryoprecipitation, ammonium sulfate fractionation, and DEAE Sepharose chromatography. SDS-PAGE under reducing condition showed both a 1:1 stoichiometric ratio of pdFI to pdFN as well as a stoichiometric ratio of 1:1 of γγ to γγ'. Only γγpdFI was discernible to be present in the DEAE chromatographic fall-through. The γγ'pdFI-pdFN complex was non-covalent in nature as it was disrupted by affinity adsorption to Gelatin Sepharose where pdFN bound strongly and the disrupted γγ'pdFI fell through the chromatographic column. The FI and FN components of the complex migrated independently on native gel confirming its noncovalent nature. The second DEAE analysis of the gelatin Sepharose fall through demonstrated that the FI population capable of binding FN at room temperature was that containing the γγ'FI heterodimer**.** Surprisingly, the purified γγ'pdFI-pdFN complex was more broadly thermally stable than pdF1 preparations not containing pdFN and was also stable at physiologic pH, ionic strength and temperature.

Introduction

The binding interactions of the general population of pdFN with pdFI have been studied in detail. Earlier studies showed that heparin could induce the formation of a cold-insoluble precipitate of fibrinogen and cold-insoluble globulin of plasma [1]. The cold-insoluble globulin is now known as fibronectin. In later studies, the main components of a pathologic plasma precipitate termed cryoglobulin made by treatment with thrombin of normal plasma were shown to be cold-insoluble globulin, fibrin and fibrinogen [2]. These studies showed that the binding of fibrinogen to cold-insoluble globulin was strong at 4^{o} C but only weakly binding at 22^{o} C. They went on to demonstrate that the COOH- terminal domain of the Aα chain of fibrin/fibrinogen is required for this interaction. Smith and Von Korff initially described the presence of fibrinogen-fibronectin complex in the plasma of patients with different inflammatory, infectious, or neoplastic diseases [3, 4]. Later analysis confirmed the existence of the complex in the plasma obtained from patients with dermatological diseases and ulcers [5, 6]. Using turbidity measurements, Mosesson and Stathukis elucidated the mechanism of cryoprecipitates formation and indicated that FN functions as a nucleus for precipitation of these complexes [7].

Recently, Makogonenko et al [8] reported the results of a detailed study on the interactions of FN with FN free plasma-derived fibrinogen and also fibrin made from that same material. Using ELISA and Surface Plasmon Resonance, this FN free fibrinogen did not bind FN, but fibrin bound with high affinity. The authors used a variety of proteolytic fragments and recombinant derived domains of fibrin to demonstrate that FN binding was due to interaction with residues 221-391 of the αC domain. These results are consistent with the earlier reports and provide a more rigorous understanding of the structural basis for the broad interaction between the two proteins.

Niewiarowsk and Cierniewski have shown that significant amount of FN was incorporated into fibrin clot when blood plasma was treated with thrombin in the presence of calcium ions or EDTA [9]. The binding was dependent on temperature, concentration, and the presence of calcium ions. Binding occurred at a temperature of 20 °C and 37 °C, however, increased amount of FN was incorporated at 4 °C. Ruoslahti and Vaheri, on the other hand, have shown that the amount of FN incorporated into the clot is greatly influenced by ambient temperature [10]. The binding of FN to fibrin clot was observed at low temperature but such binding was prevented or reversed at 37 °C. FN was also bound to Sepharose-conjugated FI at 0 °C but released by elevating the temperature.

In this study we describe, for the first time, the purification of a FI-FN complex from human plasma of healthy individual by a sequence of cryoprecipitation, ammonium sulfate precipitation, and DEAE Sepharose chromatography. Results from this report provide significant insights into the structure and function of the complex.

Materials and Methods

Materials

All reagents of highest purity were purchased from Sigma Chemical Company (St. Louis, MO) unless otherwise noted. Human plasma was donated by the U.S. Army Materials Command (Fort Detrick, MD). Human plasma fibrinogen depleted of fibronectin, plasminogen, and von Willebrand Factor was purchased from Enzyme Research Laboratories (South Bend, IN). DEAE Sepharose Fast Flow and gelatin Sepharose were purchased from GE healthcare (Uppsala, Sweden). Human fibrinogen was purified from plasma by cryoprecipitation followed by two ethanol precipitation as previously described [11]. Human fibronectin was isolated from plasma

on Gelatin Sepharose as previously described [12]. Anti-mouse fibronectin monoclonal IgG_1 antibody was obtained from Santa Cruz Biotechnology (Santa Cruz, CA). Anti-human FXIIIB monoclonal antibody was purchased from Green Mountain Antibodies (Burlington, VT). Anti-human FXIIIA polyclonal antibody was bought from US Biologicals. Anti-human α_2AP polyclonal antibody HRP was bought from US Biologicals. Anti-mouse IgG (whole molecule) peroxidase conjugate and anti-sheep IgG peroxidase conjugate were obtained from Sigma Chemical Company.

Isolation of fibrinogen-fibronectin complex

The complex was isolated from human plasma using cryo and ammonium sulfate precipitation steps followed by anion-exchange chromatography on DEAE Sepharose. The procedures are described below and summarized in Figure 2.1.

Cryoprecipitation

Fifteen units of human plasma (12.65 liters) that had been frozen at -80 °C were thawed slowly at 4 °C. The plasma was centrifuged in a Sorvall RC-5C Plus Superspeed Centrifuge (Kendro Laboratory, Newtown, CT) at 4000 rpm for 20 min at 4 °C. The supernatant was stored at -80 °C for future purification of fibronectin and other plasma-derived proteins. The fibrinogen-rich cryoprecipitate was re-suspended in a re-suspension buffer containing 20 mM tris-base, 55 mM sodium citrate, 27 mM lysine, PH 6.8 for 3 hours at room temp. Viral inactivation was carried out by adjusting the re-suspended cryoprecipitate solution to 0.15% (V/V) TNBP and 0.5% (V/V) Triton X-100. The solution was stirred at room temp for one hour.

Ammonium Sulfate Precipitation

The solvent-detergent treated solution was chilled to ~4 °C on ice then adjusted to 1 M ammonium sulfate by adding a 4 M stock solution. The sample was incubated on ice for 30 min then centrifuged at 4000 rpm at 4 °C for 20 min. The supernatant was discarded and the precipitate was re-suspended in the re-suspension buffer at room temp. The solution was dialyzed overnight against dialysis buffer containing 20 mM sodium citrate, 100 mM NaCl, pH 7.4. The solution was transferred to a fresh buffer and dialysis continued with two changes. The dialyzed solution was centrifuged for 20 min at 4000 rpm at 25 °C. Any remaining pellet was discarded and sample was analyzed by BCA protein assay, reduced and nonreduced SDS-PAGE, and Western blots analysis.

Anion-exchange Chromatography

Anion-exchange chromatography of ammonium sulfate precipitated fibrinogen solution was carried out on a 2.7 cm by 200 cm DEAE Sepharose Fast Flow (GE healthcare Bio-Sciences) column. The run was performed at room temperature using the BioCAD workstation chromatography System (Applied Biosystems) with an automated gradient controller. The run was monitored by the continuous measurement of the effluent absorbance at 280 nm. The sample was applied to the DEAE Sepharose column equilibrated with the dialysis buffer. To eliminate nonadsorbed and weakly bind proteins, the column was washed with 2 column volume of dialysis buffer until absorbance at 280 nm returned to the base line. Bound protein was eluted with a linear gradient of 0.1 M to 1.0 M NaCl in 20 sodium citrate and pH 7.4 buffers. Fractions were collected, pooled, and dialyzed versus dialysis buffer.

Gelatin Sepharose Chromatography

Ammonium sulfate precipitated fibrinogen was fractionated by affinity chromatography using Gelatin Sepharose 4B (GE healthcare). The run was done on 1.6 cm by 100 cm gelatin Sepharose 4B column using the BioCAD workstation chromatography system. The column was equilibrated with a TEC buffer containing 50 mM Tris-Base, 50 mM 6-aminocaproic acid, 20 mM sodium citrate, PH 7.5. The fibrinogen sample diluted with the same buffer was applied to the equilibrated column and washed with a 3 column volume of the equilibration buffer until absorbance at 280 nm returned to the base line. The column was further washed with a 3 column volume of the same buffer containing 1 M NaCl to remove nonspecific binding proteins. Still retained protein was desorbed with a step elution of the same equilibration buffer containing 1 M NaCl and 6 M urea. Fall through fractions were collected and dialyzed against dialysis buffer (20 mM citrate, 100 mM NaCl, PH 7.4). The elution portion was dialyzed versus a buffer containing 25 mM Tris-base, 150 mM NaCl, pH 7.5. Samples were analyzed by SDS-PAGE and Western blots analysis.

SDS-PAGE Analysis

The purity of the isolated fibrinogen was examined by SDS-PAGE under both reducing and nonreducing conditions. Samples were analyzed on 4-12% NuPAGE Bis-Tris Mini Gels (Life Technologies, Grand Island, NY) using NuPAGE LDS sample buffer. Reduced samples were treated with NuPAGE sample reducing agent. After 10 minutes incubation at 74 °C, samples were loaded onto the gel and run using 2-(N-morpholino) ethanesulfonic acid (MES) for one hour at 200 volts. Gels were stained with colloidal blue (Invitrogen, Carlsbad, CA).

Samples were also analyzed under non-denaturing condition in 3-12% NativePAGE Novex Bis-Tris Gels (Invitrogen). Samples were mixed with the NativePAGE Sample Buffer and run using the anode and cathode buffers for 115 minutes. Samples were visualized with colloidal blue.

Western Blot Analysis

Samples were analyzed on 4-12% NuPAGE Bis-Tris Mini Gels (Life Technologies) under reducing or non-reducing condition. Gels were electroblotted onto polyvinylide fluoride (PVDF) membranes (Millipore, Billerica, MA) for 45 min at 25 volts. Blots were blocked in 50 ml of 5% casein in TBST (Tris-buffered Tween-20) for 30 minutes at room temperature. Blots were incubated with the following antibodies: (a) anti-plasma fibrinogen antibody (Green Mountain Antibodies, Burlington, VT); (b) anti-plasma fibronectin monoclonal antibody (Santa Cruz Biotechnology, Santa Cruz, CA); (c) anti-plasma fibrinogen α-chain polyclonal antibody (Sigma Aldrich, Saint Louis, MO); (d) anti-plasma fibrinogen β-chain polyclonal antibody (Sigma Aldrich); (e) anti-plasma fibrinogen γ-chain monoclonal antibody (Sigma Aldrich). Blots developed with anti-plasma fibrinogen, anti-plasma fibronectin, and anti-plasma fibrinogen γ-chain antibodies were subsequently detected with an anti-mouse IgG peroxidase conjugate (Sigma Aldrich). Blots developed with anti-plasma fibrinogen α-chain and anti-plasma fibrinogen β-chain antibodies were probed with an anti-rabbit IgG peroxidase conjugate (Sigma). Blots were visualized with DAB/Metal concentrate and stable peroxide substrate buffer (Thermo Scientific, Rockford, IL) or chemiluminescence using Immun-Star HRP enhancer and peroxide buffer (Bio-Rad Laboratories, Hercules, CA).

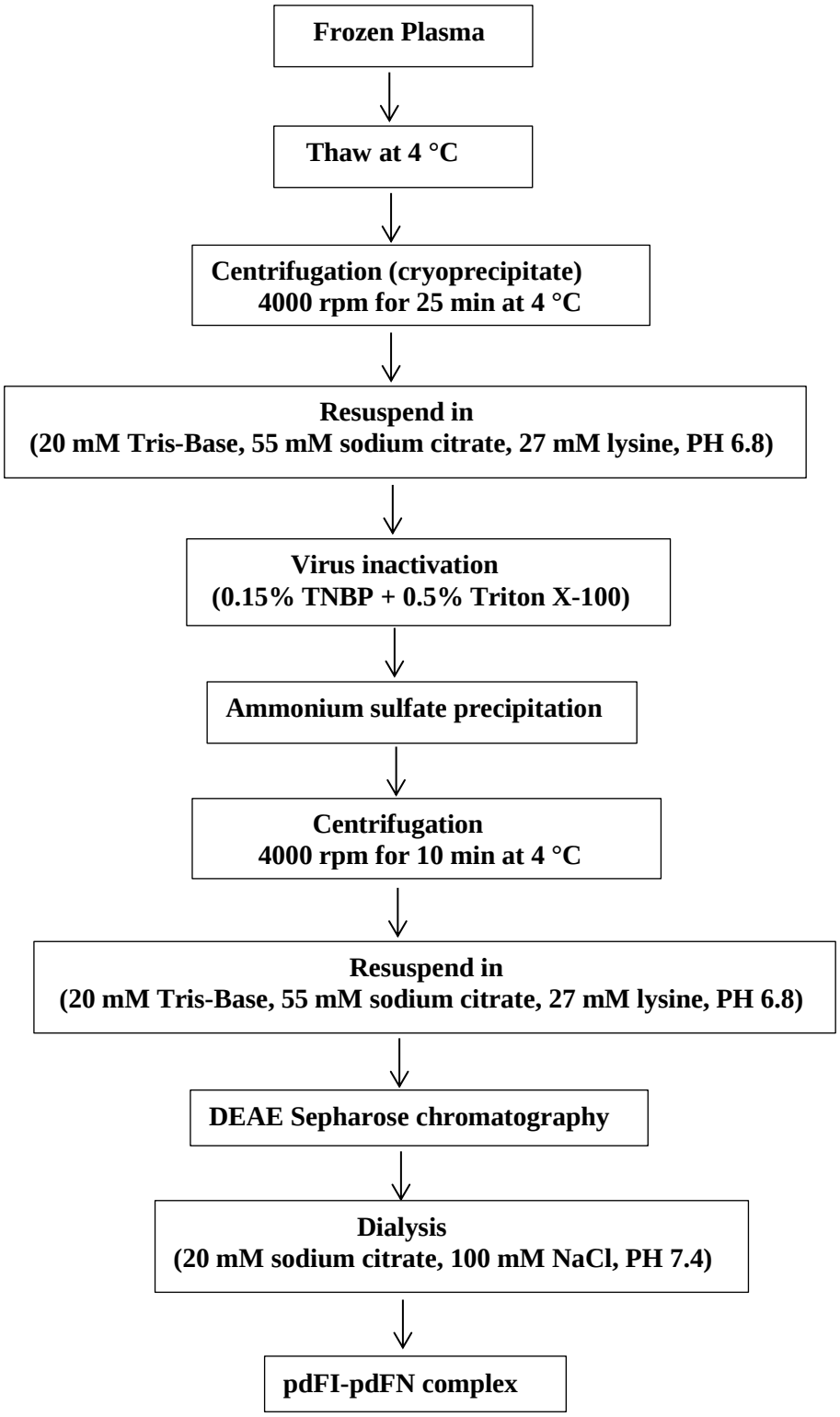

Figure 2.1 Purification procedure of fibrinogen-fibronectin complex

Dissociation of γγ'FI-FN complex by affinity Chromatography

The γγ'pdFI-pdFN complex was separated by affinity chromatography using Gelatin Sepharose 4B (GE healthcare, Uppsala, Sweden). The chromatography was carried out on 1.6 cm by 200 cm Gelatin Sepharose 4B column at room temperature. The flow rate, pressure, and absorbance at 280 nm were monitored using BioCAD workstation chromatography system. The column was equilibrated with the dialysis buffer (20 mM citrate, 100 mM NaCl, PH 7.4). The sample was applied to the column and washed with a 3 column volume of the dialysis buffer. Absorbed protein was eluted with a step elution of the dialysis buffer containing 6 M urea. Samples were collected and dialyzed against 25 mM Tris-base, 150 mM NaCl, pH 7.5 buffer.

Isolation of γγ and γγ' fibrinogen containing species

Cryoprecipitated pdFI, ammonium sulfate precipitated pdFI, DEAE Sepharose fall through (γγpdFI), and gelatin Sepharose fall through (γγ'pdFI) were resolved into γγ and γγ' fibrinogen subspecies by using a method previously described by Siebenlist [13]. Briefly, FI samples were subfractionated into γ-chain species by ion-exchange chromatography on DEAE Sepharose. The analysis was performed on 27 mm × 205 mm DEAE Sepharose column at room temperature using BioCAD system. Fibrinogen samples were dialyzed against or diluted with buffer A containing 39 mM Tris-Base, 5 mM H_3PO_4, pH 8.55 then loaded into the DEAE Sepharose column equilibrated with the same buffer. After the column was washed with buffer A until the absorbance at 280 nm returned to the base line, bound proteins were eluted with a gradient of buffer A and buffer B containing 500 mM Tris-Base, 500 mM H_3PO_4, pH 4.2. Elution fractions were pooled, dialyzed against dialysis buffer (20 mM sodium citrate, 100 mM NaCl, pH 7.4), and concentrated by ultracentrifugation on Amicon centrifugal filter units.

Results

Isolation and characterization of γγ'pdFI-pdFN complex

Cryoprecipitation, AS precipitation and DEAE chromatography

The SDS-PAGE gel electrophoresis analysis of plasma FI isolated by cryoprecipitation followed by ammonium sulfate precipitation is shown in Figure 2.2. Cryoprecipitated FI under reduced condition (lane 4) reveals three distinct bands with apparent molecular weights of ~67, 54, 47 kDa corresponding to the well-established α, β, and γ chains of FI. In addition, the same lane exhibits a minor high molecular weight band of ~220 kDa characteristic of FN monomer. Ammonium sulfate precipitated FI under reduced condition (lane 5) show similar pattern as cryoprecipitated fibrinogen. However, the primary difference is that the ammonium sulfate precipitated FI contains higher ratio of FN to FI subunits than cryoprecipitated FI. FN is not detectable in the human fibrinogen standard purchased from Enzyme Research.

Ammonium sulfate precipitated FI was applied to a column of DEAE Sepharose at 25℃ and pH 7.4. After washing with dialysis buffer until absorbance at 280 nm returned to the baseline, absorbed protein was eluted with a linear gradient of 0.1 M to 1 M NaCl. The results are depicted in Figure 2.3. The absorbance profile exhibited two major peaks. The first large peak of absorbance corresponds to the stepwise flow through region while the relatively small but symmetrical peak represents the gradient elution region.

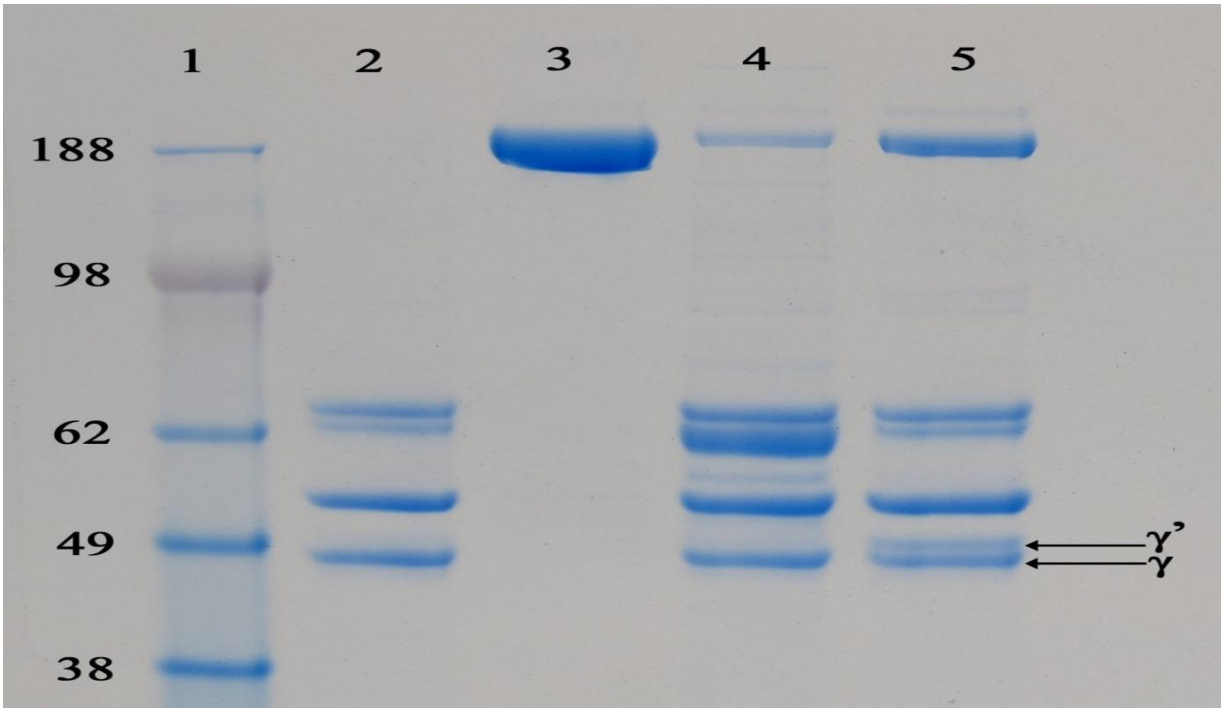

Figure 2.2 Gel electrophoresis evaluation of plasma fibrinogen purified by cryoprecipitation and ammounium sulfate precipitation. Samples were analyzed under reducing condition on 4-12% SDS-PAGE and stained with colloidal blue. Lane 1: molecular weight marker; lane 2: pdFI (reference); lane 3: pdFN (reference); lane 4: cryoprecipitated pdFI; lane 5: ammonium sulfate precipitated pdFI.

The SDS-PAGE analysis of ammonium sulfate precipitated fibrinogen fractionation on DEAE Sepharose is shown in Figure 2.4. It is clear from the figure that the majority of the pdFI in the starting material was not absorbed at pH 7.4 by the DEAE Sepharose resin. The DEAE Sepharose fall through under reduced condition is devoid of fibronectin and shows only the three peptide chains α, β, and γ of fibrinogen. Sample eluted from DEAE Sepharose under reducing condition revealed the three subunits of fibrinogen in addition to a high molecular weight band corresponding to the fibronectin. The staining intensities of these bands and their co-elution indicate a 1:1 stoichiometric ratio of fibrinogen-fibronectin complex as well as fibrinogen γ and

γ’ chains. Based on BCA protein assay, the bound fraction represented ~10 percent of the starting material.

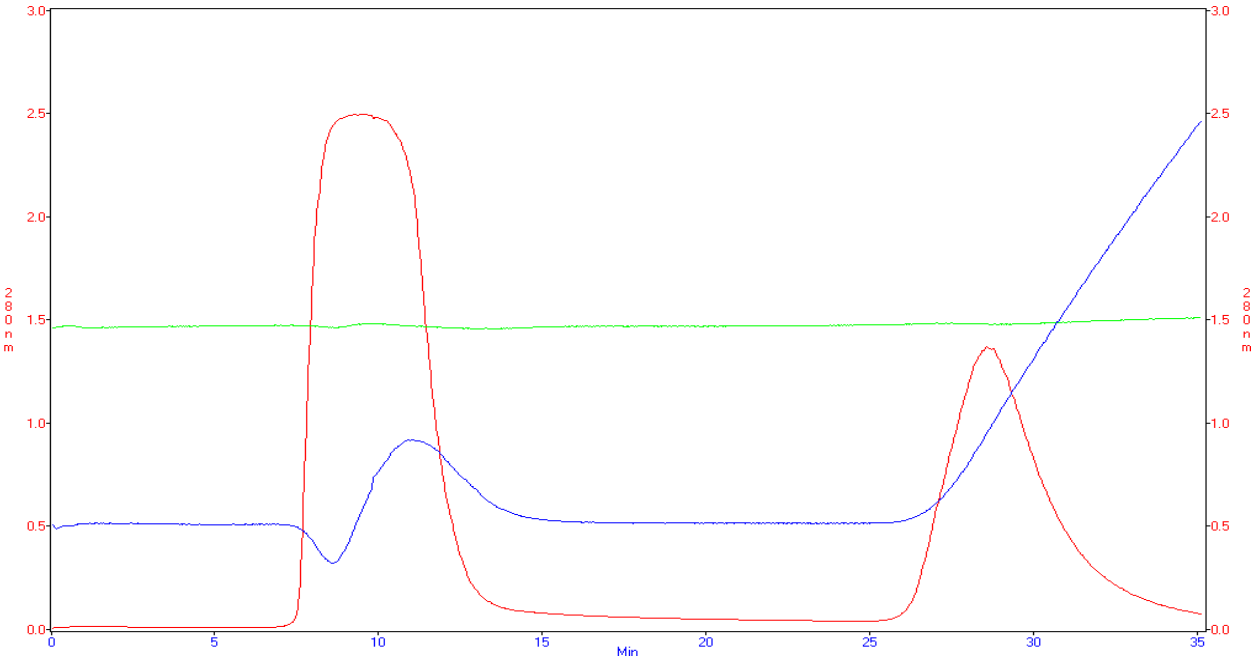

Figure 2.3 Fractionation of ammonium sulfate precipitated pdFI on DEAE Sepharose chromatography. Chromatography was performed in 2.7 cm by 20 cm DEAE Sepharose column. The broad peak represents the material not retained by the column while the small symmetrical peak represents the eluted material. Absorbance at 280 nm (red line), conductivity (blue line), and pH (green line) were monitored with the BioCAD system.

The isolated complex was analyzed under non-denaturing condition on 3-12% native gel. Results are shown in Figure 2.5. Both the isolated complex and mixtures of FN with FI species migrated as two bands. The upper band corresponds to the FN molecule, while the lower band represents FI species. Both FI and FN components of the isolated complex migrated slightly slower than the corresponding individual proteins. These data suggest that the molecule is noncovalent in nature.

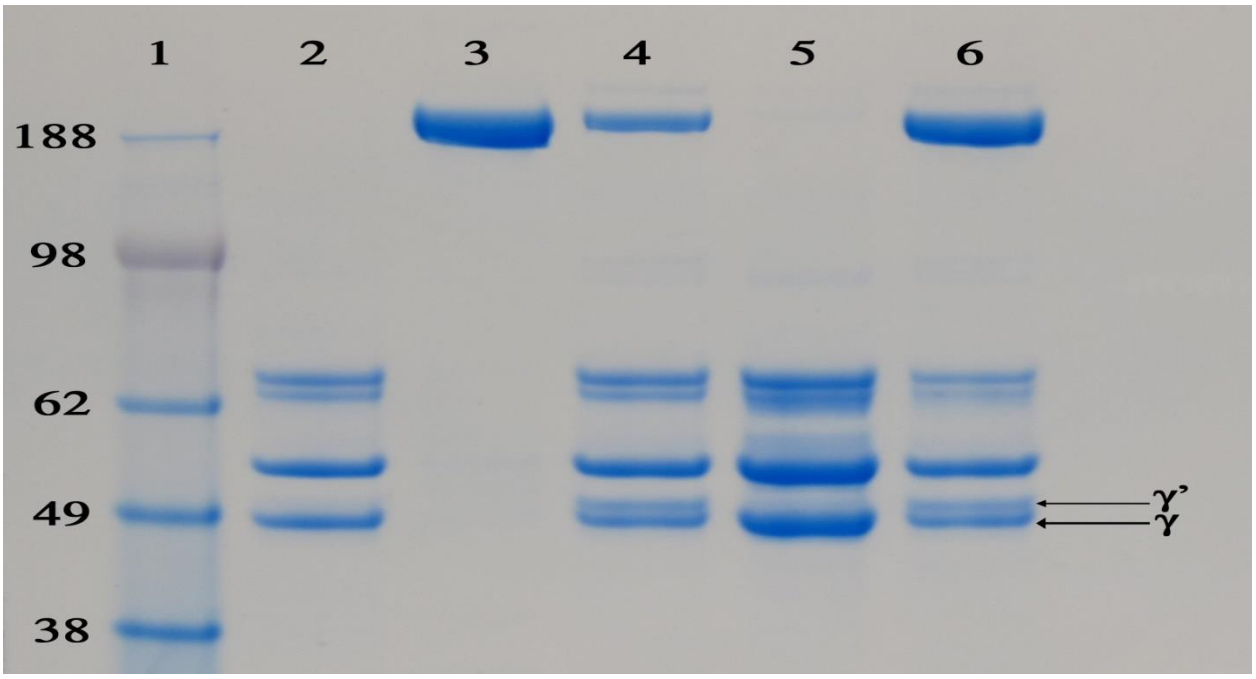

Figure 2.4 Gel electrophoresis evaluation of plasma fibrinogen-fibronectin complex purified by DEAE Sepharose chromatography. Samples were analyzed under reducing condition on 4-12% SDS-PAGE and stained with colloidal blue. Lane 1: molecular weight marker; lane 2: pdFI (reference); lane 3: pdFN (reference); lane 4: ammonium sulfate precipitated FI (loading sample); lane 5: DEAE fall through; lane 6: DEAE elution product (γγ'pdFI-pdFN complex).

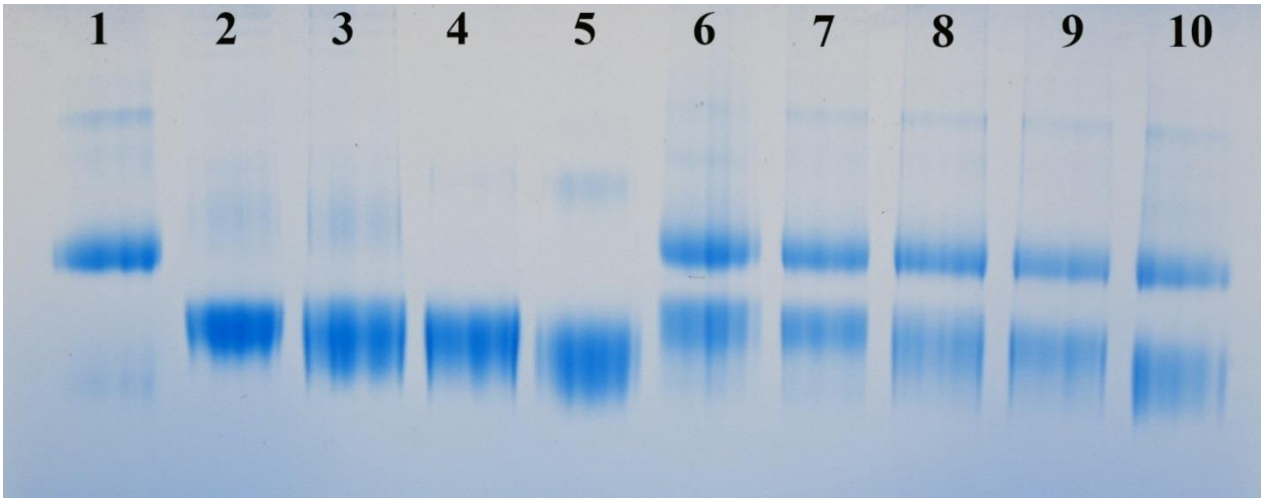

Figure 2.5 Native gel electrophoresis analysis of γγ'pdFI-pdFN complex. Samples were analyzed under native condition on 3-12% NativePAGE and stained with colloidal blue. Lane 1: pdFN; lane 2: γγpdFI; lane 3: γγ'pdFI; lane 4: γγrFI; lane 5: γγ'rFI; lane 6: γγ'pdFI-pdFN; lane 7: a mixture of γγpdFI and pdFN; lane 8: a mixture of γγ'pdFI and pdFN; lane 9: a mixture of γγrFI and pdFN; lane 10: a mixture of γγ'rFI and pdFN.

Cryoprecipitated FI, ammonium sulfate precipitated FI, and the isolated complex were subjected to immunoblot analysis on Western blots. Results are shown in figures 2.6 and 2.7. Anti-fibrinogen blot (Figure 2.6 panel A) confirmed the identity of bands corresponding to the α, β, and γ-chains of fibrinogen detected with SDS-PAGE analysis. The identity of FN bands was confirmed by an anti-fibronectin blot (Figure 2.6 panel B) which also showed that the isolated complex contained a higher percentage of FN than cryoprecipitated and ammonium sulfate precipitated FI. This indicates that the ammonium sulfate precipitation and DEAE chromatography steps enriched the amount of FN in the final product. Anti-fibrinogen α-chain (Figure 2.7 panel A) and anti-fibrinogen β-chain (Figure 2.7 panel B) revealed that these chains are intact in the three samples. Anti-fibrinogen γ-chain, which is able to cross-react with γ'-chain, revealed that the γ' content is higher in the isolated complex compared to the other two products.

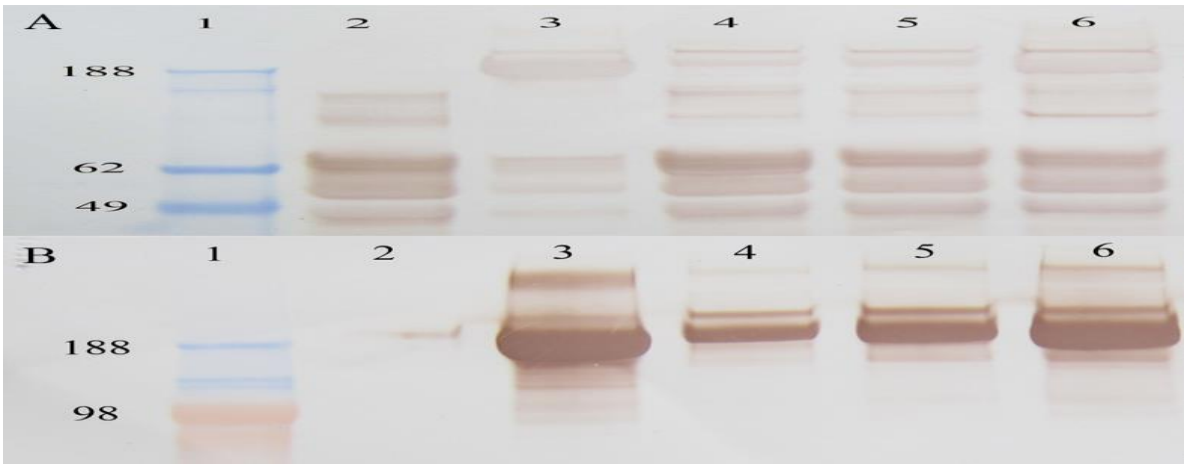

Figure 2.6 Anti-fibrinogen (A) and anti-fibronectin (B) western blot analyses of γγ'pdFI-pdFN complex. Reduced samples were analyzed in 4-12% SDS-PAGE and electrophoretically transferred to PVDF membrane. Blots were developed as described in the material methods. Lane 1: molecular weight marker; lane 2: pdFI (reference); lane 3: pdFN (reference); lane 4: cryoprecipitated pdFI; lane 5: ammonium sulfate precipitated pdFI; lane 6: γγ'pdFI-pdFN complex.

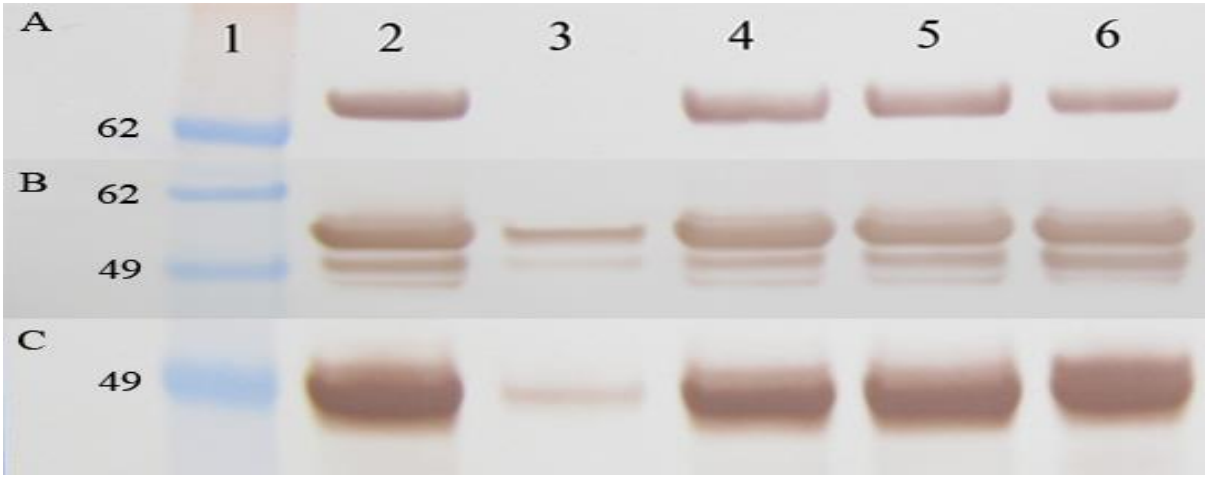

Figure 2.7 Anti-fibrinogen alpha chain (A), anti-fibrinogen beta chain (B), and anti-fibrinogen gamma chain (c) Western Blot analyses of γγ'pdFI-pdFN complex. Reduced samples were analyzed in 4-12% SDS-PAGE and electrophoretically transferred to PVDF membrane. Blots were developed as described in the material methods. Lane 1: molecular weight marker; lane 2: pdFI (reference); lane 3: pdFN (reference); lane 4: cryoprecipitated pdFI; lane 5: ammonium sulfate precipitated pdFI; lane 6: γγ'pdFI-pdFN complex.

Gelatin Sepharose chromatography

Additional experiments were conducted to determine whether the native complex can be isolated by affinity chromatography on gelatin Sepharose. The re-suspended ammonium sulfate precipitated FI was applied to a column of gelatin Sepharose. The gel electrophoresis profile of ammonium sulfate precipitated fibrinogen loaded into gelatin Sepharose is shown in Figure 2.8. Reduced 4-12% SDS-PAGE showed that the loading sample (lane 4) consist of the high molecular weight fibronectin and fibrinogen subunits. The flow through (lane 5) contains fibrinogen subunits and depleted of fibronectin. Fibronectin has been retained by the column due to its high binding affinity for collagen. The 6 M urea eluted fractions (lanes 8-10) contain fibrinogen-fibronectin complexes. Although, the ratio of fibrinogen to fibronectin in these complexes does not exhibit the same stoichiometry as DEAE eluate, there is association of fibrinogen with fibronectin. This dissociation of the complex by adsorption on gelatin Sepharose indicates that it's noncovalent in nature. Due to its high affinity for gelatin, FN was retained by the column whereas FI fell through. This is in agreement with Engvall and Ruoslahti studies showing that the FI can be separated from FN using this chromatography [14]. Separate studies have demonstrated that the incorporation of FN into blood clot is completely inhibited by gelatin [15], indicating that gelatin and FI share the same binding site in FN or more likely that the two binding sites are located next to each other. In contrast, the 1:1 FI-FN complex from pathological plasma described by Nagamatsu at el was isolated by the affinity of FN on this column.

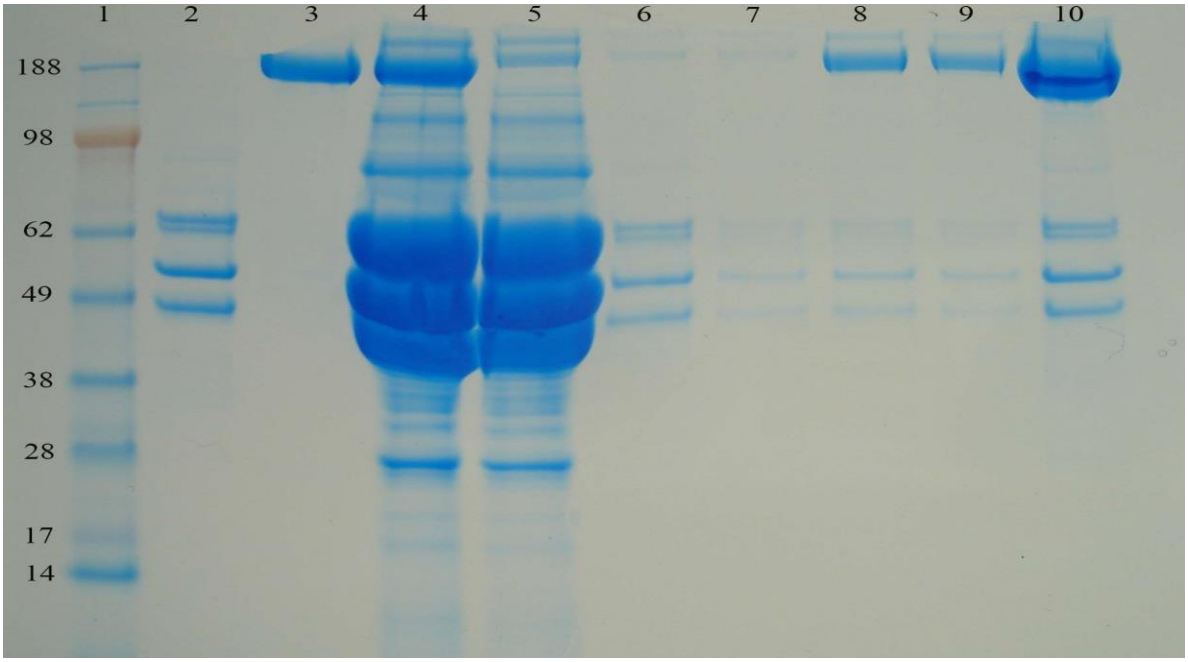

Figure 2.8 Fractionation of ammonium sulfate precipitated fibrinogen on gelatin Sepharose chromatography. Samples were electrophoresed under reduced condition on 4-12% SDS-PAGE then stained with colloidal blue. Lane 1: molecular weight marker; lane 2: pdFI (reference); lane 3: pdFN (reference); lane 4: loading sample (cryoprecipitated pdFI); lane 5: fall through; lane 6: wash; lanes 7 through 10: elution fractions.

Dissociation of γγ'pdFI-pdFN complex by affinity Chromatography

The γγ'pdFI-pdFN complex was disrupted by affinity chromatography on gelatin Sepharose. Sample of γγ'pdFI-pdFN complex was applied to gelatin Sepharose column at room temperature and washed with TEC buffer containing 1 M NaCl until absorbance reached baseline. Protein retained by the column was eluted with stepwise of TEC buffer containing 6 M urea. The chromatographic analysis is shown in Figure 2.9. The broad large peak of absorbance is the flow through region, while the small symmetrical peak of absorbance is the gradient elution.

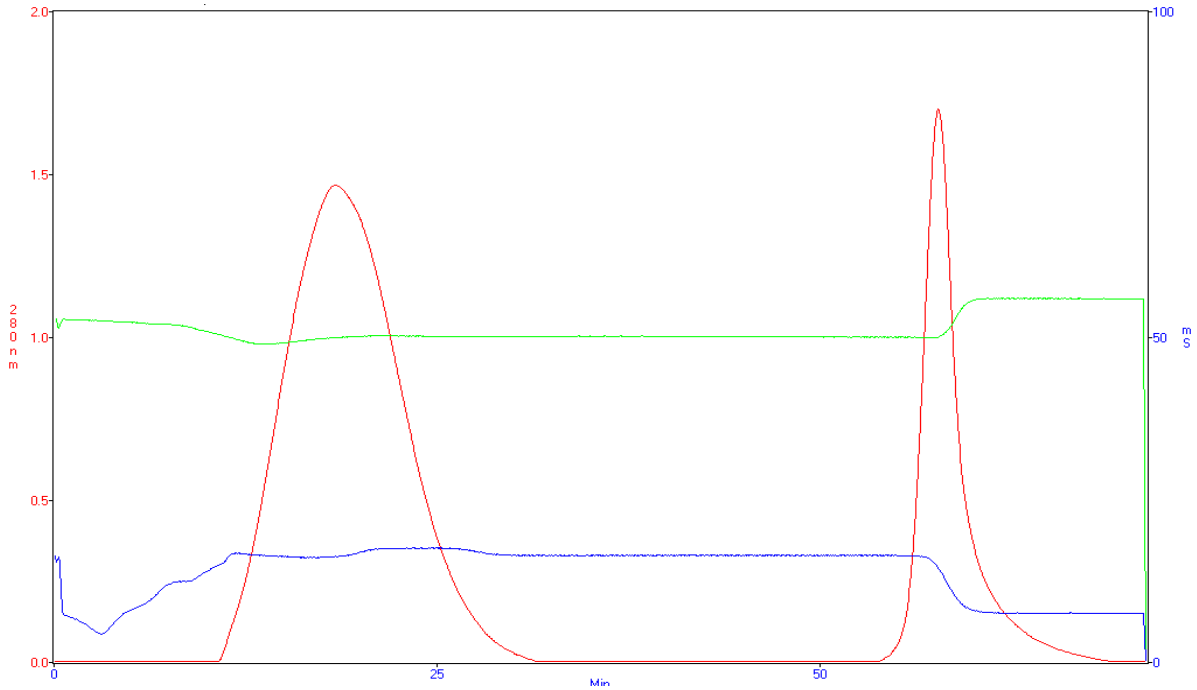

Figure 2.9 Disruption of γγ'pdFI-pdFN complex by affinity chromatography on gelatin Sepharose. Chromatographic analysis was performed on a gelatin Sepharose column (1.6 cm by 10 cm) at room temp. First peak: gelatin Sepharose fall through and wash fractions; second peak: gelatin Sepharose elution fractions. Absorbance at 280 nm (red line), conductivity (blue line), and pH (green line) were monitored with the BioCAD system.

The SDS-PAGE gel electrophoresis analysis of the purification products is shown in Figure 2.10. The loading sample (lane 4) consists primarily of FN and FI subunits. The flow through (lane 5) is devoid of fibronectin because of the high binding affinity it exhibits towards gelatin. The gelatin Sepharose elution product is shown in lane 6. It's depleted of fibrinogen species indicating that the high binding affinity of FN for gelatin Sepharose may displace a large portion of FN associated with FI.

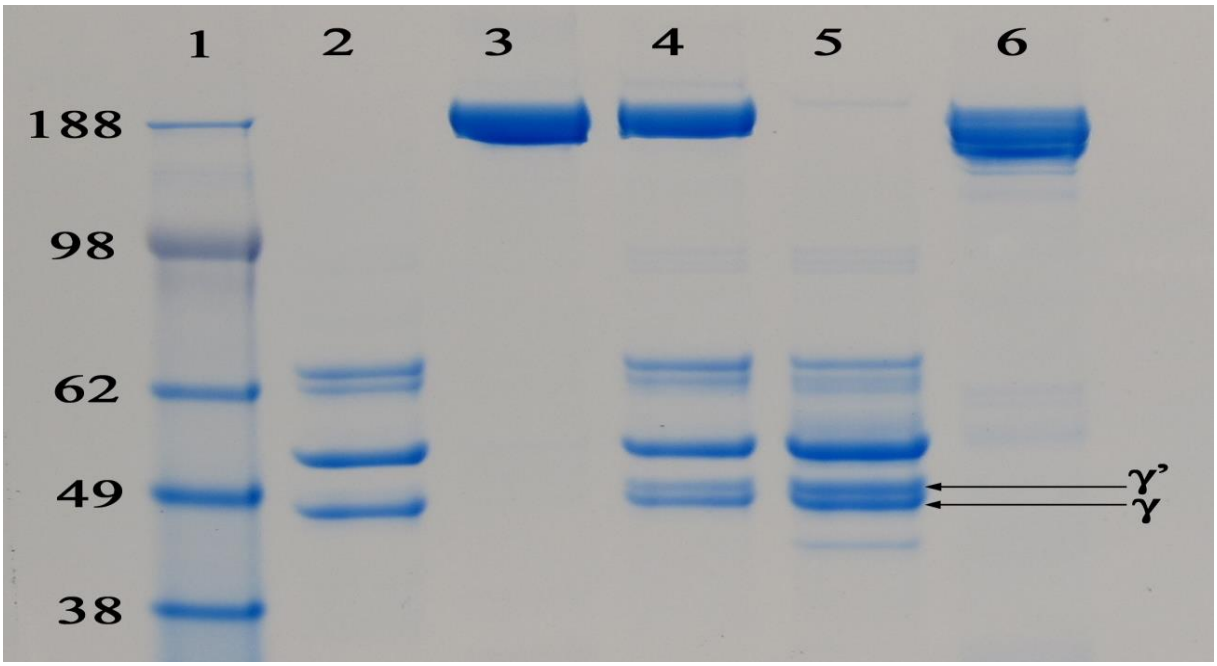

Figure 2.10 Gel electrophoresis evaluation of disrupting plasma γγ'pdFI-pdFN complex on gelatin Sepharose chromatography. Samples were analyzed under reducing condition on 4-12% SDS-PAGE and stained with colloidal blue. Lane 1: molecular weight marker; lane 2: pdFI (reference); lane 3: pdFN (reference); lane 4: γγ'pdFI-pdFN complex; lane 5: gelatin Sepharose fall through (γγ'pdFI); lane 6: gelatin Sepharose elution product (pdFN).

Isolation of γγ and γγ' fibrinogen containing species

Plasma FI, flow through from the DEAE step, and flow through from the gelatin Sepharose run of the DEAE bound material were subjected to the DEAE chromatography conditions described by Siebenlist et al. The results are shown in Figure 2.11. Plasma FI (panel A) was resolved into two peaks, a dominant sharp peak followed by smaller one. SDS-PAGE gel electrophoresis analysis (Figure 2.12) revealed that the first peak consist off the γγpdFI subspecies while the second peak contain the γγ'pdFI subspecies. The flow through of the first DEAE Sepharose exhibited two peaks, predominate peak followed by a faint one. SDS-PAGE analysis showed that both peaks contain exclusively γγpdFI subspecies. The flow through of the

gelatin Sepharose revealed smaller peak that eluted much later and consist of the γγ'pdFI subspecies. This results clearly demonstrate that the pdFI bound to pdFN at room temperature is composed of the γγ'pdFI subspecies.

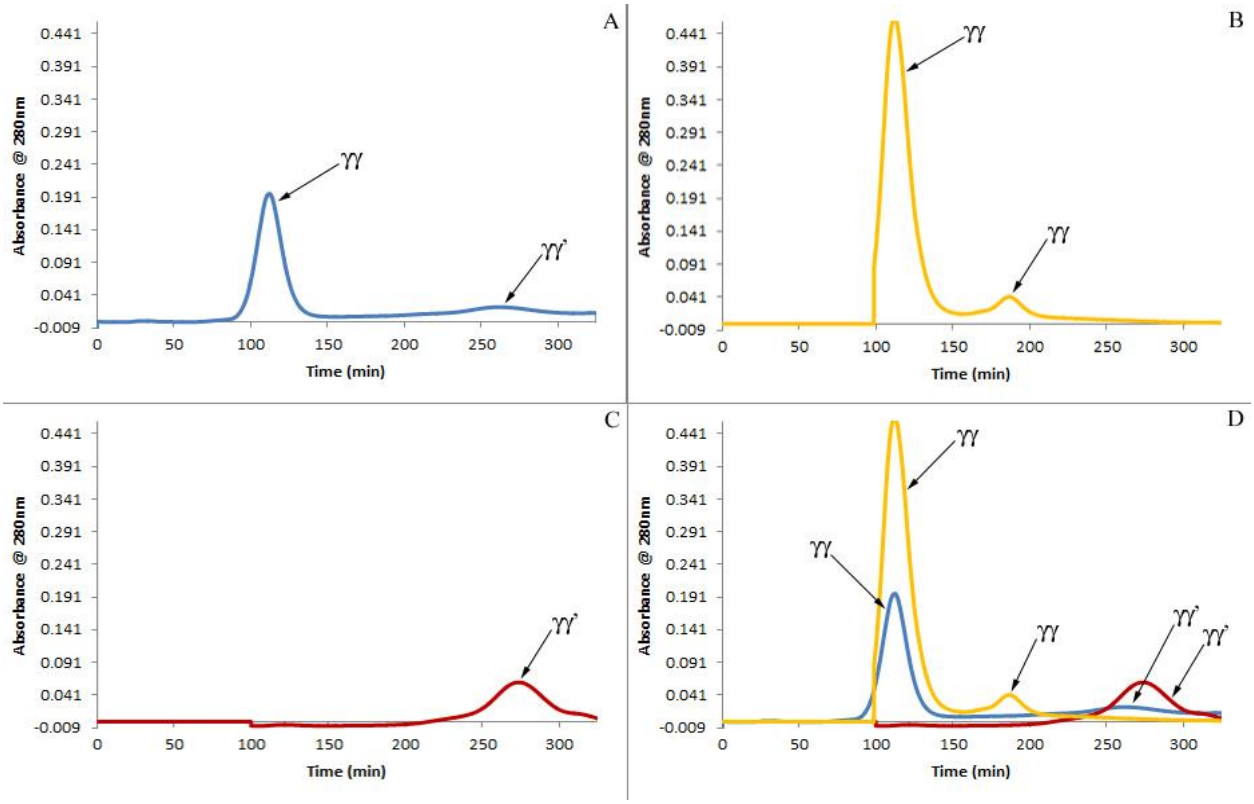

Figure 2.11 Isolation of γγ and γγ'fibrinogen subspecies by DEAE Sepharose chromatography. Samples were fractionated on 27 mm × 205 mm DEAE Sepharose column using a gradient elution of buffer A and B at room temp. Absorbance at 280 nm (red line), conductivity (blue line), and pH (green line) were monitored with the BioCAD system. Panel A: pdFI (Enzyme Research); panel B: pdFI flow through from the first DEAE column; panel C: pdFI flow through from the gelatin Sepharose; panel D: composite.

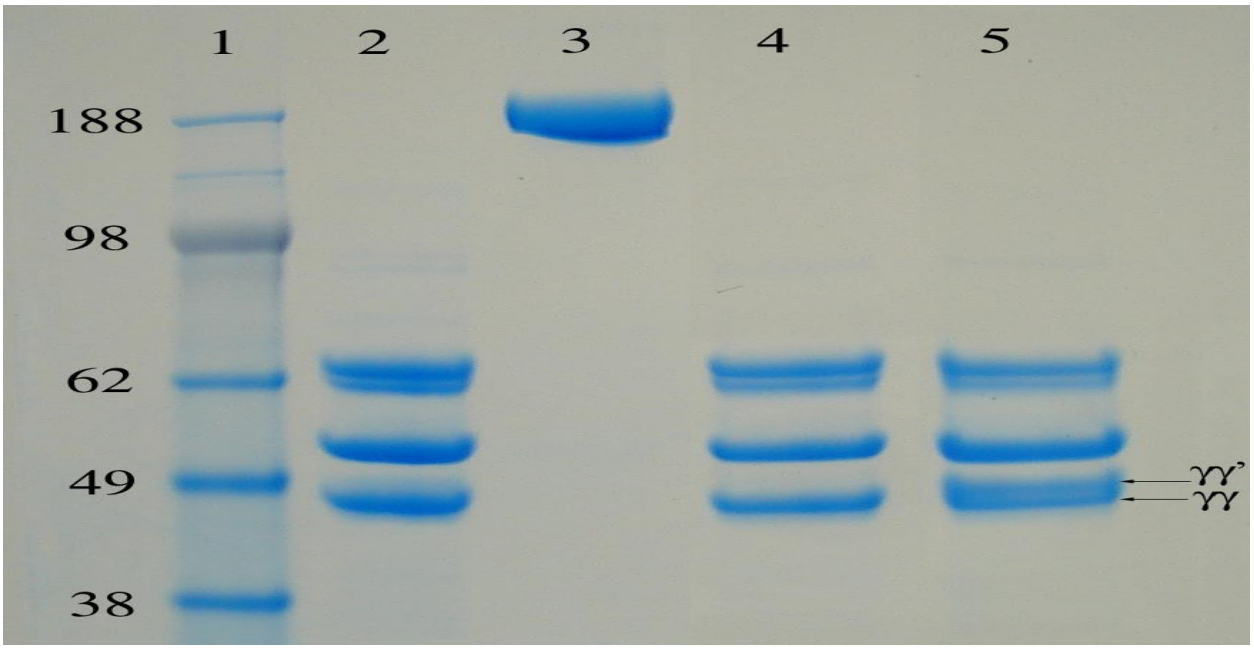

Figure 2.12 Gel electrophoresis analysis of γγ and γγ' fibrinogen subpopulation resolved by DEAE Sepharose. Samples were analyzed under reducing condition on 4-12% SDS-PAGE and stained with colloidal blue. Lane 1: molecular weight marker; lane 2: pdFI (reference); lane 3: pdFN (reference); lane 4: original DEAE Sepharose fall through (γγpdFI); lane 5: gelatin Sepharose fall through (γγ'pdFI).

Discussion

The present investigation is in contrast with earlier studies that shown complexes of fibrinogen and fibronectin exist only in the plasma of patient with inflammatory and infectious diseases. We have demonstrated that a 1:1 fibrinogen-fibronectin complex can be purified from normal human plasma of healthy individual using a sequence of cryoprecipitation, ammonium sulfate precipitation, and anion-exchange chromatography on DEAE Sepharose. The second DEAE analysis of the gelatin Sepharose fall through demonstrated that the FI component of the complex is composed exclusively of the γγ' heterodimer.

The ammonium sulfate precipitated FI contained higher percentage of fibronectin compared to cryoprecipitate or commercial FI preparations. This result is not completely novel in that Bar [16] reported that different methods of FI isolation differ in their fibronectin content. However, it was of interest that the ammonium sulfate isolation done at room temperature yielded the higher fibronectin content relative to the cryoprecipitate isolation which was done at 4^{o}C. Ammonium sulfate is known to be a relatively gentle precipitation method capable of preserving the integrity of protein-protein complexes [17]. The result indicates the presence of a room temperature stable complex of fibrinogen and fibronectin. Our studies also show that even the relatively low ratio of fibronectin to fibrinogen in the ammonium sulfate fractionated material is able to prevent aggregation/precipitation of the fibrinogen when at a high concentration at 4^{o} C.

When the ammonium sulfate fraction was applied to DEAE Sepharose in an attempt to remove solvent detergent, ~10% of the applied protein bound the column. The flow through contained the majority of the FI and was depleted of FN. The eluate contained a mixture of FI and FN in what appeared to be a 1:1 stoichiometric ratio. This result indicates that the FI associated with the DEAE resin may be due to its interaction with FN. To our knowledge, this is the first report of binding of fibrinogen as opposed to fibrin from normal human plasma to fibronectin at room temperature.

The gamma prime hetero-dimeric subpopulation of fibrinogen (γγ'FI) has several unique functional attributes arising from its 25 additional amino acids on the carboxyl terminal domain of the gamma chain [18]. The γγ'pdFI constitutes about 10 % of the total fibrinogen. Importantly, it also exhibits a much stronger anionic exchange adsorption behavior due to two more sulfation sites than the γγFI which represents the remaining 90% of the total FI. For example, using DEAE

chromatography of fibrinogen loaded at pH 8.55 and an elution gradient to pH 4.2, Siebenlist et al were able to resolve fibrinogen consisting of the γ chain from that containing the alternative splice variant γ' [13]. They went on to show that factor XIII binding was restricted to the subpopulation of fibrinogen containing the splice variant. The study also demonstrates the importance of using a relatively high pH to achieve binding of the majority of a fibrinogen sample to DEAE. However, the conditions used here, allowed us to detect and isolate the apparent fibrinogen- fibronectin complex. It is possible that there is also a subset of fibrinogen that is capable of binding fibronectin at room temperature.

The fibrinogen used in the studies of Makogonenko et al was obtained from Enzyme Research. Although the method of purification is not provided by the supplier, they do specify that it is devoid of fibronectin. That component of fibrinogen capable of binding fibronectin at room temperature could have been removed during purification. This possibility is supported by our observation that when this material was subjected to gelatin-Sepharose chromatography, there was no detectable fibrinogen or fibronectin bound to the column (data not shown).

The interaction of fibrinogen with fibronectin was confirmed by gelatin Sepharose chromatography. The re-suspended ammonium sulfate precipitate was applied to the affinity resin. The flow through was depleted of fibronectin and contained the majority of the FI. The eluate contained what appeared to be a sub- stoichiometric ratio of FI to fibronectin but did contain FI. The fact that the stoichiometry of FI to FN was reduced in the gelatin binding fraction relative to what was observed with the DEAE may be due to competition between the gelatin and fibrinogen for binding sites on fibronectin. The displacement of pdFI by gelatin suggested that FI binding site in FN is either located close to or the same as that for gelatin. Indeed, examining the structure of FN reveals that both FI and gelatin binding sites are located in close proximity to

each other. There are 5 so called F1 structural repeats in the amino terminal region and another 3 in the carboxyl terminal region of fibronectin. These two regions are thought to be the fibrin binding domains with the major fibrin binding region located in the amino terminal domain. Rostagno showed that it was repeats 4 and 5 in the amino terminal region that were responsible for binding [19]. These are immediately adjacent to the collagen/gelatin binding domain of fibronectin.

References

1. Stathakis, N.E. and M.W. Mosesson, *Interactions among heparin, cold-insoluble globulin, and fibrinogen in formation of the heparin-precipitable fraction of plasma.* J Clin Invest, 1977. **60**(4): p. 855-65.
2. Gil, G.C., W.H. Velander, and K.E. Van Cott, *Analysis of the N-glycans of recombinant human Factor IX purified from transgenic pig milk.* Glycobiology, 2008. **18**(7): p. 526-39.
3. Smith, R.T. and R.W. v. Korff, *A heparin-precipitable fraction of human plasma. I. Isolation and characterization of the fraction.* J. Clin. Invest., 1957. **36**: p. 596-604.
4. Smith, R.T., *A heparin-precipitable fraction of human plasma. II. Occurrence and significance of the fraction in normal individuals and in various disease states.* J Clin Invest, 1957. **36**(4): p. 605-16.
5. Fyrand, O. and N.O. Solum, *Heparin precipitable fraction (HPF) from dermatological patients. II. Studies on the non-clottable proteins. Identification of cold insoluble globulin as the main non-clottable component.* Thromb Res, 1976. **8**(5): p. 659-72.
6. Matsuda, M., T. Saida, and R. Hasegawa, *Cryofibrinogen in the plasma of patients with skin ulcerative lesions on the legs: a complex of fibrinogen and cold insoluble globulin.* Thromb Res, 1976. **9**(6): p. 541-52.
7. Stathakis, N.E., et al., *Cryoprecipitation of fibrin-fibrinogen complexes induced by the cold-insoluble globulin of plasma.* Blood, 1978. **51**(6): p. 1211-22.
8. Makogonenko, E., et al., *Interaction of fibrin(ogen) with fibronectin: further characterization and localization of the fibronectin-binding site.* Biochemistry, 2002. **41**(25): p. 7907-13.
9. Niewiarowska, J. and C.S. Cierniewski, *Inhibitory effect of fibronectin on the fibrin formation.* Thromb Res, 1982. **27**(5): p. 611-8.
10. Ruoslahti, E. and A. Vaheri, *Interaction of soluble fibroblast surface antigen with fribrinogen and fibrin.* J Exp Med, 1975. **141**(2): p. 497-501.
11. Burnouf-Radosevich, M., T. Burnouf, and J.J. Huart, *Biochemical and physical properties of a solvent-detergent-treated fibrin glue.* Vox Sang, 1990. **58**(2): p. 77-84.
12. Brew, S.A. and K.C. Ingram, *Purification of human plasma fibronectin.* Journal of tissue culture methods. **16**(3): p. 197-199.

13. Siebenlist, K.R., D.A. Meh, and M.W. Mosesson, *Plasma factor XIII binds specifically to fibrinogen molecules containing gamma chains.* Biochemistry, 1996. **35**(32): p. 10448-53.
14. Engvall, E. and E. Ruoslahti, *Binding of soluble form of fibroblast surface protein, fibronectin, to collagen.* Int J Cancer, 1977. **20**(1): p. 1-5.
15. Engvall, E., E. Ruoslahti, and E.J. Miller, *Affinity of fibronectin to collagens of different genetic types and to fibrinogen.* J Exp Med, 1978. **147**(6): p. 1584-95.
16. Bar, L., et al., *The binding of fibrin sealant to collagen is influenced by the method of purification and the cross-linked fibrinogen-fibronectin (heteronectin) content of the 'fibrinogen' component.* Blood Coagul Fibrinolysis, 2005. **16**(2): p. 111-7.
17. Danaie, P., et al., *Isolation of a protein complex containing translation initiation factor Prt1 from Saccharomyces cerevisiae.* J Biol Chem, 1995. **270**(9): p. 4288-92.
18. Mosesson, M.W., *Fibrinogen and fibrin structure and functions.* J. Thromb. Haemostasis, 2005. **3**(8): p. 1894-1904.
19. Rostagno, A.A., J.E. Schwarzbauer, and L.I. Gold, *Comparison of the fibrin-binding activities in the N- and C-termini of fibronectin.* Biochem J, 1999. **338 (Pt 2)**: p. 375-86.

Chapter 3 Characterize the size distribution and hydrodynamic properties of the isolated complex and comparable mixtures of FI and FN

Abstract

In this section, we estimated the molecular distribution and hydrodynamic properties of the isolated γγ'pdFI-pdFN complex utilizing different techniques that include size exclusion chromatography (SEC), dynamic light scattering (DLS), and analytical ultracentrifugation (AUC). The properties of the native complex was compared to that of free FN, unfractionated FI, γγ and γγ' FI subspecies, and equimolar mixtures of FN with FI species. Results from SEC showed that in 200 mM NaCl the complex is a more compact form than FI alone. SEC also revealed that FN interact more strongly with γγ' than γγ FI. The molecular distribution of the complex can be duplicated with a mixture containing an excess molar of γγ'FI with FN.

DLS showed that the native complex was polydisperse molecules when analyzed in high ionic strength and denaturing conditions. At higher ionic strength and chaotropic condition, the complex displayed a larger hydrodynamic radius than the value obtained in lower ionic strength solution. This indicate that the native γγ'pdF-pdFN complex is a more compact form at low ionic strength but adopt and extended conformation in high salt and denaturing conditions. The hydrodynamic properties of the γγ'pdFI-pdFN complex depend on the conformational changes of FN. At physiologic ionic strength and pH, both γγ and γγ' FI appeared as polydisperse molecules with larger hydrodynamic radius. However, the average hydrodynamic radius were decreased when an equimolar amount of FN was added, suggesting that FN interacts with both FI subspecies.

When analyzed on AUC, the native complex displayed two peaks with sedimentation constants corresponding to the individual FI and FN. The sedimentation velocity profiles of the

mixtures of γγpdFI plus pdFN and γγ'pdFI plus pdFN appear to match the profile of the native complex.

Introduction

Very few studies have investigated the hydrodynamic properties of FI-FN complexes from pathological plasma. For example, Matsuda described the properties of cryofibrinogen isolated from the plasma of male patient with leg dermal ulcers. When placed on ice, the cryofibrinogen formed precipitate that readily re-solubilized at 37 °C. Ultracentrifugation showed that the cryofibrinogen dissociated at ambient temperatures to form individual FI and FN components. Amino acid and gel electrophoresis revealed that the cryofibrinogen is a simple complex between normal plasma FI and normal plasma FN. However, quasielastic light scattering and circular dichroism analysis indicate that the cryofibrinogen possesses unique properties that are different from those of normal plasma FI and FN mixtures [1]. Nagamatsu and colleagues used affinity chromatography on gelatin-Sepharose to isolate a 1:1 complex of fibrinogen and fibronectin from plasma of patients with rheumatoid arthritis [2]. This isolated complex exhibited a compact hydrodynamic property as measured by dynamic light scattering.

Here we describe the hydrodynamic properties and size distribution of the native complex and mixtures of FI and FN utilizing techniques that include SEC, DLS, and AUC. DLS studies were performed at 25 °C using a DynaPro Molecular Sizing instrument equipped with an 830 nm laser source (Wyatt, Santa Barbara). Temperature in the MicroSampler is controlled by a Peltier effect heat pump that maintains a temperature with an accuracy of better than 1 °C in the range -4 to 60 °C. The Dynapro instrument consisted of a semiconductor diode light source that emits a laser of ~ 830 nm wave length. Light scattered by the sample is converted by an actively quenched solid State single Photon Counting Module into electrical pulses. Figure 3.1 shows the setup of DynaPro instrument. The translational diffusion coefficient (D) of the molecule is derived from the intensity of the scattered light by a mathematical process known as

autocorrelation. The hydrodynamic radius (R) is derived from the diffusion coefficient using the Stokes-Einstein equation. Data were analyzed using Dynamics V6 software.

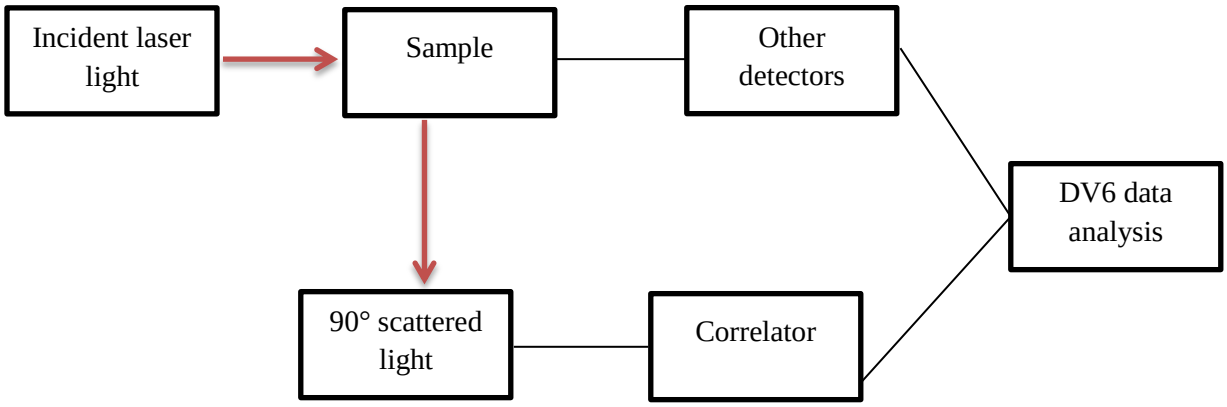

Figure 3.1 Block diagram of DLS instrument

Sedimentation equilibrium and velocity experiments were performed in a Beckman Coulter Proteome Lab XL-1 (Beckman Coulter). The instrument measures the concentration distributions of a protein under high centrifugal forces. The concentration distributions in the ProteomeLab system are determined by a combination of absorbance and interference (refractive) optical systems. The optical system consists of high-intensity xenon flash lamp that emits light in the UV/VIS range from 190 to 800 nm wavelength. The interference optical system contains laser diode light source, imaging optics, and a charge-coupled device detector. The system provides image of the cell by measuring the refractive index difference between sample and reference at the radial position. A diffusion pump or turbomolecular pump in series with a mechanical vacuum pump is used to reduce chamber pressure to below 5 microns. A solid state thermoelectric refrigeration and heating system is used to control the operating temperature in the range 0 to 40 °C with an accuracy of ± 0.3 or ± 0.5 °C.

Methods

Size Exclusion Chromatography

The molecular size distribution of the isolated γγ‘pdFI-pdFN complex was determined by SEC at room temperature. The analysis was performed on Knauer high pressure liquid chromatography (HPLC) system (Advance Scientific Instruments, Berlin, Germany) consisted of Knauer pump equipped with a sample injection valve, Conductivity meter, Smartline UV detector 2600, and fraction collector. ChromGate V3.1.7 Knauer Instrument Control Software was used to set and control pressure, flow for pump, wavelength for detector, and monitor these in real-time. Plasma γγ and γγ’ FI subspecies, FN, and the purified γγ‘pdFI-pdFN complex were exchanged into SEC buffer containing 20 mM sodium citrate, 200 mM NaCl, pH 7.0 and filtered through 0.22 μm Nylon filter. 180 μg of each sample was subjected individually to 10 mm × 300 mm Superose 6 column (GE Healthcare, Uppsala, Sweden) equilibrated with SEC buffer. The flow rate was set at 0.5 ml/min for 60 min run duration and absorbance was monitored at 280 nm. 1 min fractions were collected and analyzed by SDS-PAGE, Western blotting, and DLS. EZChrom Elite software was used to analyze the data.

DLS

SEC was used to prepare plasma derived fibrinogen (Enzyme Research, South Bend, IN), pdFN, and the purified γγ’pdFI-pdFN complex. Elutes from Superose 6 column were pooled and exchanged into different buffers that include100 mM NaCl, 150 mM NaCl, 1 M NaCl, and 6 M urea. To eliminate any potential contaminants such as dust and impurities, all samples were first

filtered through 0.22 µm Nylon membrane filter (VWR International, Radnor, PA) then through 0.02 µm disposable syringe membrane filter (Whatman, Florham, NJ).

The structure and molecular size of γγ‘pdFI-pdFN complex was determined by DLS using Protein Solutions DynaPro99 Titan with Temperature Controlled MicroSampler (Wyatt Technology Corp, Santa Barbara CA). Measurements were done at constant temperature of 25 °C. Samples were analyzed under different concentrations (1 to 5 mg/ml) and solvent conditions. 20 µl of protein sample was transferred to the DynaPro cell and inserted in the sample chamber. A further dilution was carried out if the protein sample aggregated or precipitated. A total of 20 acquisitions of 10 seconds long were obtained for each measurement. Samples were analyzed in triplicate and the scattering parameters values were averaged. Data gathered by the DynaPro Titan instrument was analyzed using Dynamics software to determine the hydrodynamic properties.

Analytical Ultracentrifugation

Sedimentation velocity

Individual proteins (γγ‘pdFI, pdFN), protein mixtures (γγ‘pdFI + pdFN) and a purified native complex (γγ‘pdFI-pdFN) were analyzed by sedimentation velocity experiments performed on an Optima XL-I analytical ultracentrifuge (Beckman coulter, Inc.) equipped with an eight-hole An50Ti rotor. Prior to analysis, proteins were dialyzed against 50 mM tris containing 150 mM NaCl, 1.1 mM $CaCl_2$, 0.6 $MgCl_2$, pH 7.5. The individual proteins and protein mixtures (400 µl) were loaded into the sample compartment of a double-sector cell. The reference compartment was filled with 430 µl of the dialysate buffer. Sample cells were then incubated at 20 ^{o}C in the rotor chamber for 2 h under vacuum. After 2 h of incubation, samples were sedimented at 35,000

rpm. A total of 250 absorbance scans (280 nm) at 3.5 min intervals were collected. Absorbance values ranged from 0.5-0.7 for the different samples. The data were analyzed by SEDFIT version 10.58d (PMID: 10692345) using the continuous *c*(*s*) distribution model and allowing the frictional ratio to float.

Sedimentation equilibrium

The oligomeric state of individual proteins (γγ‘pdFI, pdFN), protein mixtures (γγ‘pdFI + pdFN) and a purified native complex (γγ‘pdFI-pdFN) were determined at 20°C by sedimentation equilibrium using an Optima XL-I analytical ultracentrifuge (Beckman Coulter, Inc.). Proteins were dialyzed into 20 mM sodium citrate (pH 7.4) containing 100 mM NaCl. The sample cells were loaded with 110 µl of each protein (0.5 mg/ml concentrations), and reference cells were filled with the dialysis buffer. Radial scans were collected at 280 nm after 22 h at rotor speeds of 3,000, 4,000, 6,000, and 8,000 rpm. Data from the three different rotor speeds were fit by global analysis to an equation describing a single species model using Origin 6.0. Partial specific volumes of 0.7235 and 0.7281 were calculated by SedTerp for FN and γγ‘FI, respectively, and were used for the best-fit analysis. The solvent density of the buffer was calculated to be 1.0039 g/ml.

Statistical analysis

Data of repeated measurements were expressed as mean and standard deviation. Differences in hydrodynamic radius were analyzed by one-way Analysis of variance (ANOVA) using the software GraphPad Prims, version 5.0 (GraphPad Software, San Diego, CA). P values lower than 0.05 were considered to indicate statistical significance.

Results

SEC

The structure and molecular mass of the native γγ'pdFI-pdFN complex was determined by size exclusion chromatography at room temperature. 180 µg of purified samples of γγpdFI, γγ'pdFI, pdFN, and γγ'pdFI-pdFN complex were subjected individually to Superose 6 column in 200 mM NaCl citrate-buffered saline, pH 7.0. Figure 3.2 shows the elution profile of the three samples. Free γγ and γγ' pdFI were eluted as sharp peaks centered at 21.4 and 21.5 min, respectively whereas FN eluted later as a broad peak centered at 23.5 min. The earlier elution of FI variants, despite their smaller molecular weight, indicates a more linear conformation whereas FN molecules appear to adopt a more compact conformation. This agrees with previous investigations that have shown, at physiologic pH and salt condition, FN is more globular structure whereas FI tend to be more linear. Studies have shown that FN molecule is only partially extended in 200 mM NaCl in the absence of glycerol [3-5]. Therefore, the compact FN molecules are more flexible and penetrate pores of the gel more than the linear FI. It's known that elongated protein can elute at a position twice the molecular weight of a globular protein [6].

Similar to γγ and γγ'pdFI, the native complex eluted as sharp peak centered at 21.6 min with minor tailing peak that partially separated from the major form centered at 24.5 min. This indicates that at this physiologic pH and near physiologic ionic strength, the complex is a more compact form than the linear FI species.

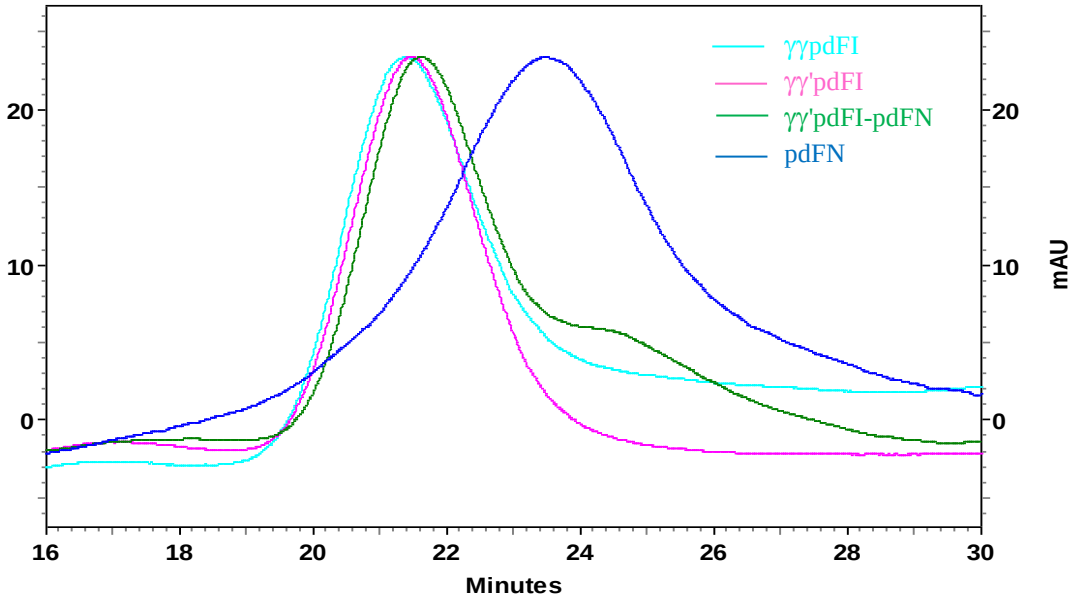

Figure 3.2 size exclusion chromatography of pdFN, isolated complex, γγ and γγ' pdFI species. Samples were chromatographed at room temperature on a Superose-6 column at 0.5 ml/min in citrate-buffered saline, pH 7.0.

We also employed SEC to study the interactions of FN with plasma unfractionated FI, γγFI, and γγ'FI subspecies. The interactions were carried out in citrate-buffered saline at room temperature. A dose response curves was created by holding the mole of FN constant while varying the mole of γγ'FI. Samples of FN and γγ'FI were incubated in a rotating mixer for 2 hours then loaded to the Superose 6 column. Figure 3.3 shows the elution profile of mixtures of γγ'FI and FN from Superose 6 column using 200 mM NaCl step elution in 20 mM sodium citrate, pH 7.0. The elution of mixtures of γγ'pdFI and pdFN, at constant level of FN, were shifted towards the void volume and FN peak started to disappear when the percentage of γγ'FI in the mixture was increased. This disappearance of FN peak was proportional to the concentration of γγ'FI added. At lower level of γγ'FI (0.25, 0.5, and 1 molar ratio) the mixture showed two peaks with elution time similar to free γγ'FI and FN. When the molar ratio of γγ'FI

was increased above 1, the FN peak disappeared and the mixture eluted as a single peak suggesting that the two molecules interact to form complexes. The higher molecular weight complexes did not elute earlier (shift to the left) than the uncomplexed FI species, suggesting that the two molecules were folded into a compact structure.

The interaction of γγpdFI with pdFN was monitored by holding the level of FN constant while varying the amount of γγpdFI. Results are displayed in Figure 3.4. All mixtures exhibited two peaks with elution times corresponding to the values of free γγFI and FN. In the 1.5:1 γγFI:FN mixture, the majority of protein eluted at 21.7 min and the rest eluted as a broad tailing peak only partially separated from the predominant form. The FN peak was not completely disappeared even when the amount of γγFI was doubled. This suggests that FN dose not interact or interact differently with γγFI at room temp.

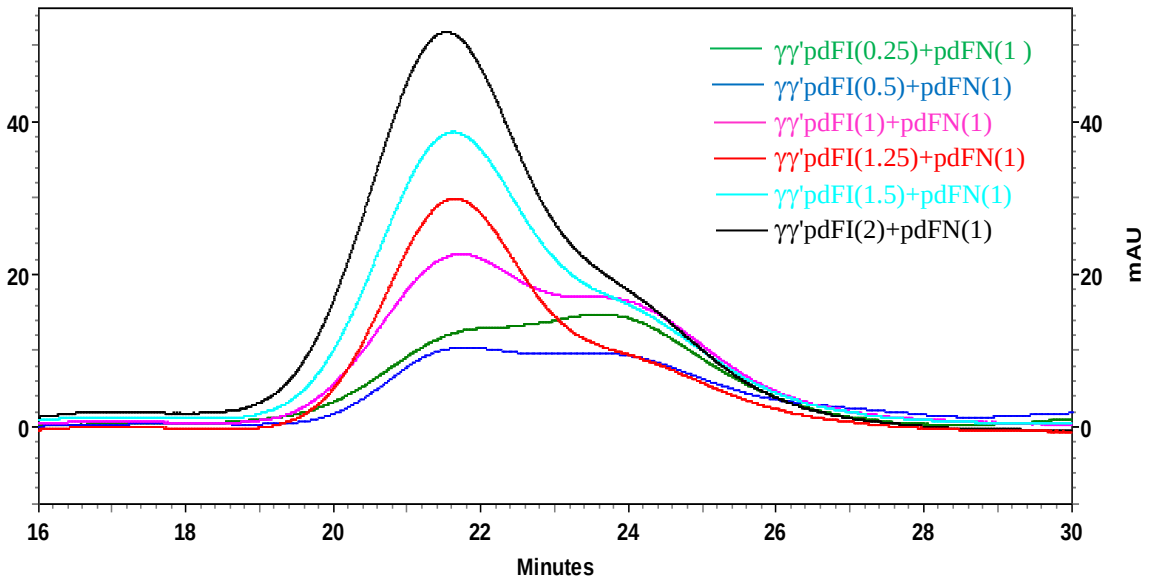

Figure 3.3 Size exclusion chromatography of a mixture of γγ'pdFI and pdFN. Samples were chromatographed at room temperature on a Superose-6 column at 0.5 ml/min in citrate-buffered saline, pH 7.0.

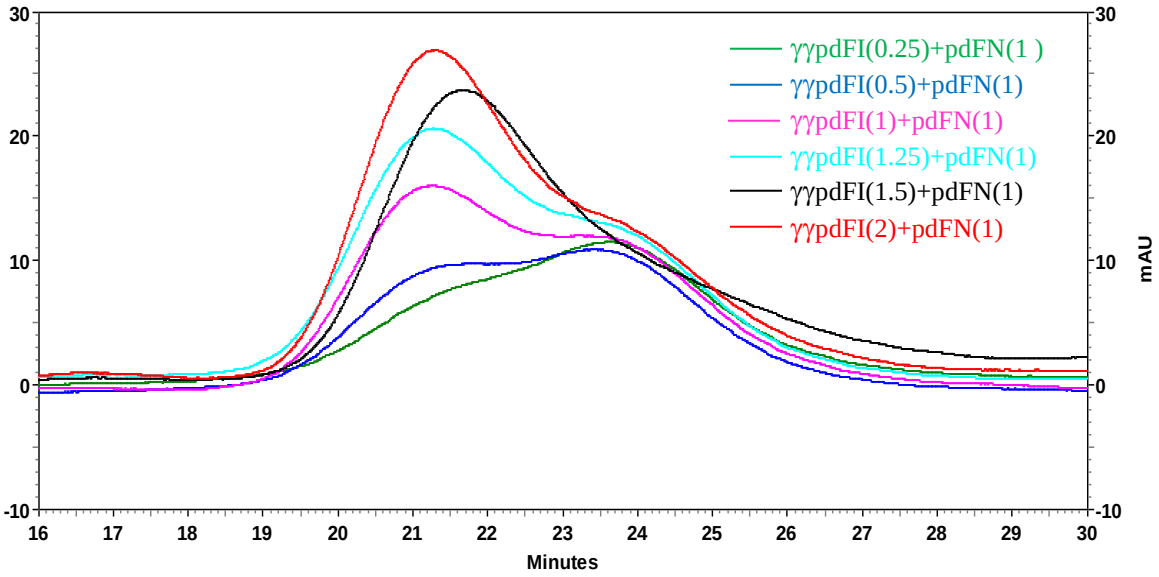

Figure 3.4 Size exclusion chromatography of a mixture of γγpdFI and pdFN. Samples were chromatographed at room temperature on a Superose-6 column at 0.5 ml/min in citrate-buffered saline, pH 7.0.

Dynamic light scattering

We employed DLS to analyze the molecular sizes of native γγ'pdFI-pdFN complex under different buffer and solvent conditions that include (1) 100 mM NaCl, (2) 150 mM NaCl, (3) 1 M NaCl, and (4) 6 M urea. DLS experiments were done using a Protein Solutions DynaPro99 Titan with Temperature Controlled MicroSampler at a constant temperature of 25℃. Proteins molecular weight and polydispersity estimations were calculated from data collected by the DynaPro Titan instrument using Dynamics software. The histogram from the regularization fit of the autocorrelation function graph shows the size distribution of the molecules at the different conditions. The polydispersity index provides a direct measure of the heterogeneity of each molecular species in sample. A polydispersity index below 20% means that the molecular species is monodisperse, otherwise it is heterogeneous.

The intensity and molecular distributions of the pdFN and γγ'pdFI-pdFN complex are presented Figure 3.5 and Table 3.1. The size distribution histogram shows that in the presence of 100 mM NaCl, γγ'pdFI-pdFN complex appeared as a prominent peak with an average hydrodynamic radius of 8.6 ± 0.24 nm and intensity distribution of 94.5%. The polydispersity of 23.9 ± 5.9% shows that the molecule is slightly polydisperse. Small population of large aggregates with a high molecular weight was also detected. Similar to the native complex, pdFI appeared slightly polydisperse but with larger hydrodynamic radius of 17.4 ± 0.4 nm. FN analyzed under similar condition appeared monodisperse (10.9 ± 5.7%) with a hydrodynamic radius of 9.5 ± 0.3 nm. This value is in agreement with the previous DLS data in which a hydrodynamic radius of 8.7 ± 0.2 nm was shown for FN in aqueous solution [7] and 8.6 ± 0.3 nm radius of gyration was shown for FN in physiological saline solution [8]. In addition, radius of gyration of 8.9 ± 0.3 nm and 9.5 ± 0.5 were obtained for FN from small-angle X-ray scattering and small-angle neutron scattering techniques respectively [9].

When salt concentration was increased to 1 M NaCl, pdFN and γγ'pdFI-pdFN complex molecules appeared larger than when 100 mM NaCl solution was used. The intensity and size distributions are shown in Figure 3.6 and Table 3.2. The average hydrodynamic radius increased to 11.1 ± 0.6 nm for the native complex and 13 ± 0.4 nm for pdFN. This indicates that exposing both molecules to the high-ionic strength buffer of 1 M NaCl caused them to undergo a conformational change from the compact structure to the more extended form. In contrast, the hydrodynamic radius of pdFI (17.4 ± 0.4 nm) was not affected by increasing the salt concentration. The measured hydrodynamic radius of pdFI is within experimental error to the value of 12 nm reported by Wasilewska [10] for pdFI in pH 9.5 solution. It's known that FI exists as a compact structure under the high ionic strength and in the extended conformation at

low ionic strength [10]. The three proteins appeared slightly polydisperse in this high salt environment.

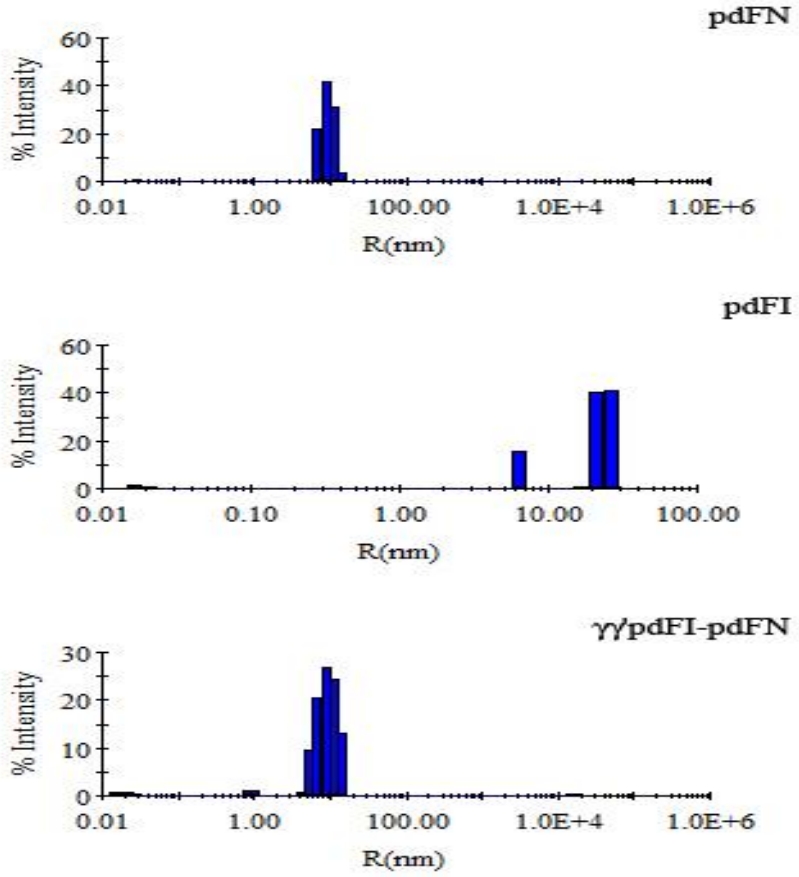

Figure 3.5 Size distribution of pdFN and γγ'pdFI-pdFN complex. Analysis was determined by DLS at 25℃ in 100 mM NaCl solution, pH 7.4.

Table 3.1 DLS parameters of pdFN, pdFI, and γγ'pdFI-pdFN complex analyzed in 100 mM NaCl.

Item	Hydrodynamic Radius (nm)	Polydispersity (%)	Molecular weight estimate (kDa)	Intensity distribution (%)
pdFN	9.5 ± 0.3	10.9 ± 5.7	648 ± 48	98.1
pdFI	17.4 ± 0.4	23.4 ± 0.6	2699 ± 137	81.9
γγ'pdFI-pdFN	8.6 ± 0.24	23.9 ± 5.9	514 ± 33	94.5

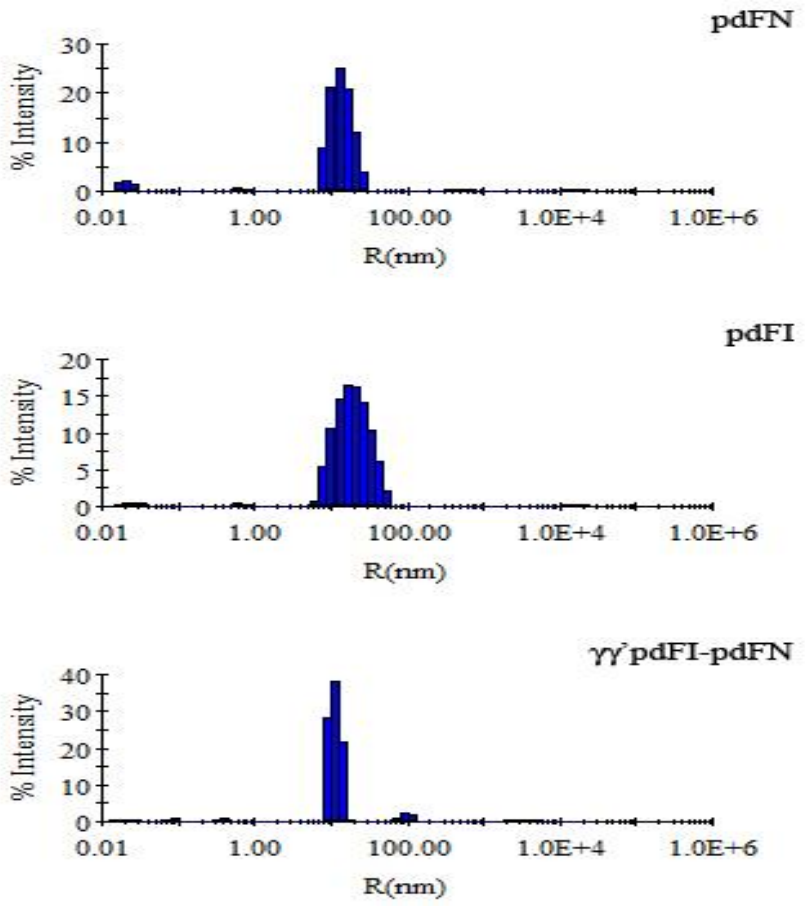

Figure 3.6 Size distribution of pdFN, pdFI, and γγ'pdFI-pdFN complex. Measurement was done by at 25℃ in 1 M NaCl citrate-buffered solution, pH 7.4.

Table 3.2 DLS parameters of pdFN, pdFI, and γγ'pdFI-pdFN complex analyzed in 1 M NaCl.

Item	Hydrodynamic Radius (nm)	Polydispersity (%)	Molecular weight estimate (kDa)	Intensity distribution (%)
pdFN	13 ± 0.4	22.1 ± 2.4	1451 ± 91	91.5
pdFI	17.4 ± 0.4	23.6 ± 0.3	2680 ± 130	93.4
γγ'pdFI-pdFN	11.1 ± 0.6	25.8 ± 5.6	953 ± 118	88.3

The intensity and mass distributions of pdFI, pdFN, and γγ'pdFI-pdFN complex molecules analyzed in 6 M urea solution are shown in Figure 3.7 and Table 3.3. Compared to the size distribution seen in 1 M NaCl, both pdFN and pdFI appeared as more monodisperse while the native complex is slightly polydisperse. Both pdFN and the isolated complex appeared larger than when analyzed in 100 nm and 1 M NaCl solutions. The hydrodynamic radius was increased to 14.4 ± 0.3 nm for pdFN and 12.5 ± 0.6 nm for the isolated complex. This indicates that both proteins extend even more to the more linear conformation in this denaturing condition of 6 M urea. Our data is consistent with previous studies that showed FN converts to the linear polymer when exposed to a denaturing condition. Pelta demonstrated that the hydrodynamic radius of FN increased by a factor of 1.6 when analyzed in 8 M urea compared to the native physiologic condition [11]. pdFI showed a smaller hydrodynamic radius than the value observed in 100 mM and 1 M NaCl solutions.

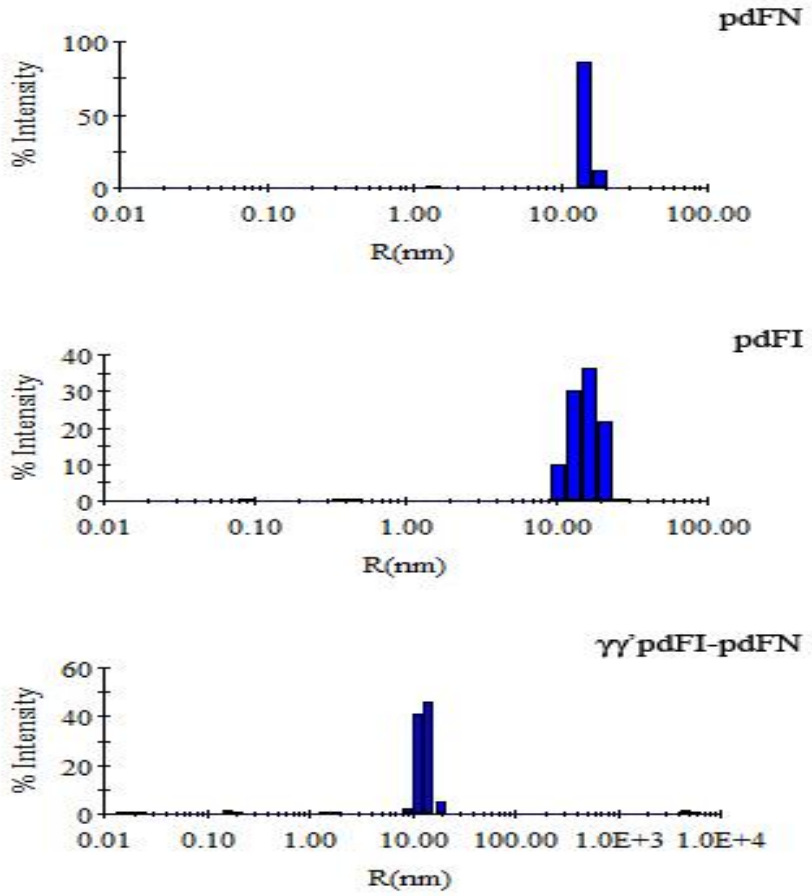

Figure 3.7 Size distributions of pdFN, pdFI, and γγ'pdFI-pdFN complex. Samples were analyzed by DLS at 25℃ in 6 M urea solution, pH 7.4.

Table 3.3 DLS parameters of pdFN, pdFI, and γγ'pdFN-pdFN complex analyzed in 6 M Urea.

Item	Hydrodynamic Radius (nm)	Polydispersity (%)	Molecular weight estimate (kDa)	Intensity distribution (%)
pdFN	14.4 ± 0.3	16.5 ± 3.6	1728 ± 85	97.7
pdFI	14.2 ± 0.2	15.2 ± 2.5	1681 ± 47	98.1
γγ'pdFI-pdFN	12.5 ± 0.6	23.5 ± 6.8	1237 ± 141	93.5

We also employed DLS to monitor the interactions of FN with γγ and γγ' FI subspecies in a buffer containing 50 mM Tris, 1.1 mM $CaCl_2$, 0.6 mM $MgCl_2$, and 150 mM NaCl. Results are displayed in Figure 3.8 and Table 3.4. FN exhibited a polydisperse distribution with a smaller hydrodynamic radius of 10.3 ± 0.3 nm. On the other hand, both γγ and γγ' FI subspecies showed a polydispersity distribution and larger hydrodynamic radius, 16.2 ± 0.5 nm and 17.1 ± 0.4 nm respectively, than the FN. The native complex appeared less polydisperse molecules than when analyzed in 100 mM NaCl and harsh conditions of 1 M NaCl and 6 M urea. The average hydrodynamic radius was 12.1 ± 0.2 nm, similar to the value obtained in 6 M Urea. The change in size distribution could be due to the presence of the calcium and magnesium in the buffer.

Interestingly, the addition of FN to γγ and γγ' FI decreased the hydrodynamic radius of both FI species. An equimolar mixture of pdFN and γγpFI showed an average hydrodynamic radius of 13.7 ± 0.9 nm and polydispersity distribution similar to that of free γγpdFI. An equimolar mixture of pdFN and γγ'pdFI displayed an average hydrodynamic radius of 13.0 ± 0.4 nm and polydispersity distribution similar to that of free γγ'pdFI. These results indicate that FN interacts with both γγ and γγ'. The reductions in hydrodynamic radius of both mixtures suggest that the two molecules are interacting to create a more compact product. This can be visualized as the more linear FI molecules folding around the globular FN.

The hydrodynamic radius of γγ'pdFI-pdFN complex is similar to the published value for FI. At physiological pH and ionic strength of 0.15 M, the hydrodynamic radius of FI was 12.7 nm [10]. However, the values obtained for γγpdFI and γγ'pdFI are much higher.

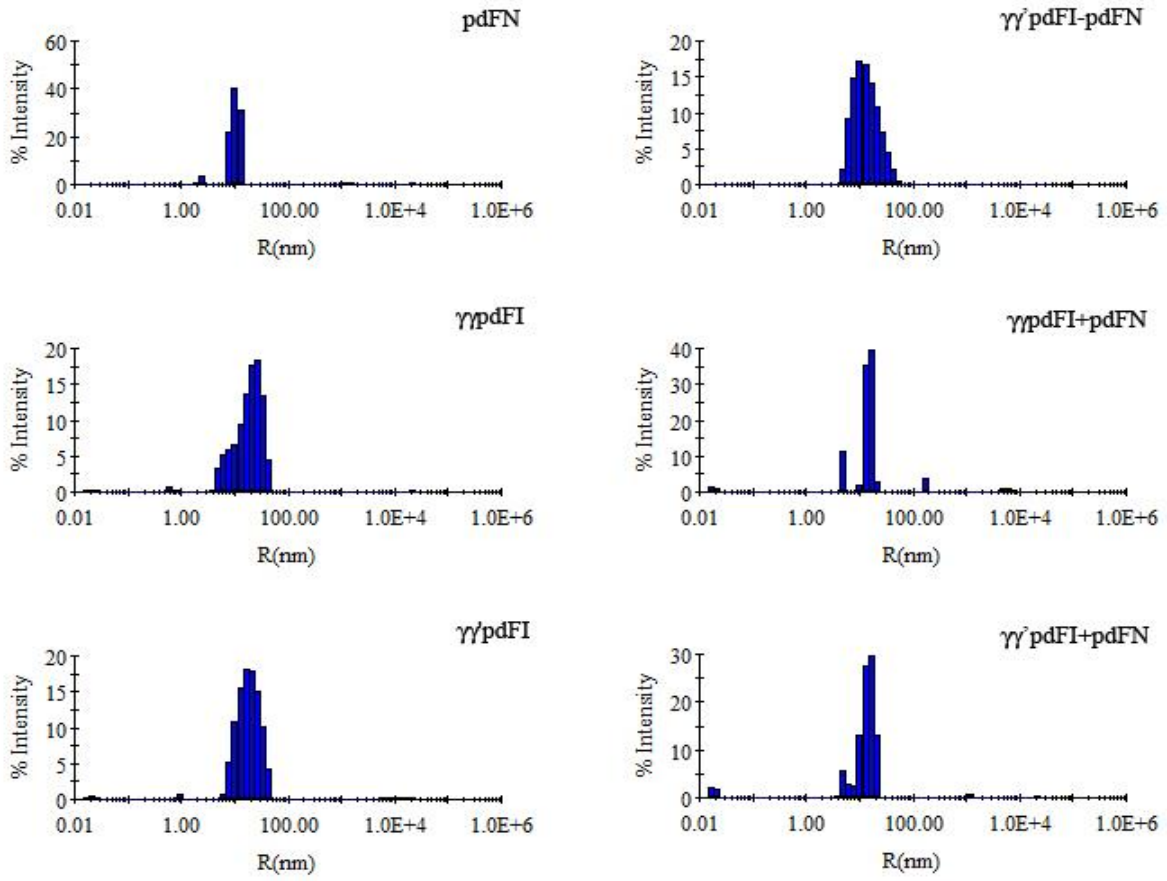

Figure 3.8 Size distributions of pdFN, γγpdFI, γγ'pdFI, γγ'pdFI-pdFN complex, and mixtures of pdFN with γγpdFI and γγ'pdFI. Measurements were performed by DLS at 25℃ in 150 mM NaCl tris-buffered solution containing physiological calcium and magnesium and pH 7.4.

Table 3.4 DLS parameters of pdFN, γγpdFI, γγ'pdFI, γγ'pdFI-pdFN complex, and mixtures of pdFN with γγpdFI and γγ'pdFI species analyzed in 150 mM NaCl.

Item	Hydrodynamic Radius (nm)	Polydispersity (%)	Molecular weight estimate (kDa)	Intensity distribution (%)
pdFN	10.3 ±0.3	22.5 ± 2.2	786 ± 63	92.8
γγpdFI	16.2 ± 0.5	28.4 ± 4.8	2268 ± 167	98.1
γγ'pdFI	17.1 ± 0.4	23 ± 1.3	2599 ± 145	97.1
γγpdFI+pdFN	13.7 ± 0.9	29 ± 12.2	1541 ± 240	79.9
γγ'pdFI+pdFN	13.0 ±0.4	21.2 ± 1.6	1368 ± 99	83.4
γγ'pdFI-pdFN	12.1 ± 0.2	20.2 ± 2	1150 ± 54	99.5

Analytical Ultracentrifugation

Sedimentation velocity

The sedimentation coefficients of pdFN, γγ'pdFI, γγ'pdFI-pdFN complex, and an equimolar mixture of γγ'pdFI and pdFN were measured by sedimentation velocity experiment at 35,000 rpm. In these experiments, the sedimentation coefficient distributions of the proteins were monitored. The sedimentation coefficients and frictional ratios were calculated from the fitted data. FN exhibited a single dominant peak with sedimentation coefficient of 13 S and molecular weight of 545 kDa (Figure 3.9). The calculated molecular value is higher than the value of 450 kDa estimated from mobility in sodium dodcylsulfate gel electrophoresis. This difference in molecular weight value from our experiments may reflect ionic strength differences in the buffer. The S value is consistent with the established sedimentation constant of FN which is in the range 12-14 S at physiological pH and salt [3, 12-14]. However, at higher pH and salt concentration, FN adopt an extended conformation that sediment at 6-8 S [3, 4, 15]. The frictional ratio was high, 1.85, a value that characteristic of the extended length of FN. This value falls within the reported 1.7 frictional coefficient of FN [16]. The γγ'pdFI showed a sharp dominant peak at 7.7 S and molecular weight of 229 kDa less than the established molecular weight of FI (Figure 3.10). A minor peak at 11.2 S with molecular weight of 402 kDa was also seen indicating the presence of some aggregate. The calculated frictional ratio was 1.8. The S(20, w) value is similar to the reported value of unfractionated plasma FI (7-8S) [17].

The native γγ'pdFI-pdFN complex exhibited two major peaks with characteristics similar to the individual FI and FN molecules (Figure 3.11). The faster sedimenting peak has an S (20, w) value of 7.8 and molecular weight of 237 kDa, while the second peak had a higher

sedimentation coefficient of 13.7 S and molecular weight of 545 kDa. A faint peak trailing the first and leading the second major two peaks was seen with an S (20, w) value of 10.6 and molecular weight of 376 kDa. The overall frictional coefficient of the complex was 1.82. This agrees with Matsuda et al who showed that the FI and FN component of cryofibrinogen dissociated from each other when analyzed by ultracentrifugation in 300 mM NaCl solution at 22-24 °C. Matsuda also showed that the FN from cryofibrinogen sedimented at 11.3 S and 12.8 S which are similar to the value we obtained. The sedimentation velocity profiles for equimolar mixtures of γγ'pdFI plus pdFN (Figure 3.12) and γγ pdFI plus pdFN (Figure 3.13) were very similar to that of the native complex. Both mixtures displayed peaks corresponding to the individuals FI and FN molecules. The frictional ratio of a mixture of γγ'pdFI plus pdFN was identical to that of γγ'pdFI and slightly larger than the frictional ratio of a mixture of γγpdFI plus pdFN. Altogether, the sedimentation profiles of the plasma mixtures of fibronectin and fibrinogen subspecies appear to match the profile of the native complex. A component with a sedimentation coefficient beyond that of fibronectin was not observed in the sedimentation velocity experiments.

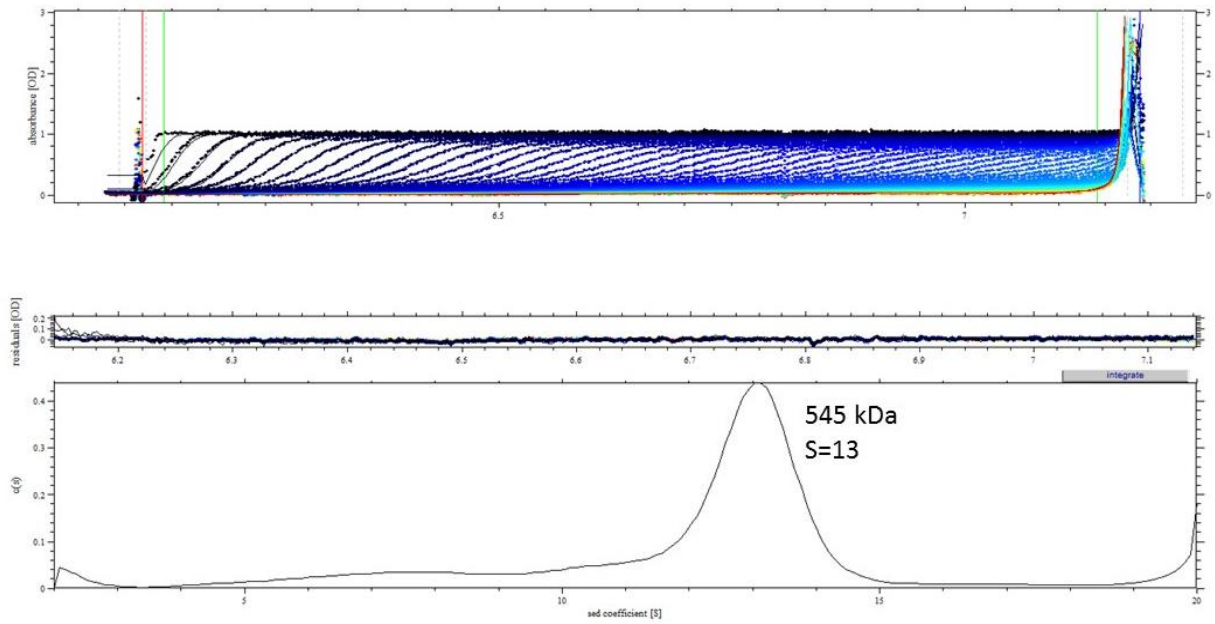

Figure 3.9 Sedimentation velocity data of pdFN. A set of 250 scans were collected at 3.5 min intervals in a Beckman Coulter XL-1 analytical ultracentrifuge using the absorbance optical system. Samples were analyzed at 35,000 rpm and 20 °C in Tris/NaCl buffer, pH 7.5.

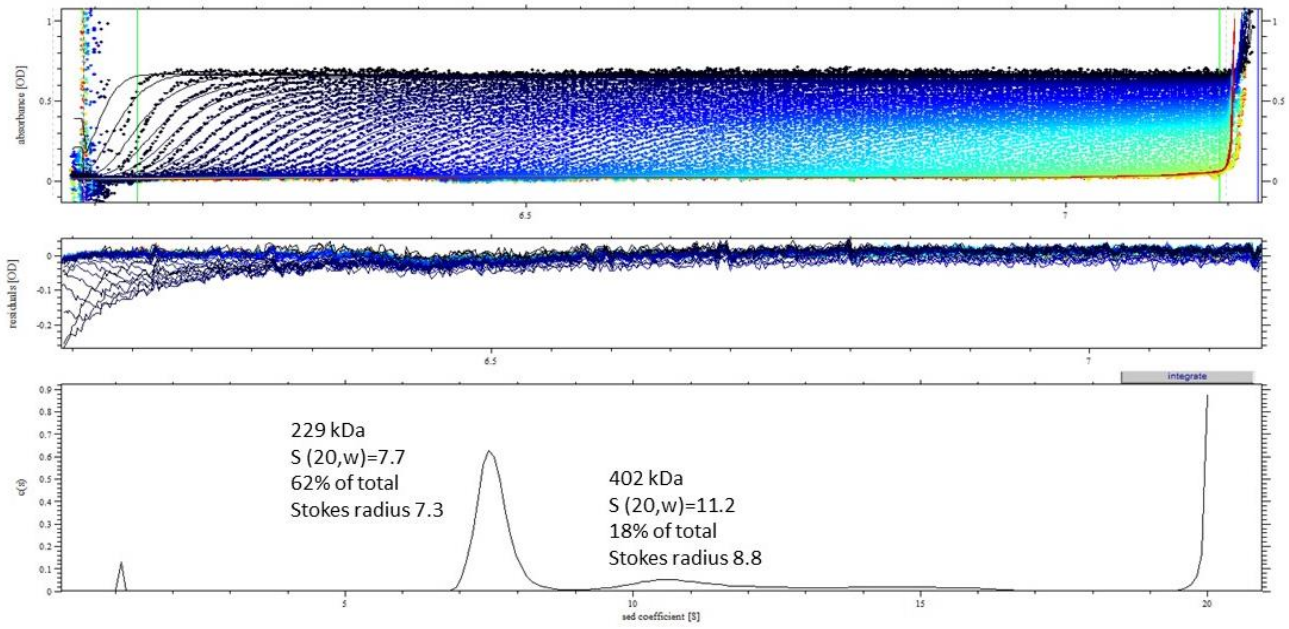

Figure 3.10 Sedimentation velocity data of γγ'pdFI. A set of 250 scans were collected at 3.5 min intervals in a Beckman Coulter XL-1 analytical ultracentrifuge using the absorbance optical system. Analysis was performed at 35,000 rpm and 20 °C in Tris/NaCl buffer, pH 7.5.

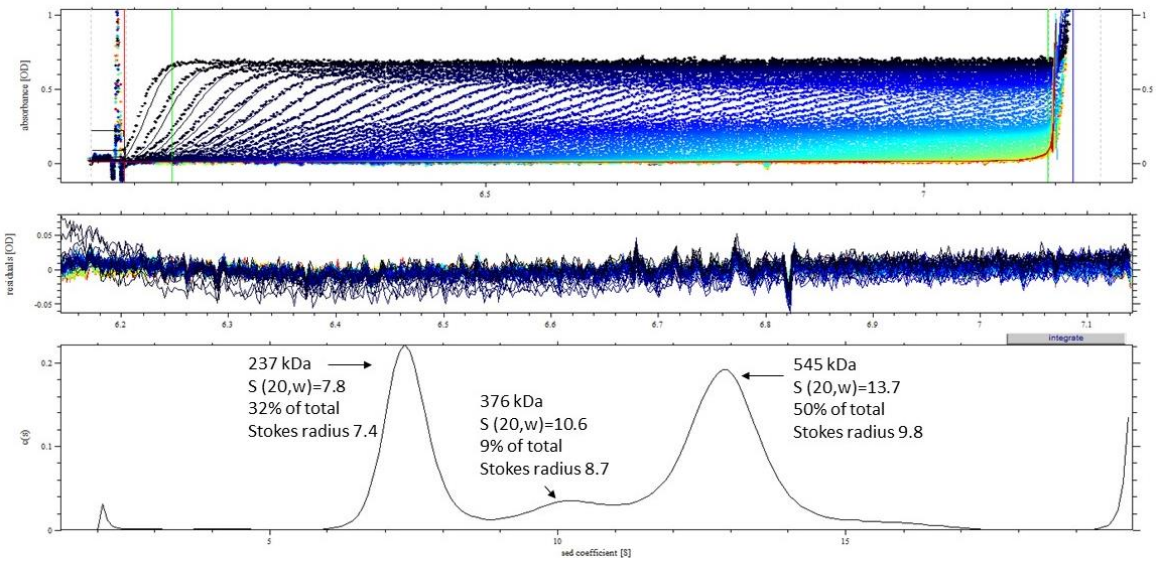

Figure 3.11 Sedimentation velocity data of the isolated γγ'FI-FN complex. A set of 250 scans were collected at 3.5 min intervals in a Beckman Coulter XL-1 analytical ultracentrifuge using the absorbance optical system. Samples were analyzed at 35,000 rpm and 20 °C in Tris/NaCl buffer, pH 7.5.

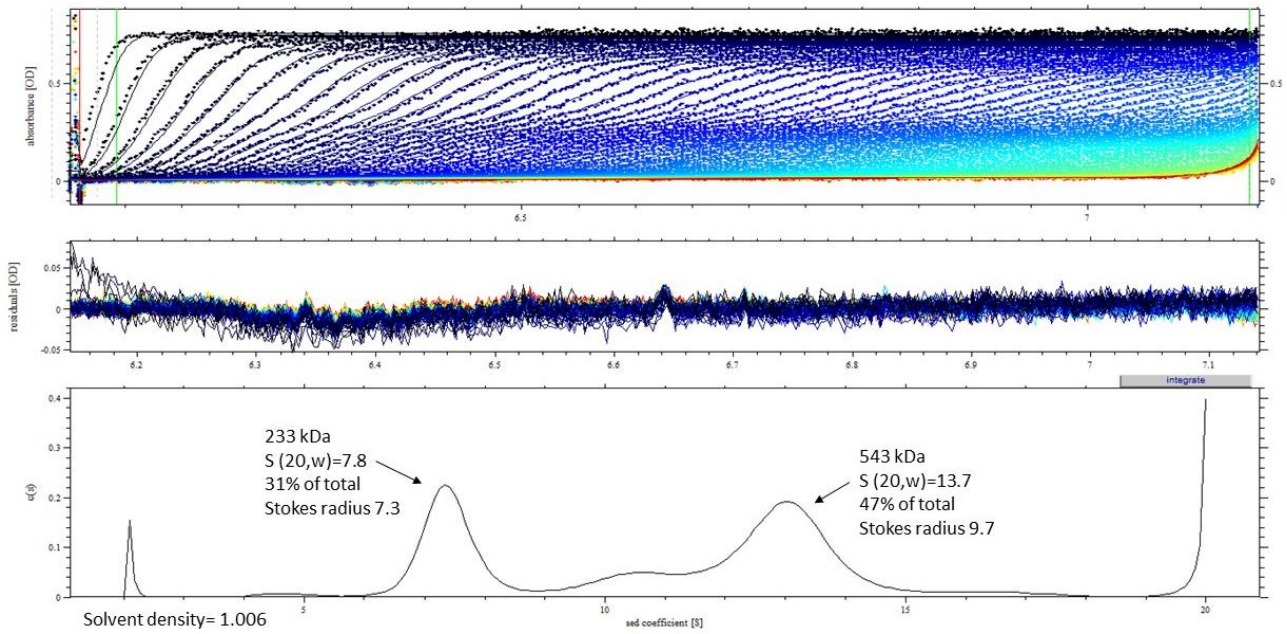

Figure 3.12 Sedimentation velocity data of an equimolar mixture of γγ'pdFI and pdFN. A set of 250 scans were collected at 3.5 min intervals in a Beckman Coulter XL-1 analytical ultracentrifuge using the absorbance optical system. Data was collected at 35,000 rpm and 20 °C in Tris/NaCl buffer, pH 7.5.

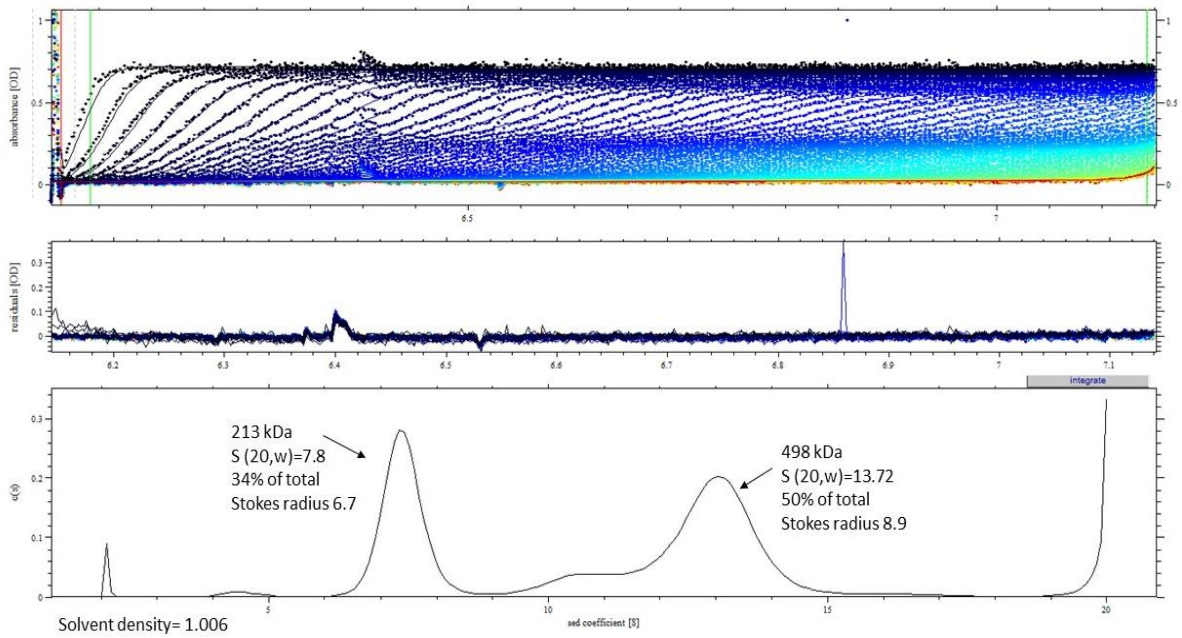

Figure 3.13 Sedimentation velocity data of an equimolar mixture of γγpdFI and pdFN. A set of 250 scans were collected at 3.5 min intervals in a Beckman Coulter XL-1 analytical ultracentrifuge using the absorbance optical system. Data was collected at 35,000 rpm and 20 °C in Tris/NaCl buffer, pH 7.5.

Sedimentation Equilibrium

Sedimentation equilibrium data of pdFI, pdFN, γγ'pdFI-pdFN, and a mixture of γγ'pdFI and pdFN were collected at different rotor speeds (3000 to 8000 rpm) and fitted to the single ideal species model. Fitting the data to a self-association model did not improve the fitting or change the molecular weight estimates and thus was not used. The results of sedimentation equilibrium experiments are presented in Figures 3.14 through 3.17 which show the concentration gradients obtained during sedimentation equilibrium at four different rotor speeds. The combined data of unfractionated pdFI collected at 4000, 6000, and 8000 rpm fit to a molecular weight of 342.1 ± 11.6 kDa (Figure 3.14), which is similar to the reported molecular weight of pdFI (340 kDa). The residuals are distributed randomly and tightly about the fit,

indicating that the single ideal species model describes the data well. FN fit returned a molecular weight of 494.9 ± 29.5 (Figure 3.15), which is within the calculated molecular weight for FN (450 kDa). The residuals are randomly distributed in all data sets, indicating that the self-association model can describe the reaction independent of the rotor speed and initial protein concentration.

Fitting the combined data of the native complex at 3000 and 6000 rpm returned a molecular weight of 645.8 ± 36.2 kDa (Figure 3.16), which is lower than the expected 790 kDa molecular weight of the complex. Residuals are randomly distributed around zero, indicating the single ideal species model is a good description of the data. The combined data for a mixture of γγ'pdFI and pdFN fit to a molecular weight of 288.6 ± 14.7 kDa (Figure 3.17). There is no established molecular weight for a mixture of γγ'pdFI and pdFN or γγpdFI and pdFN to compare to. Residuals are randomly distributed around zero.

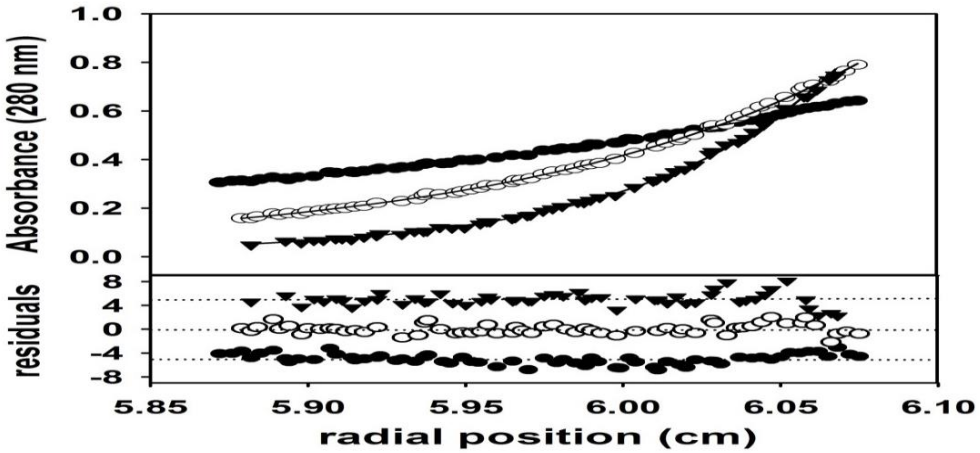

Figure 3.14 Sedimentation equilibrium data of unfractionated pdFI. Protein samples were centrifuged for 22 h at 4000 (solid circles), 6000 (open circles) and 8000 (triangles) rpm at 20 °C. The solid line through the points is the weighted nonlinear least-squares fit to an ideal single-species model. Molecular weight (kDa) estimate of 342.1 (± 11.6) for pdFI was generated from the fitting analysis. The residuals of each fit speed (4000 rpm, solid circles; 6000 rpm, open circles; 8000 rpm, triangles) are displayed in the bottom.

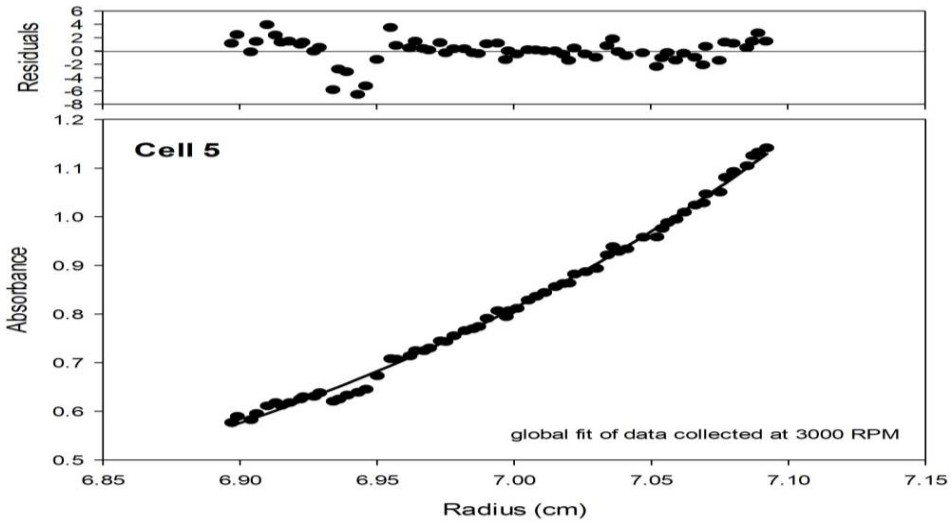

Figure 3.15 Sedimentation equilibrium data of pdFN. Protein samples were centrifuged for 22 h at 3000 and 6000 rpm at 20 °C. Shown is the combined fitting of data collected at 3000 and 6000 rpm. The solid line through the points is the weighted nonlinear least-squares fit to an ideal single-species model. Molecular weight (kDa) estimate of 494.9 (± 29.5) for pdFN was generated from the fitting analysis. The residual for the best-fit analysis at each speed is shown above.

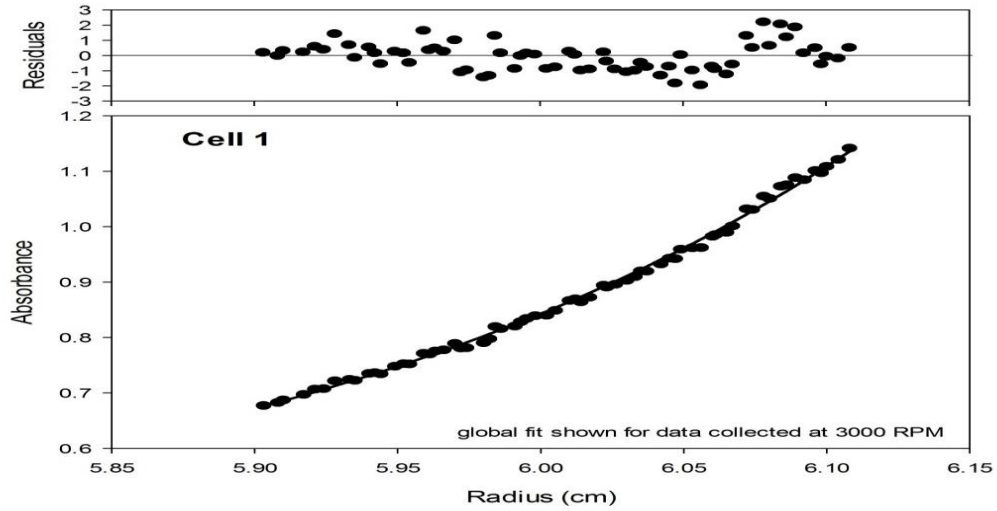

Figure 3.16 Sedimentation equilibrium data of γγ'pdFI-pdFN. Protein samples were centrifuged for 22 h at 3000 and 6000 rpm at 20 °C. Shown is the combined fitting of data collected at 3000 and 6000 rpm. The solid line through the points is the weighted nonlinear least-squares fit to an ideal single-species model. Molecular weight (kDa) estimate of 645.8 (± 36.2) for γγ'pdFI-pdFN was generated from the fitting analysis. The residual for the best-fit analysis at each speed is shown above.

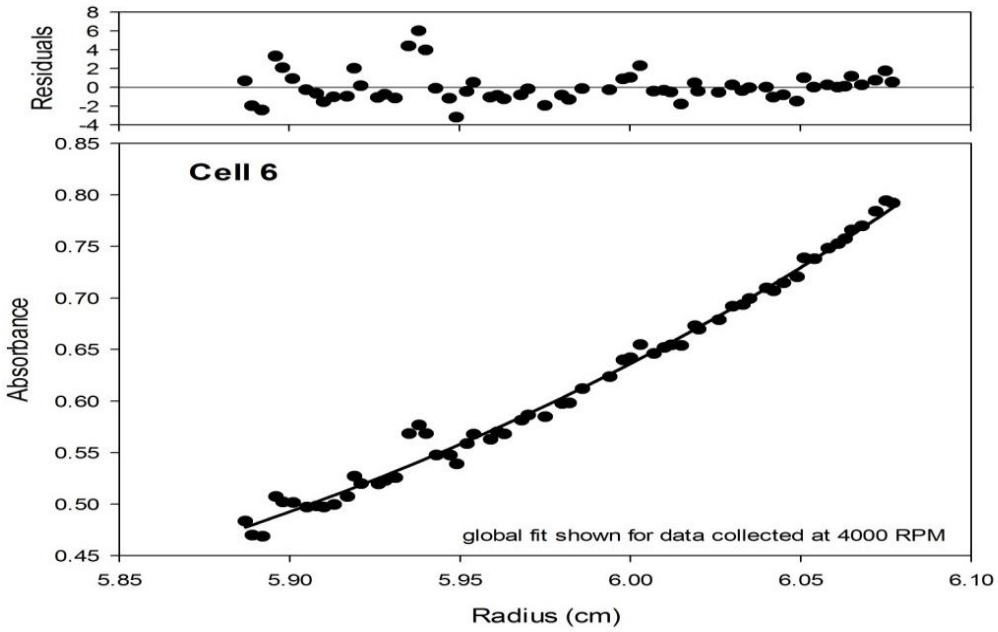

Figure 3.17 Sedimentation equilibrium data of a mixture of γγ'pdFI and pdFN. Protein samples were centrifuged for 22 h at 3000 and 6000 rpm at 20 °C. Shown is the combined fitting of data collected at 3000 and 6000 rpm. The solid line through the points is the weighted nonlinear least-squares fit to an ideal single-species model. Molecular weight (kDa) estimate of 288.6 (± 14.7) for γγ'pdFI+ pdFN was generated from the fitting analysis. The residual for the best-fit analysis at each speed is shown above.

Discussions

When analyzed on SEC at room temperature, the complex did not dissociate to form individual FI and FN providing further evidence for a room-temperature stable γγ'pdFI-pdFN complex. This in contrast to the complex obtained from pathological plasma by heparin at near-freezing temperature which tends to dissociate at room temperature. SEC also demonstrated that the complex is a compact structure at 200 mM NaCl and pH 7.0. We attempted to reconstitute the complex using mixtures of FN plus γγFI and FN plus γγ'pdFI. SEC indicated that a mixture of FN with an excess molar of γγ'pdFI exhibited characteristics similar to the isolated complex.

DLS measurements of the size and mass distribution of the native complex were performed under physiologic, high and low ionic strength, and denaturing conditions and compared to measurements of individual pdFN, γγ and γγ' pdFI species. Results showed that the hydrodynamic radius of the complex increased when analyzed in 1 M NaCl compared to the low ionic strength of 100 mM NaCl. When a denaturing condition of 6 M urea is used, the complex exhibited a much larger hydrodynamic radius. This corroborates the SEC results that the complex is a more compact structure at low ionic strength condition but unfold into the linear conformation under harsh condition in a manner similar to free FN. This agrees with Nagamatsu at el results that showed the complex as a more compact structure at low ionic strength. The conformation of the complex was dependent on solvent conditions as that of free FN.

These findings agree with the physicochemical studies that showed FN structure is highly flexible and depends on the solution conditions. It is known that FN assumes a more compact structure at near physiological condition but undergo a conformational change to the extended form under high salt and chaotropic conditions. Studies have demonstrated that under a denaturing condition of 8 M urea, FN unfolds into a linear polymer with a radius of gyration of 30 nm [11]. FN flexibility is also apparent from SEM studies that showed the molecule in different shapes that ranged from a compact structure, elongated, and rod-like structure.

Based on the DLS and SEC results, we assume that the compact structure of the complex results from the complete or partial folding of the linear FI around the more compact FN. The proposed structure is schematically depicted in Figure 3.18. This hypothesis is supported by the observation that FN exists in a compact conformation at physiological pH and ionic strength. Rotary shadowing electron microscopy showed that FN in the compact conformation appeared more bent and folded upon itself [15]. Electron microscopy revealed that FN molecules are more

strongly curved or bent to generate an irregularly coiled compact structure in low ionic strength, the strand bent. These observations support the hypothesis that at low ionic strength, FN curved, or folded back on itself to form a more compact structure. A possible explanation is that the oppositely charged parts of FN molecules interact electrostatically causing the extended strand to fold into a compact structure [18]. Another possible explanation is that folding is generated by short range electrostatic interactions at many points along the strand. At high ionic strength FN exists as extended strands.

The binding sites involved in the crosslinking of FN to fibrinogen or fibrin are localized in the NH- terminal region of the FN molecule and the COOH-terminal region of the FI α-chains [19-21] . This indicates that both γγ and γγ' FI variants interact with FN through their α-chains. It's known that the γγ'FI is longer and contains more anionic groups than γγFI [22]. This enables γγ'FI to fold more tightly around the FN molecule than γγFI.

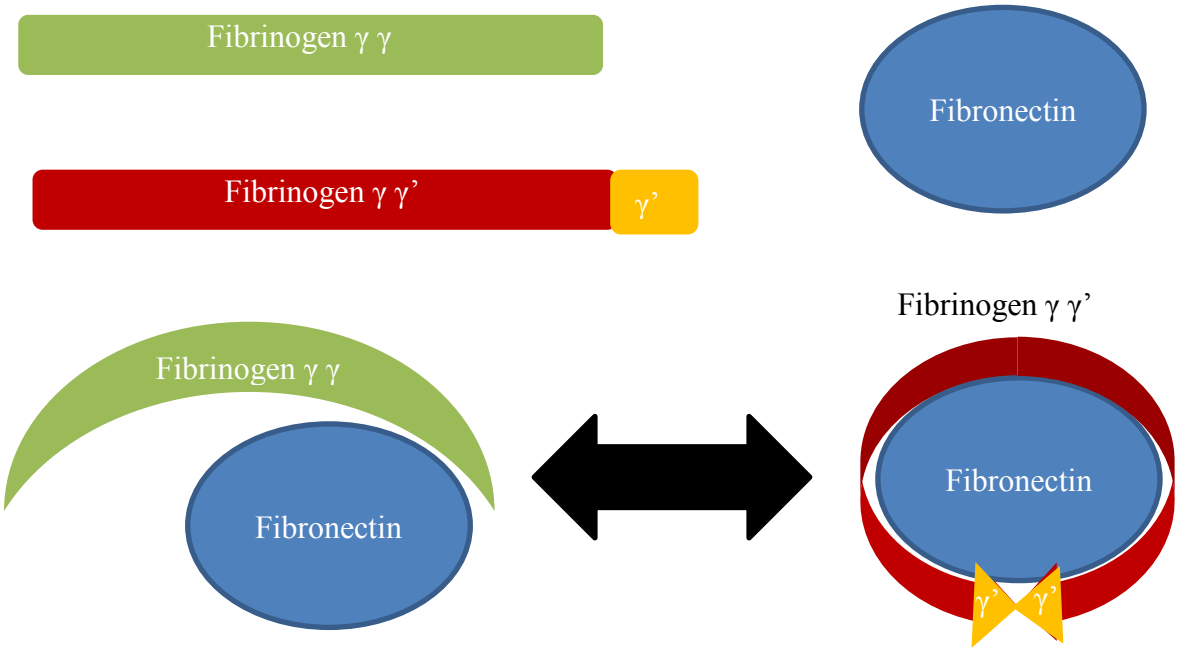

Figure 3.18 schematic diagram of γγ and γγ' interactions with FN.

References

1. Matsuda, M., et al., *Distribution of cold-insoluble globulin in plasma and tissues.* Ann N Y Acad Sci, 1978. **312**: p. 74-92.
2. Nagamatsu, K., et al., *Dynamic light scattering studies on hydrodynamic properties of fibrinogen-fibronectin complex.* J Biomol Struct Dyn, 1992. **9**(4): p. 807-20.
3. Alexander, S.S., Jr., G. Colonna, and H. Edelhoch, *The structure and stability of human plasma cold-insoluble globulin.* J Biol Chem, 1979. **254**(5): p. 1501-5.
4. Williams, E.C., et al., *Conformational states of fibronectin. Effects of pH, ionic strength, and collagen binding.* J Biol Chem, 1982. **257**(24): p. 14973-8.
5. Rocco, M., et al., *Dependence of the shape of the plasma fibronectin molecule on solvent composition. Ionic strength and glycerol content.* J Biol Chem, 1983. **258**(23): p. 14545-9.
6. Erickson, H.P., *Size and shape of protein molecules at the nanometer level determined by sedimentation, gel filtration, and electron microscopy.* Biol Proced Online, 2009. **11**: p. 32-51.
7. Nelea, V., Y. Nakano, and M.T. Kaartinen, *Size distribution and molecular associations of plasma fibronectin and fibronectin crosslinked by transglutaminase 2.* Protein J, 2008. **27**(4): p. 223-33.
8. Lai, C.S., et al., *Solution structure of human plasma fibronectin under different solvent conditions. Fluorescence energy transfer, circular dichroism and light-scattering studies.* J Mol Biol, 1993. **230**(2): p. 625-40.
9. Sjoberg, B., et al., *Solution structure of human plasma fibronectin using small-angle X-ray and neutron scattering at physiological pH and ionic strength.* Arch Biochem Biophys, 1987. **255**(2): p. 347-53.
10. Wasilewska, M., Z. Adamczyk, and B. Jachimska, *Structure of fibrinogen in electrolyte solutions derived from dynamic light scattering (DLS) and viscosity measurements.* Langmuir, 2009. **25**(6): p. 3698-704.
11. Pelta, J., et al., *Statistical conformation of human plasma fibronectin.* Biochemistry, 2000. **39**(17): p. 5146-54.
12. Mosesson, M.W. and R.A. Umfleet, *The cold-insoluble globulin of human plasma. I. Purification, primary characterization, and relationship to fibrinogen and other cold-insoluble fraction components.* J Biol Chem, 1970. **245**(21): p. 5728-36.
13. Mosesson, M.W., A.B. Chen, and R.M. Huseby, *The cold-insoluble globulin of human plasma: studies of its essential structural features.* Biochim Biophys Acta, 1975. **386**(2): p. 509-24.
14. Miekka, S.I., K.C. Ingham, and D. Menache, *Rapid methods for isolation of human plasma fibronectin.* Thromb Res, 1982. **27**(1): p. 1-14.
15. Erickson, H.P. and N.A. Carrell, *Fibronectin in extended and compact conformations. Electron microscopy and sedimentation analysis.* J Biol Chem, 1983. **258**(23): p. 14539-44.
16. Mosher, D.F. and L.T. Furcht, *Fibronectin: review of its structure and possible functions.* J Invest Dermatol, 1981. **77**(2): p. 175-80.
17. Shulman, S., *The size and shape of bovine fibrinogen. Studies of sedimentation, diffusion, and viscosity.* J. Am. Chem. Soc., 1953. **75**: p. 5846-52.

18. Hormann, H., *Fibronectin--mediator between cells and connective tissue.* Klin Wochenschr, 1982. **60**(20): p. 1265-77.
19. Mosher, D.F., *Cross-linking of cold-insoluble globulin by fibrin-stabilizing factor.* J Biol Chem, 1975. **250**(16): p. 6614-21.
20. Iwanaga, S., K. Suzuki, and S. Hashimoto, *Bovine plasma cold-insoluble globulin: gross structure and function.* Ann N Y Acad Sci, 1978. **312**: p. 56-73.
21. Mosher, D.F. and R.B. Johnson, *Specificity of fibronectin--fibrin cross-linking.* Ann N Y Acad Sci, 1983. **408**: p. 583-94.
22. Wolfenstein-Todel, C. and M.W. Mosesson, *Carboxy-terminal amino acid sequence of a human fibrinogen gamma-chain variant (gamma').* Biochemistry, 1981. **20**(21): p. 6146-9.

Chapter 4 Characterize the kinetics and viscoelastic properties of the isolated γγ'pdFI-pdFN complex and comparable mixtures of FI and FN

Abstract

Clottability of the native γγ'pdFI-pdFN complex was evaluated by Thromboelastography (TEG) assay. Clots derived from the native complex had appreciably enhanced clot strength than any other species. The effect of fibronectin on the polymerization rate and viscoelastic properties of fibrin clots made from unfractionated FI and fractionated γγ and γγ' subspecies was also evaluated by TEG. Results showed that FN in the concentration range 0.5-4.5 mg/ml did not perturb polymerization rates and gelation of clots. The clot initiation and propagation time was not influenced by the presence of FN. The initiation and propagation of γγ and γγ' FI clots were inhibited in the absence of FXIII. Interestingly, the addition of FN without crosslinking restored the initiation and propagation time of these clots.

FN, even at the near physiological level of concentration, has shown effect on the rigidity of fibrin clots. Results showed an increase in the maximal amplitude and shear elastic modulus of clots made from unfractionated FI and γγ'FI as a function of supplementing with measured doses of the purified FN (0.5-4.5 mg/ml). FN had dual effect on the rigidity of clots from plasma and recombinant γγFI. While lower level of FN (0.5 and 2 mg/ml) decreased the shear modulus and maximal amplitude of γγFI clots, higher level of FN (3 and 4.5 mg/ml) increased the modulus and maximal amplitude. Even without rFXIIIa mediated crosslinking, FN improved the shear modulus of both γγ and γγ' FI clots.

Introduction

It's well established that FN is covalently incorporated into fibrin clots by activated FXIII. The influence of FN when present on the polymerization and gel structure of fibrin clots is not well resolved. For example, Kamykowski and colleagues [1] measured the effect of FN on shear moduli and creep compliances of fine clots with little lateral aggregation of the fibrin protofibrils and coarse clots with substantial lateral aggregation of the fibrin protofibrils. They found that FN crosslinked to fine clots decreased the shear modulus of clots whereas the addition of FN with or without crosslinking to coarse clots increased the rate and final magnitude of shear modulus. The authors believed that the formation of alpha-fibronectin bonds increased the binding of protofibrils together and stiffened the protofibrils bundles leading to increase in the shear modulus. In contrast to Kamykowski's finding, Chow reported that pdFN had little impact on the mechanical properties of fibrin clots derived from platelet free plasma (PFP) and platelet rich plasma (PRP) [2].

The effect of FN on the polymerization of fibrin was also investigated by using liquid permeation of gels formed in the present of FN [3]. This approach provided information on the size, shape, and orientation of the gel pores associated with FN incorporation. The results indicated that the rate of activation and polymerization of FI is not affected by the presence of FN. The covalent incorporation of FN, however, increased the turbidity of the fibrin gel and significantly reduced the permeability coefficient. The authors concluded that increase in turbidity indicates increase in the thickness of the fibrin strands while decrease in permeability was due to increase in width of the strands. In separate studies, Niewiarowsk and Cierniewski reported that FN inhibited formation of blood clots by influencing the polymerization process and decreasing thrombin clotting time [4]. Using turbidity measurement, the addition of FN to FI

at a molar ratio of 1:5 inhibited the early phase of polymerization leading to prolongation of the lag period. The polymerization processes was completely inhibited when the molar concentration of FN to FI was increased to 1:2. It was speculated that the inhibitory effect of FN is due to the steric hindrance of either thrombin peptide bonds or the polymerization sites in FI. Other studies have demonstrated that FN inhibits fibrin polymerization by maintaining fibrin monomers solubility and re-solubilize fibrin at 37 C. The authors presumed that such solubilization permit fibrin to move in the circulation until it is cleared [5].

Measuring the rheology of fibrin clots

Various techniques were developed to measure the tensile strength and shear strength of clots derived from fibrin sealants formulations. Most of these methods attempt to detect a liquid-to-solid transition during coagulation. These techniques include TEG, shear viscosity measurements, and complex shear modulus measurements such as controlled stress and controlled strain rheometers. Photometric methods such as turbidimetry are also used to measure clot's physical properties. For instance, Chow employed Rheometrics Fluid rheometer to study the effect of FN on clotting of PFP and PRP [6]. The device measures the rheological properties of fluids using either steady shear or dynamic testing modes. Studies by Kamykowski were conducted on a Plazek torsional creep and recovery apparatus in which disk-shaped clot is deformed in torsion. Many of these techniques provide little information on the kinetics of the clot formation. We employed TEG to evaluate the effect of FN on the shear elastic modulus and kinetics of clot formation.

The TEG, developed by Hartert in 1948, is a coaxial cylinder rheometer that measures the growth of elasticity during clot formation. The instrument measures elasticity by monitoring the

motion of the inner cylinder (pin) suspended on a torsion wire, when the outer cylinder (cup) is oscillated back and forth [7]. TEG measure continuously the evolution of viscoelasticity during the course of fibrin polymerization. The adherence of the clot in the cup ensures that retraction is negligible. The TEG was shown to provide reliable, reproducible information on the rheology of clots from fibrin sealant preparations. Herring and colleagues have demonstrated that TEG can be used as a simple, rapid, and reproducible technique for evaluating the mechanical properties of clots derived from different fibrin sealant preparation [8]. Compared to other techniques, the TEG can provide kinetic data on the rheology of fibrin clot formation. It can provide a real-time determination of the onset of clot formation, the rate of clot formation, maximum clot strength, and degradation of the clots.

Shear elastic modulus measurements were done on a TEG 5000 Thromboelastograph Hemostasis Analyzer System. The instrument consisted of a temperature-controlled chamber with two independent measuring channels. Each channel contained a cup and a pin suspended on a torsion wire. To measure the shear elastic modulus, clotting factors are placed in TEG cup and a pin suspended in a torsion wire is lowered into the sample. The cuvette rotates slowly back and forth around its vertical axis through very small angle of 4°45’. The rotation of the cuvette takes 3.5 sec for one direction then comes to standstill for 1 sec and moves back in the other direction for 3.5 sec. Clotting factors transmit little or no torque from cup to pin. As clot develops, fibrin fibers fill the gap between the cup and pin coupling the motion of the cup and the pin. This coupling is directly proportional to the clot strength. The movement of the torsion wire is converted by an electrical-mechanical transducer into electrical signal which then amplified and recorded on computer. Data analysis is done using the TEG analytical software which automatically and independently calculates the TEG parameters. Pin movement in both the

clockwise and counterclockwise directions is simultaneously recorded and plotted in the computer as separate peaks (Figure 4.1). Five parameters are recorded:

- The reaction time (R or r) is the time needed to initiate clot formation and measured as the time or distance from the start of the reaction to the point of first significant clot formation with an amplitude of 2 mm.
- The coagulation or propagation time (K) is the time or distance taken to generate a clot with amplitude of 20 mm. It indicates the rate of increase of elastic modulus in the sample or how fast the clot structure is forming.
- The angle (α) reflects the kinetics of clot formation and measured between the midline of the tracing and a line drawn from the 1 mm wide point tangential to the curve.
- The maximum amplitude (MA) is the width of the curve at its widest point. It shows the maximum clot elastic shear modulus attainable.
- The shear elastic modulus (G) is measured in dynes/cm^2

The absolute elastic shear modulus can be estimated from thromboelastograph amplitude as follows:

$$G = \frac{(5000A)}{(100 - A)}$$

Where G is the elastic shear modulus in dynes/cm^2 and A is the width of the tracing in millimeters.

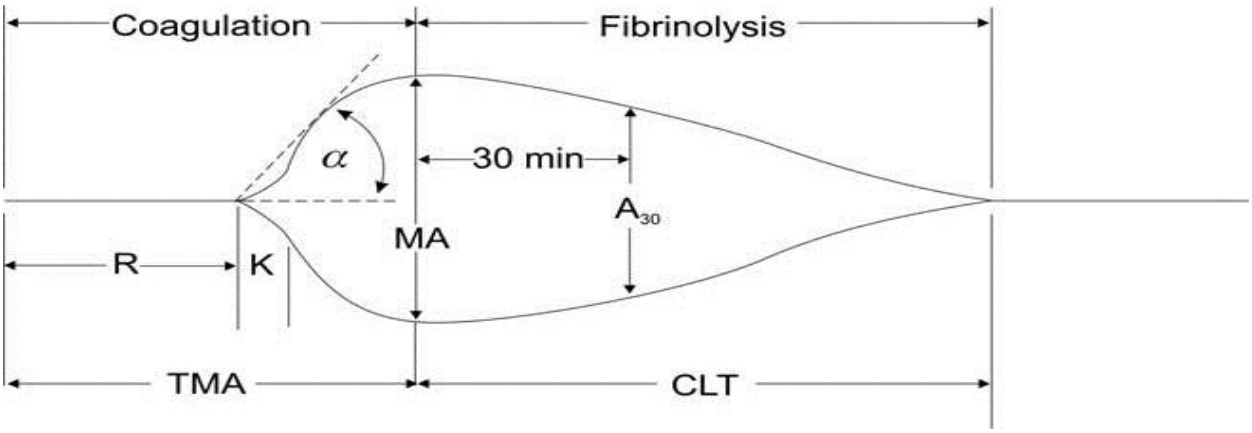

Figure 4.1 TEG tracing parameters

In this section, the effect of FN on the clotting of FI was investigated with the aid of TEG. The role of FN was studied by comparing the kinetic parameters and the dynamic elastic shear modulus of plasma and recombinant unfractionated FI, γγFI, and γγ'FI samples with and without FN.

Materials and Methods

Materials

All reagents of highest purity were purchased from Sigma Chemical Company (St. Louis, MO) unless otherwise noted. Human plasma fibrinogen depleted of fibronectin, plasminogen, and von Willebrand Factor was purchased from Enzyme Research Laboratories (South Bend, IN). Fibrinogen and fibronectin were purified from pool of human plasma donated by the U.S. Army Materials Command (Fort Detrick, MD). Human fibrinogen was purified from plasma by cryoprecipitation followed by two ethanol precipitation as previously described. Human fibronectin was isolated from plasma on Gelatin Sepharose as previously described.

Recombinant fibrinogen (rFI), expressed in the milk of transgenic cows, was kindly supplied by Nick Masiello (LFB). Recombinant human thrombin (rFIIa) was purchased from The Medicines Company (Parsippany, NJ). Recombinant human FXIII (rFXIIIa), expressed in Pichia Pastoris, was purified on His-Bind Resin (Novagen, CA). TEG disposable cups and pins were bought from Haemoscope (Niles, IL).

Evaluating Clottability of FI-FN complex by Thromboelastography

The clotting kinetics of purified γγ'pdFI-pdFN complex was evaluated by TEG Hemostasis system 5000 series (Haemoscope Corporation, Niles, IL). Samples of γγ'pdFI-pdFN complex or pdFI (final concentrations of 9 mg/ml) were placed in a TEG cup, which is kept at 37^{o}C by the instrument. rFXIIIa (final concentration of 0.36 mg/ml), $CaCl_2$ solution (final concentration of 12 mM) and Ringer's solution (155 mM NaCl, 5 mM KCl, 2 mM $CaCl_2$, and 1 mM $MgCl_2$) were added followed immediately by rFIIa (final concentration of 105.6 U/ml) to trigger clot formation. The TEG analyzer collected clot parameters such as the time to reach 2 mm clot strength (R), the time to reach 20 mm clot strength (K), and the maximum clot strength (MA) every five seconds for 30 minutes. The data was collected and analyzed in Microsoft Excel.

Effect of FN on the clottability of FI

The effect of FN on the kinetics and mechanical properties of fibrin clots was also evaluated by TEG Hemostasis system 5000 series. FN effect was measured for both plasma derived and recombinant unfractionated FI and fractionated γγ and γγ' FI subspecies that were isolated on DEAE Sepharose as previously described. Dose response curves were created by

holding the concentration of FI constant (4.5 mg/ml) while varying the level of FN (0.5, 2, 3, and 4.5 mg/ml).

Statistical analysis

Data of repeated experiments were expressed as mean and standard deviation. Differences in the maximal amplitude and shear modulus were analyzed by one-way ANOVA analysis using the software GraphPad Prims, version 5.0 (GraphPad Software, San Diego, CA). P values lower than 0.05 were considered to be significant.

Results

Clottability of γγ'pdFI-pdFN complex by Thromboelastography

The kinetics and mechanical properties of γγ'pdFI-pdFN clots were measured by TEG and compared to the properties of clots derived from plasma FI. Results are shown in Figure 4.2 and Table 4.1. Both types of clots showed very similar clotting kinetics as evident by the clot initiation time (R) and propagation time (K). The formation of both types of clots was initiated 10 seconds after rFIIa was added to the complex and FI. The clot propagation time was also identical, both types of clots needed 50 seconds to reach 20 mm amplitude. However, clots made from γγ'pdFI-pdFN showed superior mechanical properties than pdFI clots. The maximum amplitude (MA) of γγ'pdFI-pdFN clots (79.93 ± 1.37 mm) was 13% higher than the maximum amplitude of pdFI clots (70.57 ± 1.89 mm). In addition, the shear elastic modulus strength (G) of γγ'pdFI-pdFN clots (20004.30 ± 1790 dynes/sec) was 60% stronger than that of pdFI (12048.20 ± 1062.45 dynes/sec). This result is significant considering that the TEG measurements were

performed at a concentration of 9 mg/ml for both samples but the pdFI content of the complex was ~50% of the commercially purified pdFI (Enzyme Research Laboratories).

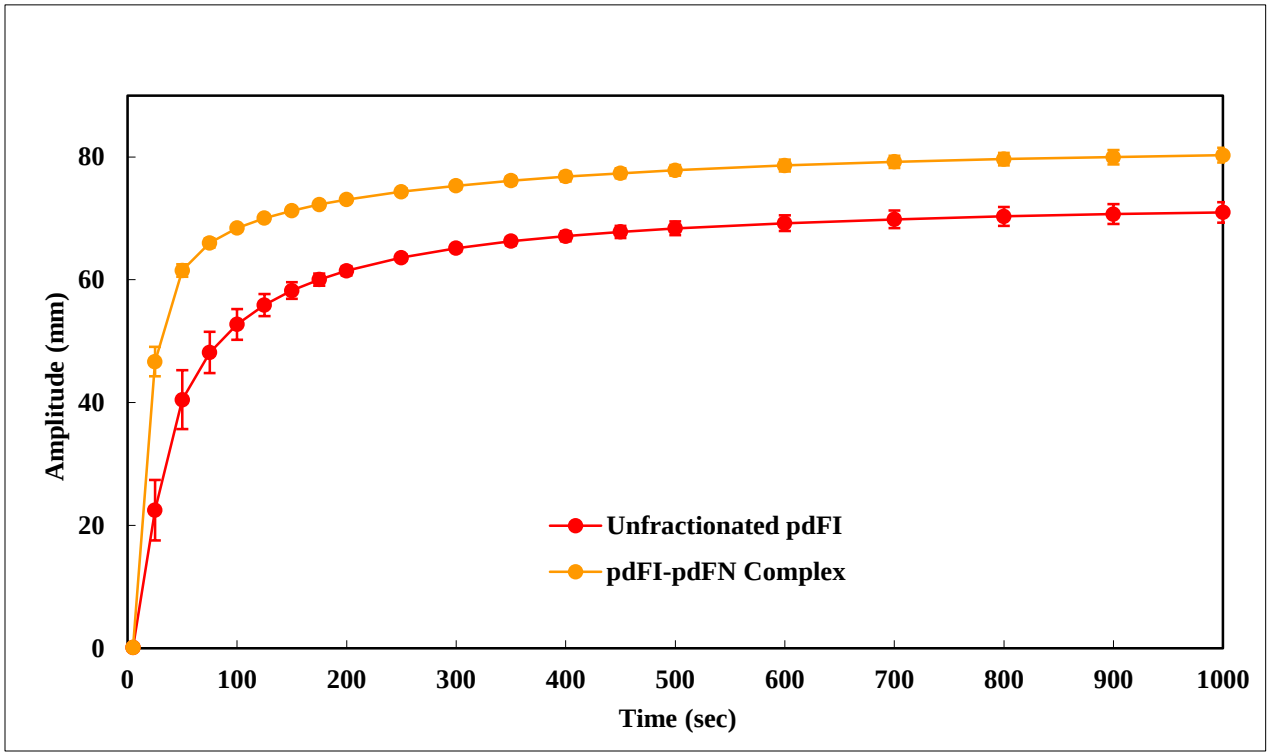

Figure 4.2 Thromboelastography analysis of clots formed from pdFI and native γγ'pdFI-pdFN complex. Viscoelastic and kinetic parameters were measured by TEG Hemostasis system 5000 series. Clotting mixtures included pdFI (9 mg/ml), pdFI-pdFN complex (9 mg/ml), rFXIIIa (0.36 mg/ml), rFIIa (105.6 U/ml), $CaCl_2$ (12 mM), and Ringer's solution.

Table 4.1 Kinetics and viscoelastic parameters of clots from pdFI and γγ'pdFI-pdFN complex.

Type of clot	R (sec)	K (sec)	Angle (deg)	MA (mm)	G (dynes/sec)
Unfractionated pdFI	10.00	50.00	85.80	70.57	12048.20
pdFI-pdFN Complex	10.00	50.00	86.93	79.93	20004.30

The effect of FN on the clotting of unfractionated pdFI

The impact of pdFN on viscoelastic and kinetic parameters of clot developed by normal unfractionated pdFI containing ~80% γγ and 15% γγ' subspecies was evaluated by TEG assay. The study was conducted using commercially available pdFI (Enzyme Research Laboratories) that has been depleted of FN. Measurements were made by holding pdFI concentration constant (4.5 mg/ml) while dosing pdFN (2 and 4.5 mg/ml). Results are displayed in Figure 4.3. TEG parameters R, K, Angle, MA, and G are presented in Table 4.2. As expected, FN alone demonstrated no clot formation or any sign of viscoelastic properties as evident by the flat line. As shown in the table, the addition of FN had no effect on the kinetics of pdFI clots. The time to clot initiation as determined by R is identical (10 seconds) for clots made with and without FN. The propagation time as determined by K is also identical (50 seconds) for both clots. The inclusion of pdFN, however, increased the maximum amplitude and shear strength of the clots. The increase was proportional to the amount of FN added. A lower level of FN (2 mg/ml) increased the maximum amplitude by 7.8% and shear strength by 14.4% whereas a higher level of FN (4.5 mg/ml) elevated the maximum amplitude by 21.1% and shear strength by 44.2%.

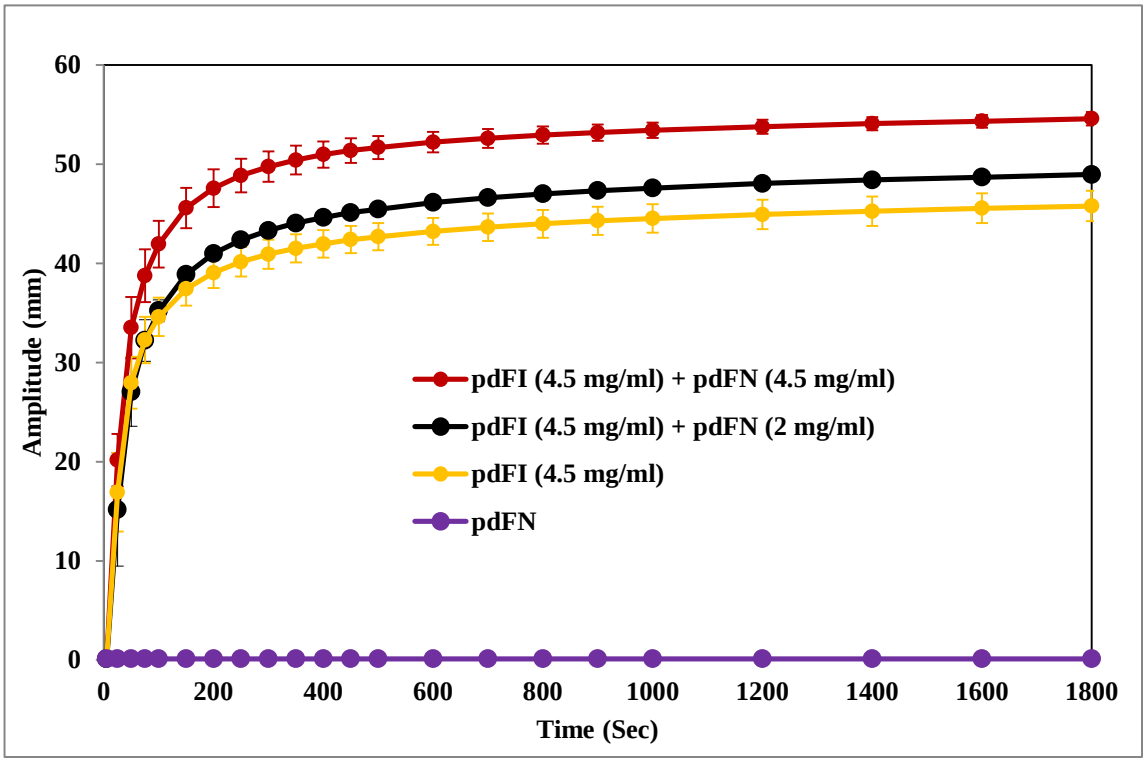

Figure 4.3 Thromboelastography analysis of clots formed from unfractionated pdFI. Viscoelastic and kinetic parameters were measured by TEG Hemostasis system 5000 series. Clotting mixtures included pdFI (4.5 mg/ml), rFXIIIa (0.36 mg/ml), rFIIa (105.6 U/ml), $CaCl_2$ (12 mM), and Ringer's solution.

Table 4.2 Kinetics and Viscoelastic parameters of clots from unfractionated pdFI

Type of clot	R (sec)	K (sec)	Angle (deg)	MA (mm)	G (dynes/sec)
pdFI (4.5 mg/ml) + pdFN (4.5 mg/ml)	10.00	50.00	84.70	52.60	5552.23
pdFI (4.5 mg/ml) + pdFN (0.5 mg/ml)	10.00	50.00	84.10	49.18	4842.75
pdFI (4.5 mg/ml) + pdFN (2 mg/ml)	10.00	50.00	83.77	46.83	4406.43
pdFI (4.5 mg/ml)	10.00	50.00	83.83	43.45	3850.73

The effect of FN on the clotting of γγ and γγ' pdFI

The effect of pdFN on the viscoelastic and mechanical properties of clots formed by γγ'pdFI and γγpdFI was examined by TEG at 37℃. The results are depicted in Figure 4.4 and Table 4.3. A dose response curve was generated by keeping the concentration of

γγpdFI or γγ'pdFI constant while varying pdFN levels (0.5, 2, 3, and 4.5 mg/ml). The presence of FN did not influence the kinetic of γγ'pdFI clot formation. It took the same time (10 sec) to initiate clot formation after rFIIa was added to γγ'pdFI and a mixture of γγ'pdFI plus pdFN. Similarly, the time to reach 20 mm clot strength was the same (50 sec) for both types of clots. However, the presence of FN increased the shear modulus and maximal strength of clots in a manner that dependent on the amount of FN added. A low concentration of FN (0.5 mg/ml) increased the maximum amplitude by 4.9% and shear modulus by 10.3%, while a high level of FN (4.5 mg/ml) increased the maximum amplitude by 42.3% and shear modulus 146.6%. Increasing FN concentration from 2 to 3 mg/ml resulted in the largest increase in maximal amplitude (22.4%) and shear strength (88.4%). On the other hand, going from 3 to 4.5 mg/ml produced the smallest increase in maximal amplitude (3.5%) and shear strength (19.5%), suggesting a saturation level was attained.

Similar to γγ'pdFI clots, FN did not affect the kinetic of γγpdFI clot formation (Figure 4.5 and Table 4.4). Formation of clot in the presence or absence of FN was initiated 10 sec following the addition of rFIIa. Also, it took all clots 50 sec to reach 20 mm amplitude. The addition of FN, however, had a mixed effect on the maximum amplitude and shear modulus of γγpdFI clots. While lower levels of FN (0.5 and 2 mg/ml) decreased the shear modulus, higher levels (3 and 4.5 mg/ml) increased the shear modulus. The inhibitory effect of FN on clot strength was maximal at FN concentration 0.5 mg/ml, which lowered maximum amplitude by 15% and shear modulus by 28%. FN at 4.5 mg/ml enhanced the maximum amplitude by 19.3% and shear modulus 55.4%.

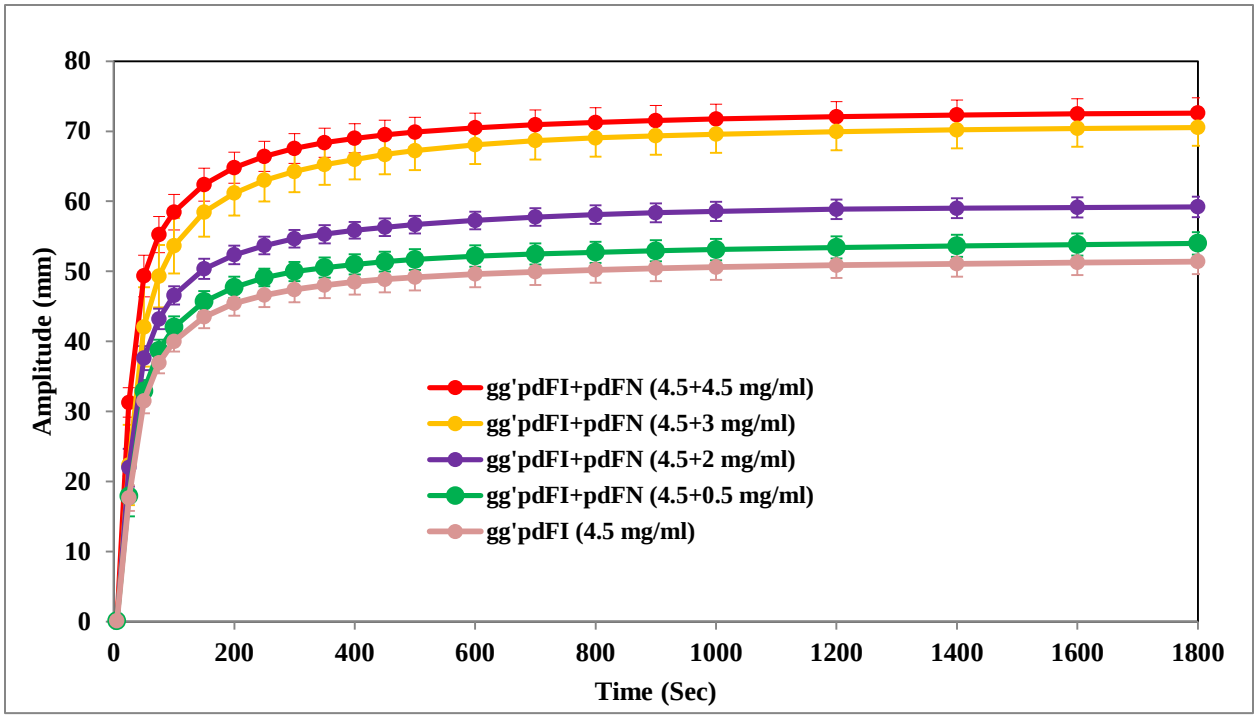

Figure 4.4 Thromboelastography analysis of clots formed from mixtures of γγ'pdFI and pdFN. Viscoelastic and kinetic parameters were measured by TEG Hemostasis system 5000 series. Clotting mixtures included γγpdFI (4.5 mg/ml), pdFN (0.5, 2, and 3 mg/ml), rFXIIIa (0.36 mg/ml), rFIIa (105.6 U/ml), $CaCl_2$ (12 mM), and Ringer's solution.

Table 4.3 Kinetics and viscoelastic parameters of clots from mixtures of γγ'pdFI and FN

Type of clot	R (sec)	K (sec)	Angle (deg)	MA (mm)	G (dynes/sec)
gg'pdFI+pdFN (4.5+4.5 mg/ml)	10.00	50.00	86.40	71.03	12,322.93
gg'pdFI+pdFN (4.5+3 mg/ml)	10.00	50.00	85.88	69.28	11,348.25
gg'pdFI+pdFN (4.5+2 mg/ml)	10.00	50.00	85.37	58.07	6,928.63
gg'pdFI+pdFN (4.5+0.5 mg/ml)	8.33	50.00	84.60	52.37	5,510.43
gg'pdFI (4.5 mg/ml)	10.00	50.00	84.57	49.93	4,997.23

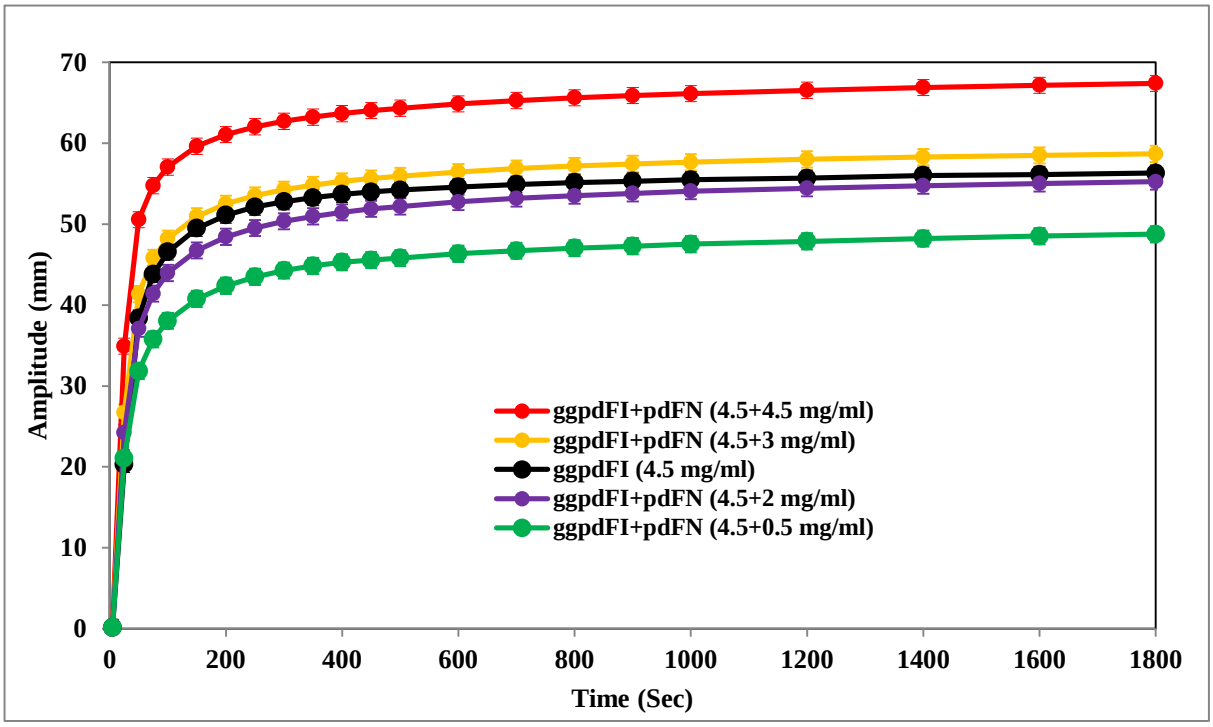

Figure 4.5 Thromboelastography analysis of clots formed from mixtures of γγpdFI and pdFN. Viscoelastic and kinetic parameters were measured by TEG Hemostasis system 5000 series. Clotting mixtures included γγpdFI (4.5 mg/ml), pdFN (0.5, 2, and 3 mg/ml), rFXIIIa (0.36 mg/ml), rFIIa (105.6 U/ml), $CaCl_2$ (12 mM), and Ringer's solution.

Table 4.4 Kinetics and viscoelastic parameters of clots from mixtures of γγpdFI and FN

Type of clot	R (sec)	K (sec)	Angle (deg)	MA (mm)	G (dynes/sec)
ggpdFI+pdFN (4.5+4.5 mg/ml)	10.00	50.00	86.27	65.20	9,418.67
ggpdFI+pdFN (4.5+3 mg/ml)	10.00	50.00	85.50	57.05	6692.78
ggpdFI (4.5 mg/ml)	10.00	50.00	85.50	54.67	6062.07
ggpdFI+pdFN (4.5+2 mg/ml)	10.00	50.00	85.20	53.43	5764.37
ggpdFI+pdFN (4.5+0.5 mg/ml)	10.00	50.00	84.43	46.47	4365.47

The viscoelastic and mechanical properties of the native γγ'pdFI-pdFN complex and mixtures of γγ'pdFI plus pdFN and γγpdFI plus pdFN complex are shown in Figure 4.6 and Table 4.5. FN did not interfere with the clotting kinetics of native and reconstituted complex; time to clot initiation and propagation was similar for both the complex and the control γγ and γγ'

FI. However, the addition of exogenous FN to γγ'pdFI and γγpdFI did not create clots with mechanical strength as those of native complex. The maximum amplitude of clots made from the native γγ'pdFI-pdFN complex was 7.1% and 14.3% greater than the amplitude of clots from a mixture of γγ'pdFI with pdFN and γγpdFI with pdFN, respectively. This shows that the viscoelastic properties of the native complex can only be partially duplicated using exogenous mixtures of γγ'pdFI and pdFN.

We also examined the polymerization rate and gel structure of γγ and γγ' FI variants by TEG. Results were averaged from several experiments. Figure 4.6 and Table 4.5 illustrate that there is no kinetic difference between γγ'pdFI and γγpdFI clots. However, the maximal amplitude attained by γγ'pdFI clots was 3.7% greater than the amplitude of γγpdFI clots. In addition, the shear strength of γγ'pdFI clots was 8.2% greater than the shear strength of γγpdFI clots. The higher shear strength of clots made from γγ'pdFI can be attributed to the FXIII mediated crosslinking of fibrin monomers. It's well established that fibrinogen γγ' contains binding sites for FXIII and serve as a carrier for the transglutaminase in the circulation. Therefore, clots made from γγ'FI are more extensively cross-linked and resistant to proteolytic degradation than clots derived from γγpdFI. γγ' affects clot properties by concentrating and increasing the rate of FXIII activation at the site of vascular injury. It has been shown that the more extensively cross-linked γγ' fibrin clots are more resistant to clot lysis than γγ [9]. The higher rate of FXIII associated with γγ' fibrinogen was thought to be responsible for the large increase in fibrinolysis resistance of γγ' fibrin compared with γγ fibrin.

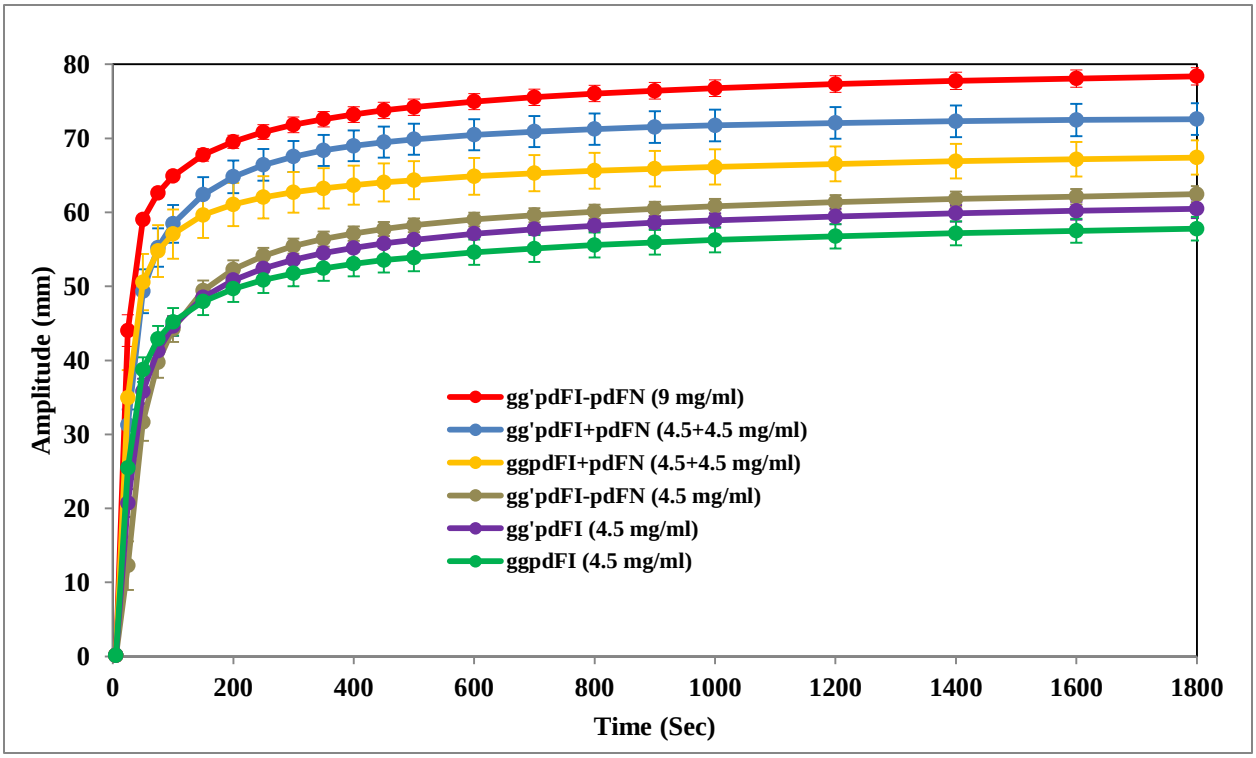

Figure 4.6 Thromboelastography comparison of clots formed from the native and reconstituted γγ'pdFI-pdFN complex. Viscoelastic and kinetic parameters were measured by TEG Hemostasis system 5000 series. Clotting mixtures included γγ'pdFI (4.5 mg/ml), γγ'pdFI-pdFN complex (4.5 or 9 mg/ml), γγ'pdFI (4.5 mg/ml) + pdFN (4.5 mg/ml). rFXIIIa (0.36 mg/ml), rFIIa (105.6 U/ml), $CaCl_2$ (12 mM), and Ringer's solution.

Table 4.5 Viscoelastic and kinetic parameters of clots from the native and reconstituted γγ'pdFI-pdFN complex.

Type of clot	R (sec)	K (sec)	Angle (deg)	MA (mm)	G (dynes/sec)
gg'pdFI-pdFN (9 mg/ml)	10.00	50.00	86.90	76.10	15,960.77
gg'pdFI+pdFN (4.5+4.5 mg/ml)	10.00	50.00	86.40	71.03	12322.93
ggpdFI+pdFN (4.5+4.5 mg/ml)	10.00	50.00	86.27	65.20	9418.67
gg'pdFI-pdFN (4.5 mg/ml)	11.00	50.00	84.78	60.20	7571.34
gg'pdFI (4.5 mg/ml)	10.00	50.00	85.07	57.75	6848.72
ggpdFI (4.5 mg/ml)	10.00	50.0	82.43	55.7	6328.59

The effect of adding FN without crosslinking on the clotting of γγ and γγ'

We also examined the effect of adding FN without FXIII mediated crosslinking on the strength and kinetics of clots derived from γγ and γγ' pdFI. Results are shown in Figure 4.7 and Table 4.6. It was found that in the absence of FXIIIa and FN, the propagation time of both γγ (748.75 sec) and γγ' (93.33 sec) clots were delayed. The clot initiation time of the γγ clots were also delayed (18.75 sec). However, the inclusion of FN restored the initiation and propagation time of both types of clots to the values of samples containing FXIIIa.

Even without FXIII mediated crosslinking, the addition of FN increased the maximal strength and shear modulus of both γγ and γγ' FI clots. FN increased the maximal strength of γγpdFI clots by 60.6% and γγ'pdFI clots by 19%. The increase in shear strength was 94.7% for γγpdFI clots and 26.3% for γγ'pdFI clots. This contrast the finding that, without crosslinking by FXIII, γγFI clots were 2.7 times stiffer than γγ' [10]. However, the maximal amplitude and shear strength of unligated clots from a mixture of γγpdFI plus pdFN clots was 1.59 and 5.53 times lower than the crosslinked γγpdFI clots. Likewise, the maximal amplitude and shear strength of unligated clots from a mixture of γγ'pdFI plus pdFN was 0.77 and 2.24 times lower compared to the ligated γγ'pdFI clots. This shows that the difference in clot strength is due to the FXIIIa mediated covalent crosslinking of FN. It's well established that FXIIIa catalyze the formation of γ and α dimers between adjacent fibrin strands. FXIIIa also covalently crosslinks FN to fibrin by catalyzing the formation of bonds between Lys residue in the C-terminal of the fibrin α-chain and Gln receptor residues in the N-terminal of FN [11]. The formation of additional fibrin-FN was thought to contribute to clot strength.

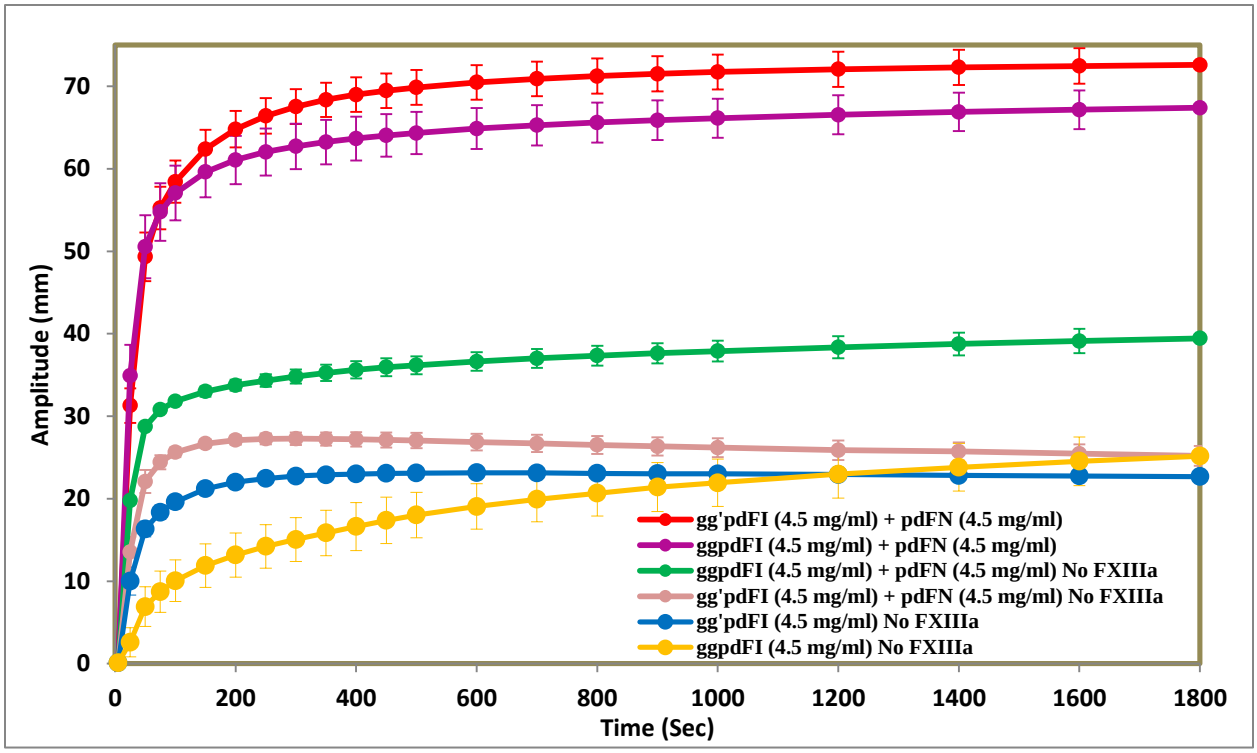

Figure 4.7 Thromboelastography analysis of clots formed from γγ and γγ'pdFI with or without FXIII and pdFN. Viscoelastic and kinetic parameters were measured by TEG Hemostasis system 5000 series. Clotting mixtures included γγpdFI (4.5 mg/ml), γγ'pdFI (4.5 mg/ml), pdFN (4.5 mg/ml). rFXIIIa (0.36 mg/ml), rFIIa (105.6 U/ml), $CaCl_2$ (12 mM), and Ringer's solution.

Table 4.6 Kinetics and viscoelastic parameters of clots from γγ and γγ'pdFI with or without FXIII and pdFN

Type of clot	R (sec)	K (sec)	Angle (deg)	MA (mm)	G (dynes/sec)
gg'pdFI + pdFN (4.5 + 4.5 mg/ml)	10.00	50.00	86.4	71.033	12,322.93
ggpdFI + pdFN (4.5 + 4.5 mg/ml)	10.00	50.00	86.27	65.20	9,418.67
ggpdFI + pdFN (4.5 + 4.5 mg/ml) No FXIIIa	10.00	50.00	83.67	36.73	2,902.57
gg'pdFI + pdFN (4.5 + 4.5 mg/ml) No FXIIIa	10.00	50.00	82.00	27.38	1,885.95
gg'pdFI (4.5 mg/ml) No FXIIIa	10.00	93.33	79.30	23.00	1,493.00
ggpdFI (4.5 mg/ml) No FXIIIa	18.75	748.75	66.80	22.88	1,490.43

The effect of FN on the clotting of γγ and γγ' rFI

The effect of FN on the clotting of γγ and γγ' rFI was also investigated by TEG at 37. The results are shown in Figures 4.8 and 4.9. TEG parameters are displayed in Tables 4.7 and 4.8. FN showed no inhibitory effect on the initiation and propagation of both γγ and γγ' rFI clots. In fact, FN improved the propagation of γγ'rFI clots. FN, however, had mixed effect on the viscoelastic properties of γγ'rFI clots. While FN concentration 2 and 3 mg/ml slightly increased the maximal amplitude and shear strength, 0.5 mg/ml concentration appears to weaken the amplitude and strength of γγ'rFI clots. FN concentration 4.5 mg/ml enhanced the maximal amplitude by 24.2% and shear strength by 38.5%. FN also had dual effect on the maximal amplitude and shear strength of γγ rFI clots. While FN concentrations 0.5 and 2 mg/ml retarded maximal amplitude and shear strength, FN concentrations 3 and 4.5 mg/ml improved the amplitude and shear strength of γγ rFI clots. Figure 4.10 compares the impact of FN on the shear strength of clots developed from plasma and recombinant unfractionated FI and fractionated γγ and γγ'FI variant.

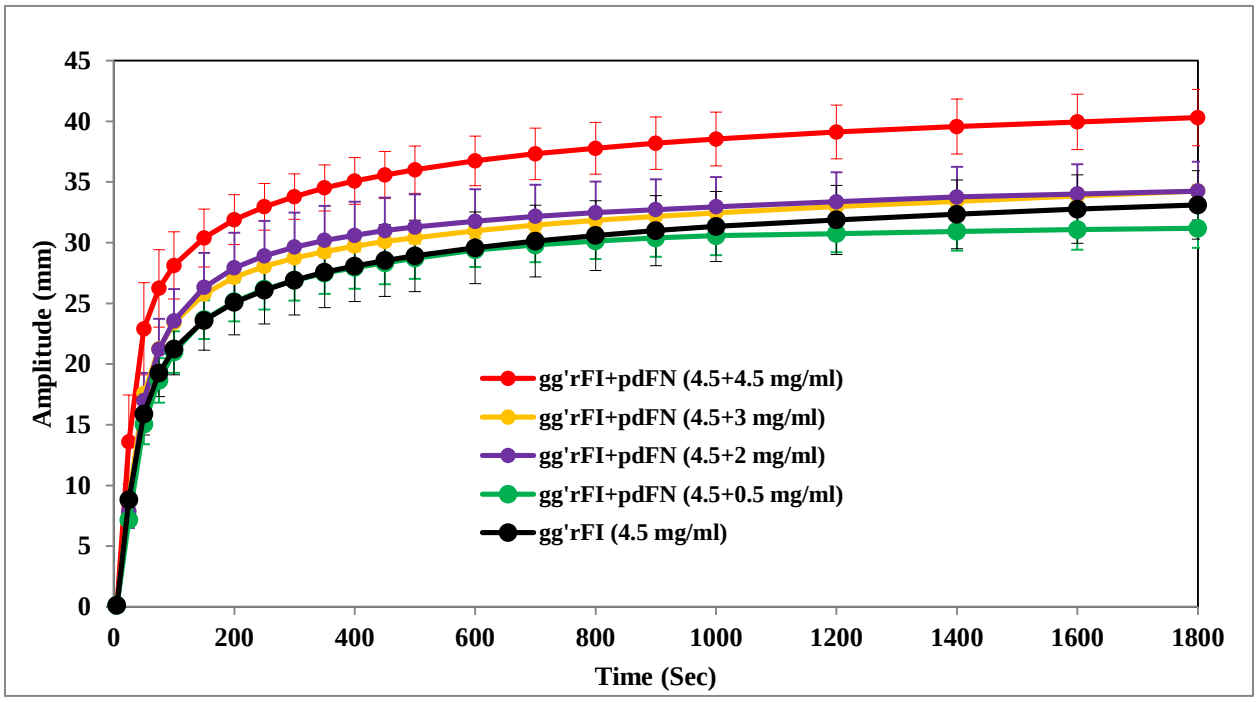

Figure 4.8 Thromboelastography analysis of clots formed from mixtures of γγ'rFI and pdFN. Viscoelastic and kinetic parameters were measured by TEG Hemostasis system 5000 series. Clotting mixtures included γγpdFI (4.5 mg/ml), pdFN (0.5, 2, and 3 mg/ml), rFXIIIa (0.36 mg/ml), rFIIa (105.6 U/ml), $CaCl_2$ (12 mM), and Ringer's solution.

Table 4.7 Kinetics and viscoelastic parameters of clots from mixtures of γγ'rFI and FN

Type of clot	R (sec)	K (sec)	Angle (deg)	MA (mm)	G (dynes/sec)
gg'rFI+pdFN (4.5+4.5 mg/ml)	10.00	50.00	82.33	37.78	3042.85
gg'rFI+pdFN (4.5+3 mg/ml)	10.00	50.00	80.57	30.90	2237.23
gg'rFI+pdFN (4.5+2 mg/ml)	10.00	56.67	80.33	32.10	2373.73
gg'rFI+pdFN (4.5+0.5 mg/ml)	10.00	71.67	79.07	29.97	2143.03
gg'rFI (4.5 mg/ml)	10.00	72.00	79.52	30.42	2196.30

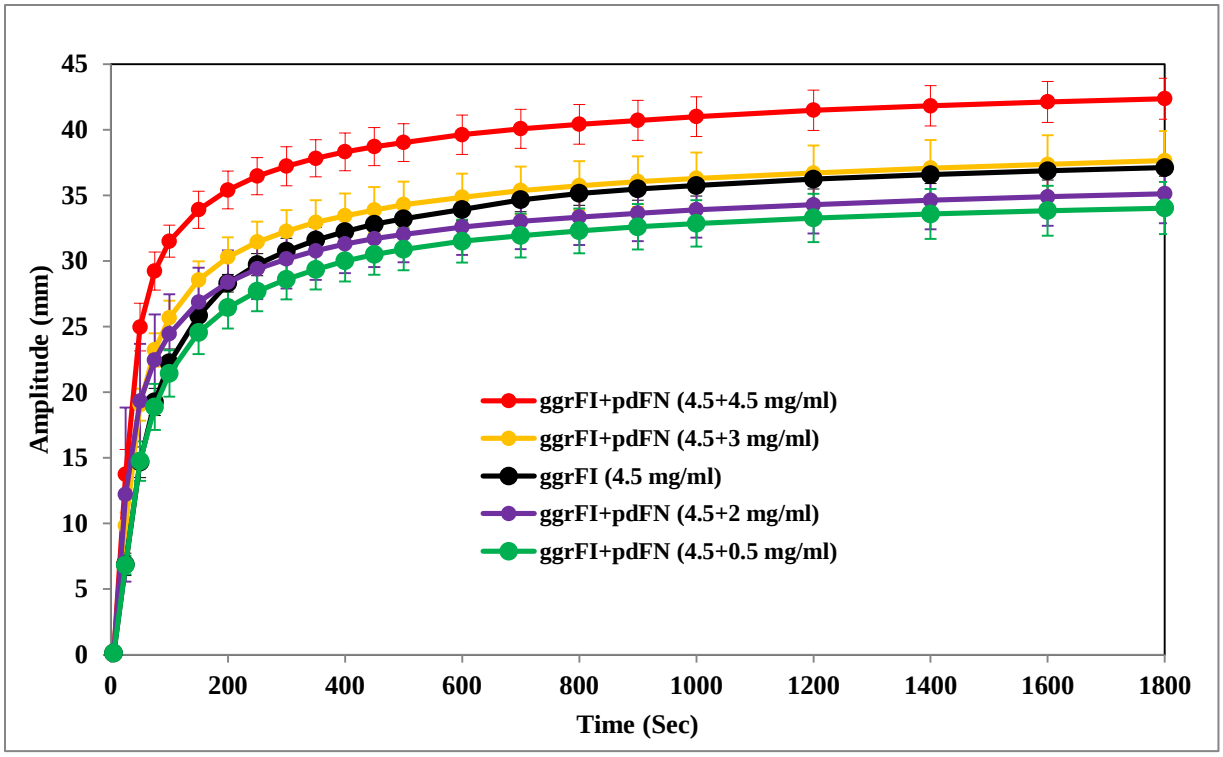

Figure 4.9 Thromboelastography analysis of clots formed from mixtures of γγrFI and pdFN. Viscoelastic and kinetic parameters were measured by TEG Hemostasis system 5000 series. Clotting mixtures included γγpdFI (4.5 mg/ml), pdFN (0.5, 2, and 3 mg/ml), rFXIIIa (0.36 mg/ml), rFIIa (105.6 U/ml), $CaCl_2$ (12 mM), and Ringer's solution.

Table 4.8 Kinetics and viscoelastic parameters of clots from mixtures of γγrFI and FN

Type of clot	R (sec)	K (sec)	Angle (deg)	MA (mm)	G (dynes/sec)
ggrFI+pdFN (4.5+4.5 mg/ml)	10.00	50.00	83.17	40.17	3360.83
ggrFI+pdFN (4.5+3 mg/ml)	10.00	50.00	81.30	35.47	2752.60
ggrFI+pdFN (4.5+2 mg/ml)	10.00	51.67	81.00	32.87	2453.67
ggrFI+pdFN (4.5+0.5 mg/ml)	10.00	68.33	79.13	32.40	2397.80
ggrFI (4.5 mg/ml)	10.00	63.33	79.30	35.37	2733.87

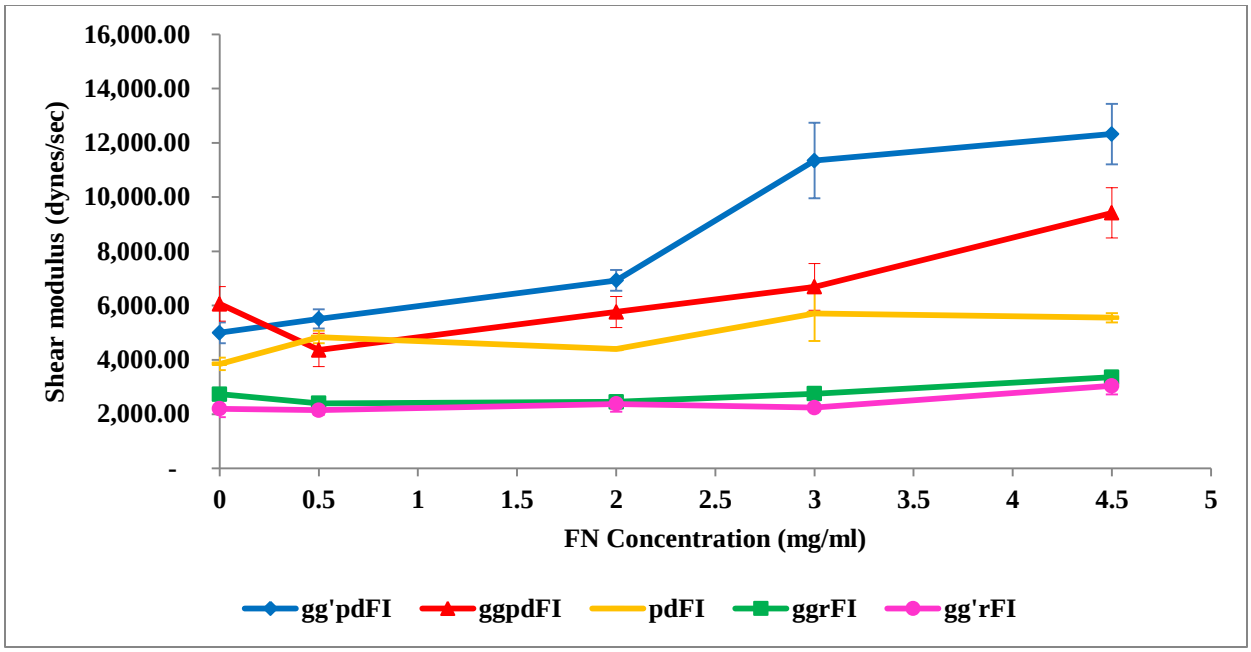

Figure 4.10 Effect of FN on the shear modulus of clots made from unfractionated FI and fractionated γγ and γγ' FI as determined by TEG.

Discussion

The viscoelastic properties of a fibrin clot are essential for its functions and will determine how it responds to the mechanical challenge created by the following blood. The clot must be strong enough to stem the flow of blood and elastic enough to withstand the shear forces generated by the flowing blood. Fibrin clot is a viscoelastic polymer with both viscous and elastic components [12]. The viscoelasticity determines how the clot responds to the forces created by the flowing blood. It has been shown that the inclusion of other proteins from plasma greatly influenced the mechanical properties of fibrin clots [13]. Studies have shown that fibrin clots made from plasma possess different properties than those created from purified proteins [14-16]. Clots formed *in vivo* can be different in certain conditions where some other proteins may be present in different quantities and under different conditions and thereby may be

responsible for modulating clot structure. Since FN is the second largest component of the clot, 4% of the total weight of the clot, measuring the effect of FN on clot's properties is essential.

The influence of FN on the kinetics and rigidity of various types of fibrin clots was assessed by TEG assay. Results showed that pdFN in the concentration range 0.5-4.5 mg/ml had no influence on the kinetics of clot formation of different FI containing species. FN, however, had a greater influence on the rigidity of fibrin clots. FN enhanced the maximal amplitude and shear elastic modulus of clots made from unfractionated plasma FI, plasma and recombinant γγ'FI subspecies. FN had dual effect on the rigidity of plasma and recombinant γγFI. While FN concentration 0.5-2 mg/ml decreased the shear modulus and maximal amplitude of γγFI clots, FN concentration 3-4.5 mg/ml increased the modulus and maximal amplitude.

Exogenous FN increased the rigidity of γγFI, and γγ'FI clots even in the absence of FXIII mediated crosslinking. However, the increase in strength of clots containing FN without FXIII mediated crosslinking is significantly lower than the strength of crosslinked clots. With ligation, FN improved the shear modulus of γγpdFI by a factor of 1.6 and γγ'pdFI by a factor of 2.5. Without ligation, the improvement was by a factor of 1.9 for γγpdFI and by a factor of 1.3 for γγ'pdFI.

The results presented here show that the native γγ'pdFI-pFN complex formed clots with viscoelastic properties that higher than any other species. The mechanical properties of the native complex clots can be partially duplicated with mixture of γγ'pdFI and FN, which formed clots with shear strength that 22.8% lower than the strength of the native complex clot. The higher stiffness displayed by clots from the native γγ'pdFI-pdFN complex and a mixture of γγ'pdFI plus pdFN can be attributed to the γγ' crosslinking. This is consistent with previous functional studies

that showed that fibrin clot containing γγ' species are more far cross-linked by FXIIIa than fibrin clot containing γγ [17]. Furthermore, clot lysis experiments demonstrated that fibrin derived from γγ'pdFI has greater resistance to fibrinolysis [9]. Another possible explanation is that the interaction of FN with γγ' result in the formational of multiple FN- γγ' bonds. We have shown that the native complex contains exclusively γγ'FI subspecies in a 1:1 mixture with FN.

The augmentation of clot rigidity by plasma fibronectin is in agreement with the finding of Kamykowski et al that shown, depending on the ionic strength and the pH during polymerization, FN either increase or decrease the shear modulus of clot. FN has decreased the elastic modulus of fine clots formed at high ionic strength and pH and increased the modulus of coarse clots formed at physiological ionic strength and neutral pH. FN enhanced the shear modulus of coarse clots by a factor of 2.0 without crosslinking and by a factor 2.4 with crosslinking. The enhancement was explained by the formation of additional FN-α bonds that stiffen protofibrils by binding them together. Our clots were formed at physiologic pH and ionic strength conditions that favors the generation of coarse clots. Our results contrasts the finding of Chow et al who reported that pdFN had little impact on the mechanical properties of fibrin clots derived from platelet free plasma and platelet rich plasma.

Okada et al found that the presence of FN did not affect the clotting time or the initial rate of increase in turbidity which corresponds to the clot propagation time [3]. FN did not affect the clotting time nor the release of fibrinopeptides and consequently had no influence on the polymerization and gelation of fibrinogen. Incorporated FN, however, increased the turbidity and slightly decreased the permeability coefficient. The authors conclude that FN increases the width of the strands and proposed a model in which FN diffuse through the loosely assembled

fibrin strands resulting in a sandwich-like arrangement of fibrin polymers separated by an array of FN molecules. This gel structures is expected to become much stronger than the structure stabilized solely by g and α crosslinks within the polymers of the strand. Our studies are in support of this conclusion. Separate studies by Niewiarowska and Cierniewski et al have revealed that FN inhibited fibrin formation by delaying the early phase of fibrin formation and decreasing the thrombin clotting time. In contrary, our studies showed that FN had no influence on the initiation of fibrin formation and propagation of the clot. In fact, FN speeds up clot development in some instances.

The increased shear modulus of clots derived from γγ' is likely due to the presence of FXIII. Biochemical studies have shown that the γ' chain of FI contains binding sites for FXIII and FII and also serves as a carrier for FXIII in the circulation. Therefore, γ' chain has been thought to modulates the activity of FXIII and FII, alter clot architecture, and interfere with platelet fibrinogen interaction. The association of rFII and FXIII with γγ'FI indicates that the later may influence the structure and properties of fibrin clots. For instance, it has been suggested that γγ' concentrate and speed up the rate of FXIII activation leading to extensive crosslinking of fibrin monomers. This alters the stability of fibrin clot developed *in vitro* by increasing clot's ability to resist lysis by plasmin and other proteases.

References

1. Kamykowski, G.W., et al., *Modification of shear modulus and creep compliance of fibrin clots by fibronectin.* Biophys Chem, 1981. **13**(1): p. 25-8.
2. Chow, T.W., L.V. McIntire, and D.M. Peterson, *Importance of plasma fibronectin in determining PFP and PRP clot mechanical properties.* Thromb Res, 1983. **29**(2): p. 243-8.
3. Okada, M., et al., *Fibronectin and fibrin gel structure.* J Biol Chem, 1985. **260**(3): p. 1811-20.

4. Niewiarowska, J. and C.S. Cierniewski, *Inhibitory effect of fibronectin on the fibrin formation.* Thromb Res, 1982. **27**(5): p. 611-8.
5. Kaplan, J.E. and P.W. Snedeker, *Maintenance of fibrin solubility by plasma fibronectin.* J Lab Clin Med, 1980. **96**(6): p. 1054-61.
6. Chow, T.W.Y., *A rheological study of platelet-fibrin interaction*. 1984. p. 125 pp.
7. Hartert, H., *Fibrin elasticity and coagulation.* Biorheology, 1988. **25**(1-2): p. 137-45.
8. Glidden, P.F., C. Malaska, and S.W. Herring, *Thromboelastograph assay for measuring the mechanical strength of fibrin sealant clots.* Clin Appl Thromb Hemost, 2000. **6**(4): p. 226-33.
9. Falls, L.A. and D.H. Farrell, *Resistance of gammaA/gamma' fibrin clots to fibrinolysis.* J Biol Chem, 1997. **272**(22): p. 14251-6.
10. Allan, P., et al., *Evidence that fibrinogen gamma' directly interferes with protofibril growth: implications for fibrin structure and clot stiffness.* J Thromb Haemost, 2012. **10**(6): p. 1072-80.
11. Matsuka, Y.V., M.M. Migliorini, and K.C. Ingham, *Cross-linking of fibronectin to C-terminal fragments of the fibrinogen alpha-chain by factor XIIIa.* J Protein Chem, 1997. **16**(8): p. 739-45.
12. Ferry, J.D. *Structure and rheology of fibrin networks*. 1988. Elsevier Appl. Sci.
13. Weisel, J.W., *Fibrinogen and fibrin.* Adv Protein Chem, 2005. **70**: p. 247-99.
14. Blomback, B., et al., *Fibrin in human plasma: gel architectures governed by rate and nature of fibrinogen activation.* Thromb Res, 1994. **75**(5): p. 521-38.
15. Carr, M.E., *Fibrin formed in plasma is composed of fibers more massive than those formed from purified fibrinogen.* Thromb Haemost, 1988. **59**(3): p. 535-9.
16. Shah, G.A., C.H. Nair, and D.P. Dhall, *Comparison of fibrin networks in plasma and fibrinogen solution.* Thromb Res, 1987. **45**(3): p. 257-64.
17. Moaddel, M., et al., *Interactions of human fibrinogens with factor XIII: roles of calcium and the gamma' peptide.* Biochemistry, 2000. **39**(22): p. 6698-705.

Chapter 5 Characterizing the cell adhesion properties of the native γγ'pdFI-pdFN complex

Abstract

In this section, the biological activity of the isolated complex was tested with an *in vitro* cell adhesion assay. Human Foreskin Fibroblasts and Human Umbilical Vein Endothelial cells (HUVEC) were tested for their abilities to adhere to fibrin clots made from unfractionated pdFI, the purified γγ'pdFI-pdFN complex, and an equimolar mixture of pdFI and pdFN. Results showed that the rate and number of cells attaching was diminished in the absence of FN. Relatively few cells attached to fibrin matrix made from pdFI. Cell attachment was only modestly greater in fibrin made from the same FI but with FN added to a stoichiometric level with respect to the total FI initially present. Conversely, an increased amount of cells were adhered to clots made from the native complex. The greatly increased efficiency of fibroblast and HUVEC attachment to fibrin made from γγ'pdFI-pdFN complex indicates a more efficient presentation of FN relative to that of fibrin made from an equivalent amount of FI an FN, but having a more random presentation due to a predominance of γγF1. The nature by which FN is presented within fibrin clots to facilitate the initiation of wound healing is not well detailed.

Introduction

FN within ECM provides substrates that facilitate cell adhesion and migration during development, wound healing, and other processes. FN also participates in other cellular functions including proliferation, survival, and differentiation. Following vascular injury, the blood clotting system is activated leading to the formation of a clot that seal the injured site and stop bleeding. In addition to restoring the integrity of the vascular system, the clot also serves as provisional matrix for cell adhesion and migration into the wounded tissue to initiate the healing process. These functions are mediated by the clot's main protein components, fibrin with ~94.9% and fibronectin with ~4.4% of the total mass of the clot [1]. FN covalently cross-linked to fibrin clot by FXIIIa plays critical roles in the subsequent remodeling and cellular responses. It forms stable matrix at the wounded area to which different cell types and ECM components can attach and spread. This process is enabled when FN incorporated into fibrin-FN complex adopts an extended conformation within the complex which results in exposure of cryptic cell binding domains to facilitate cellular processes [2]. Bound FN also plays important roles in tissue debridement, wound repair, and augmenting the binding of fibrin clot to macrophages for subsequent phagocytosis [3].

Numerous studies have demonstrated the ability of FN to mediate the attachment of various cell types [4]. For instance, studies investigating the migration of macrophages in three-dimensional fibrin clot revealed that both FXIII and FN exhibited inhibitory effect on macrophage spreading on fibrin surface [5]. FN cross-linked to fibrin polymer inhibits macrophage migration by linking cells to the fibrin clot [5]. The linking occurs between R on macrophage surface and specific domain of FN containing the RGDS sequence [6-10]. The migration inhibitory effect of FN was reversed by adding an excess of a synthetic peptide

containing the RGDS FN cell binding sequence to the fibrin gel. The synthetic peptide saturated binding sites on cross-linked FN and greatly enhanced macrophage migration. Other studies have shown that cells did not migrate into clots formed from FN-depleted plasma. Cells migration was reversed by the addition of FN to plasma prior to clotting indicating that FN has to be incorporated by FXIIIa [11].

FN covalently cross-linked to fibrin clot promotes hemostasis and stabilize the clot by binding to collagen and glycosaminoglycans. Corbett have shown that the covalent crosslinking of FN to fibrin is needed for optimal adhesion of the clot to cellular and ECM [12] specifically collagen. Separate studies found that the adherence of clot to collagen is largely dependent on the concentration of FN component of the fibrin sealant [13]. FN covalently incorporated into fibrin clot is also critical in enhancing the binding of fibrin to macrophages for subsequent phagocytosis.

FN incorporated into fibrin clots by FXIII significantly improves clot retraction by nucleated cells expressing the integrin $\alpha_5\beta_1$, suggesting that FN influence the process of tissue remodeling. The extent of retraction was shown to depend on the RGD, synergy sites in FN, and the covalent incorporation of FN into the fibrin matrix. During clot formation, fibronectin assist in removing soluble fibrin that leaves the area of clotting. Furthermore, the inclusion of FN in fibrin clot may play role in macrophage clearance of fibrin from circulation following trauma or inflammation.

Materials and Methods

Materials

All chemicals of highest purity were purchased from Sigma Chemical Company (St. Louis, MO). Materials for cell culture were purchased from Lonza (Walkersville, MD). The native complex, fibrinogen, and fibronectin were purified from pool of human plasma donated by the U.S. Army Materials Command (Fort Detrick, MD) as described previously. Recombinant FXIII, expressed in Pichia Pastoris, was purified on His-Bind Resin. Recombinant thrombin was bought from The Medicines Company (Parsippany, NJ). Human foreskin fibroblasts and HUVEC cells were kindly provided by Dr. Mark A. Carlson (University of Nebraska Medical Center).

Cell culture

All procedures were performed under sterile condition in NUAIRE Biological Safety Cabinets. Human foreskin fibroblasts and HUVEC were cultured in 75 cm^2 flasks coated with 2 μg/ml pdFN. Cells were grown at 37 °C in a humidified 5% Co_2 in DMEM supplemented with 20% FBS, 20 ng/ml FGF1, 19 U/ml heparin, 2 mM L-glutamine, 100 U/ml penicillin, and 100 μg/ml streptomycin. After cells were grown to confluence, culture media was removed and cells were rinsed with PBS buffer then harvested by addition of 2 ml of 1x trypsin in PBS buffer. Flasks were incubated in CO_2 incubator and gently pipetted until cells were visibly released from the flask's surface. Trypsin was inactivated by the addition of 30 ml of growth media. Cell suspension was transferred to 50 ml conical tube and cells were pelleted by centrifugation at 600 xg for 5 minutes. Supernatant was removed and cells pellet were re-suspended in 50 ml growth medium. To determine the number of cells, cells were mixed with Trypan Blue Stain (Gibco by

life Technologies), transferred to dual chamber counting slides and counted using TC20 automated cell counter (Bio-Rad).

Preparation of coated plate wells

Cell attachment properties of the different fibrin clots preparations were examined using 96 and 24 well plates. Clots were formed at 2 mg/ml of fibrinogen concentration. Isolated γγ'pdFI-pdFN complex, pdFI, and an equimolar mixture of pdFI and pdFN were added to the designated wells. Appropriate amounts of rFXIIIa, $CaCl_2$ solution, and ringer's solution were added followed by rFIIa to trigger clot formation. Plates were incubated on a rotating mixer at room temperature for 2 hours to allow the formation of maximum cross-linked clots. Un-treated wells served as control.

Cell adhesion assays

Before seeding, plates were exposed to UV lights for 30 min to eliminate any potential pathogens. HUVEC were seeded in DMEM at 47,800 cells per well whereas human foreskin fibroblasts were seeded at 4,000 cells per well. Cells were allowed to attach for either 30 min, 1 hour, or 3 hours at 37 °C in a humidified 5% Co_2 environment. Wells were washed 3 times with PBS buffer containing calcium and magnesium, and cells were fixed for 15 min by adding 3.7% formaldehyde in PBS buffer. Formaldehyde solution was removed and wells were washed 3 times with PBS buffer containing calcium and magnesium. Fixed cells were stained with 300 nM diamidino-2-phenylindole (DAPI) (Thermo Fisher Scientific) in PBS for 5 minutes. DAPI was removed and wells were washed with PBS buffer. Attached cells were visualized with EVOS fluorescent Microscope (Advanced Microscopy Group, Life Technologies) using a 10X

objective. Plates were kept wrapped with aluminum foil during the staining and visualization process.

Statistical analysis

The number of cells adhering to the various types of wells was quantified with ImageJ software (The National Institute of Health). All data are expressed as means and standard deviations. Differences in the number of adhered cells were analyzed by one-way Analysis of variance (ANOVA) using the software GraphPad Prims, version 5.0 (GraphPad Software, San Diego, CA). P values lower than 0.05 were considered to indicate statistical significance.

Results

Human fibroblasts and human umbilical vein endothelial cells are examples of cell types which are stimulated by fibronectin at wound surfaces. Human fibroblasts and HUVEC adhesion to fibrin matrices made from the isolated γγ'pdFI-pdFN complex was examined with an *in vitro* adhesion model and compared to adhesion to fibrin made from pdFI or an equimolar mixture of pdFI and pdFN. Clots formed from γγ'pdFI-pdFN complex isolated from human plasma contained an equal amount of FN and γγ'FI. Human fibrinogen used consist of the typical levels of 8 to 15% γγ'FI, 90% homodimeric γγFI, as typically found in human plasma. rFXIIIa covalently cross-linked FN to the α-chain of fibrin to form high molecular weight heterodimers and polymers.

Cells were harvested with trypsin digest and therefore devoid of cell-surface fibronectin [14]. This ensures that cells will not utilize their own FN to facilitate adhesion. The number of cells adhering was quantified and the results obtained are shown in Figures 5.1 through 5.4. As

expected cell attachment was markedly decreased in the absence of FN. After 3 hours of incubation, few cells were attached to untreated wells and wells containing clots made from plasma FI. This corroborates previous observations that FN is essential in augmenting the adhesion and spreading of various types of cells [15-18]. Additional cell adhesion experiments were conducted to determine whether the covalent incorporation of FN into fibrin clot by FXIII can improve cell adhesion. These set of experiments were also designed to reveal whether the biological activity of the native complex could be replicated with an equimolar mixture of exogenous FI and FN. The covalent incorporation of FN into fibrin clots resulted in a marked increase in cell attachment. The adhesion of HUVECs cells was increased by a factor of 1.6 and fibroblasts by a factor of 8.5. This agrees with the previous observations that FN covalently bound to fibrinogen or fibrin substrata by FXIII greatly enhanced the ability of the substrata to support cell adhesion [19]. FN covalently bound to substrata was thought to result in an orientation of FN molecules more favorable for cell interactions than the orientation that would occurs with noncovalently bound FN.

Both HUVEC and fibroblasts cells demonstrated an increase in the rate and number of cells attached when the native complex was present. The adhesion of both types of cells was significantly increased on clots made from the native complex. The attachment of HUVEC cells was increased by a factor of 2.5 and fibroblasts by a factor of 2.6 than the attachment observed on clots from a mixture of pdFI and pdFN. These results show that despite the presence of an equal amount of FN on the native complex and a mixture of FI and FN, the orientation of FN in the native complex is more favorable for cell adhesion. The covalent of incorporation of exogenous FN into fibrin clots could not duplicate the cell adhesion properties of the isolated complex. The rates of attachment of HUVECs and fibroblasts cells to the different types of clots

are shown in Figures 5.5 and 5.6. Rates of cells attachment to clots made from the native complex were faster compared to clots from pdFI and a mixture of pdFI and pdFN.

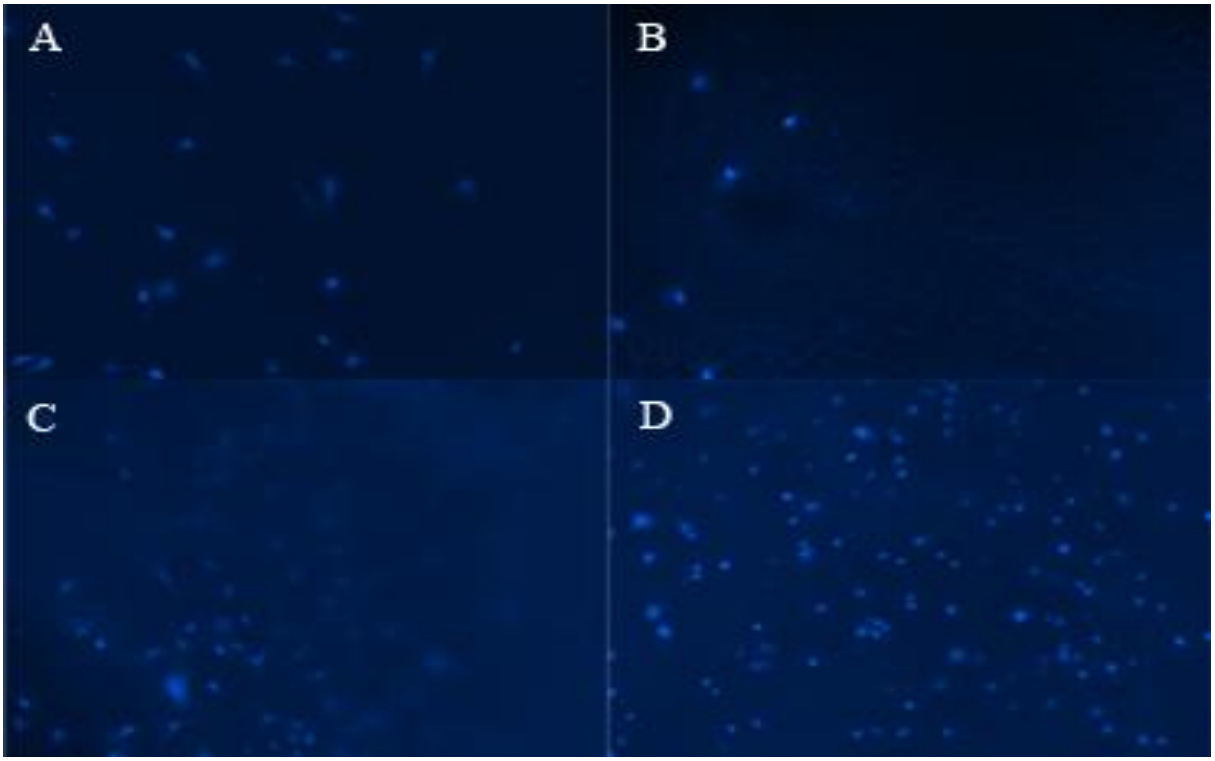

Figure 5.1 Fibroblasts adhesion to A) propylene; B) fibrin clots formed from plasma pdFI; C) fibrin clots formed from equimolar concentration of pdFI and pdFN; D) fibrin clots formed from the isolated γγ'pdFI-pdFN complex. Cells were allowed to adhere for 3 hour then visualized using EVOS fluorescent Microscope

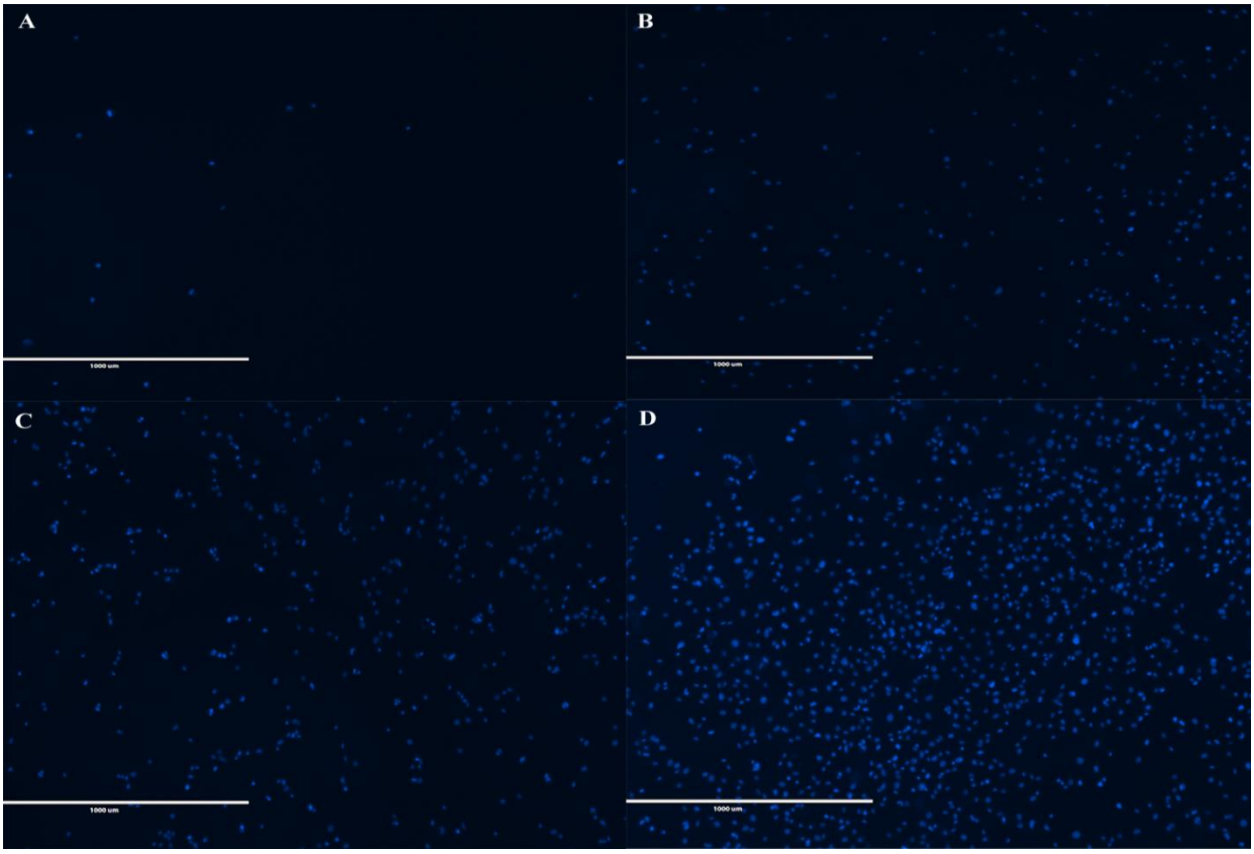

Figure 5.2 HUVECs adhesion to: A) propylene; B) fibrin clots formed from pdFI; C) fibrin clots formed from equimolar concentration of pdFI and pdFN; D) fibrin clots formed from γγ'pdFI-pdFN complex. Cells were allowed to adhere for 3 hours then visualized on EVOS fluorescent Microscope.

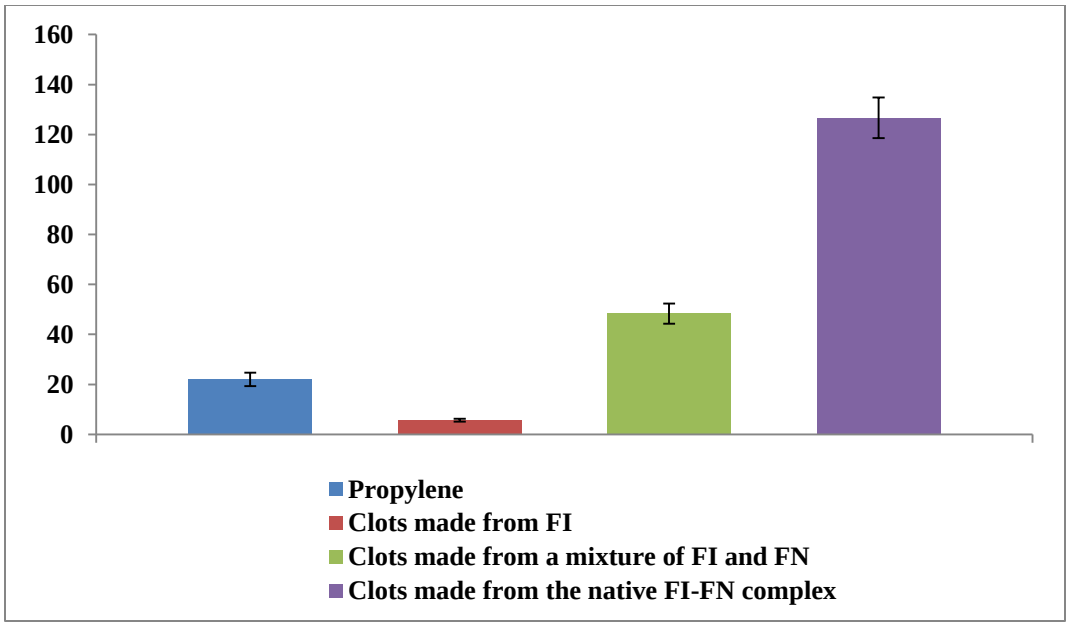

Figure 5.3 Quantitation of fibroblasts cells attachment. Equal numbers of cells were seeded onto wells containing clots derived from FI, native complex, and a mixture of pdFI and pdFN. Cells were allowed to attach for 3 hours and the extent of cell adhesion was quantitated with ImageJ.

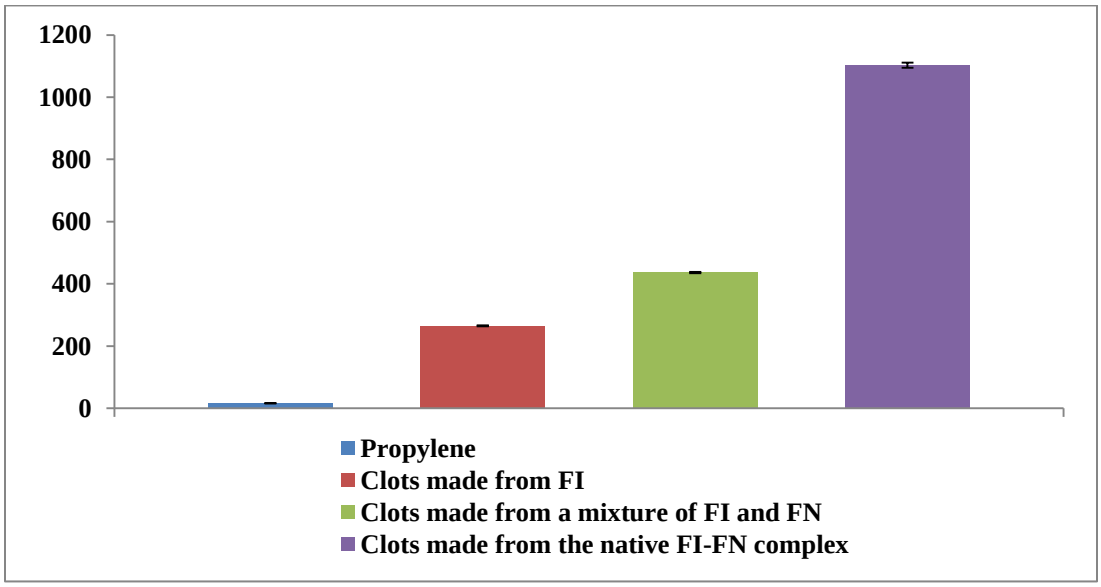

Figure 5.4 Quantitation of HUVEC cells attachment. Equal numbers of cells were seeded onto wells containing clots derived from FI, native complex, and a mixture of pdFI and pdFN. Cells were allowed to attach for 3 hours and the extent of cell adhesion was quantitated with ImageJ.

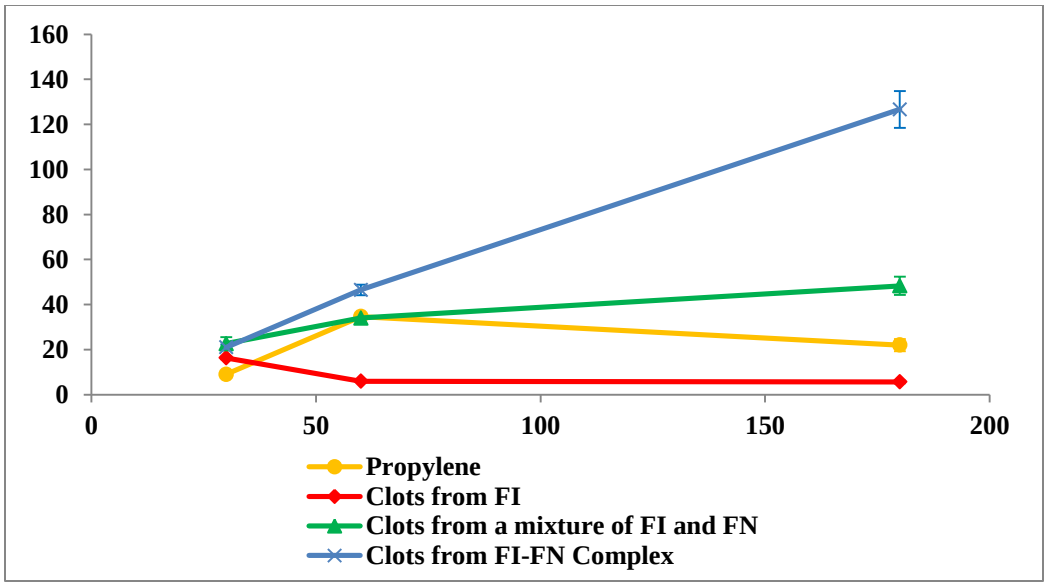

Figure 5.5 Time course of fibroblasts cells adhesion. Cells were allowed to attach for 30 min, 1 h, and 3 h at 37 then visualized with EVOS fluorescent Microscope. The number of cells attached was calculated from three independent experiments. Cells were quantified with ImageJ.

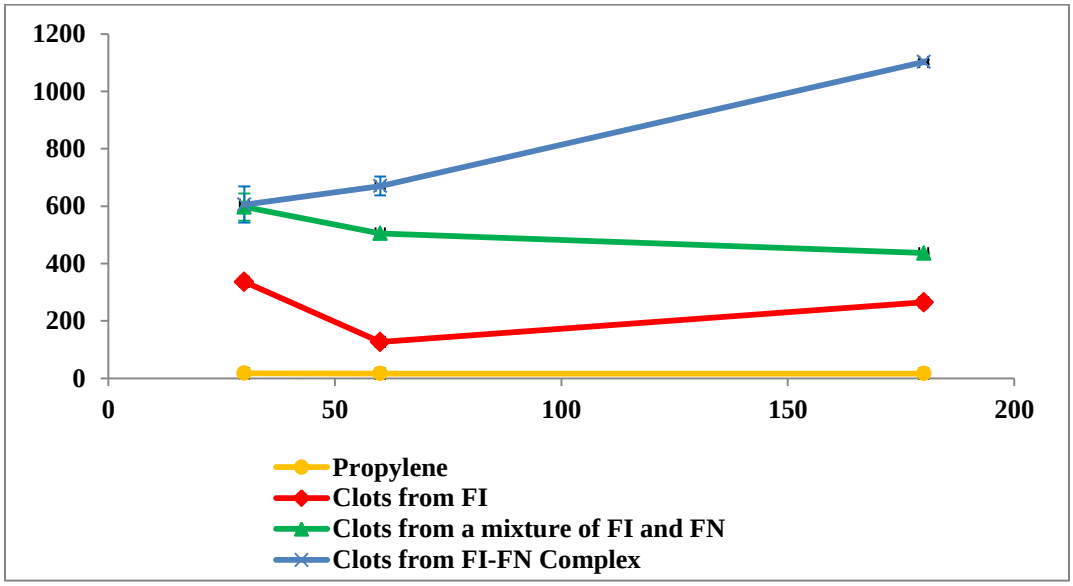

Figure 5.6 Time course of HUVECs cells adhesion. Cells were allowed to attach for 30 min, 1 h, and 3 h then visualized with EVOS fluorescent Microscope. The number of cells attached was calculated from three independent experiments. Cells were quantified with ImageJ.

Discussion

Cell culture studies were performed to assess whether and to what extent the isolated γγ'pdFI-pdFN complex affect cell adhesion. Our studies showed that fibrin matrices derived from γγ'pdFI-pdFN complex induced greater human fibroblasts and HUVEC attachment than fibrin matrices made from an equimolar mixture of pdFI and pdFN or pdFI alone. Unlike an exogenous mixture of FI and FN coated on surface, the γγ'pdFI-pdFN complex provides a more accurate substrate that resembles the provisional matrix found during wound healing. More cells were adhered to clots developed from an equimolar mixture of FI and FN than clots from FI. This agrees with the finding of Corbett at el that FXIIIa mediated covalent crosslinking of FN to fibrin clot is required for maximal cell adhesion. Cells attachment and spreading was maximal on FN-fibrin clots but significantly decreased on non-crosslinked clots.

It's well known that soluble FN is a poor substrate for many cell types; however, the cell binding avidity of FN is enhanced upon deposition on surfaces. Immobilization is thought to cause FN to undergo an irreversible conformational change to the more extended form that exposes cell binding sites previously hidden in the molecule. Under physiological pH and salt concentration, soluble FN assumes a compact structure stabilized by hydrophobic interactions between acidic and basic residues. In contrast, SEM studies revealed that immobilized pdFN exists as elongated thread-like particles with greater separation between the two N-termini of the dimer. This reversible change in pdFN conformation is thought to expose several cryptic binding sites that promote the interactions of cells with fibronectin. It is possible that interaction of FN with γγ'FI causes a conformational change of FN that is different than the interaction of FN with FI that contains ~ 10% γγ' and 85% γγ FI subspecies. We have shown, using methods that

include gel filtration, analytical ultracentrifugation, and dynamic light scattering that FN interact more tightly with γγ'FI than γγFI. Perhaps cells binding sites in FN covalently cross-linked to γγ'FI are more ordered compared to binding sites on FN bound to FI. The covalent binding of FN to γγ'FI may also exposes additional cell binding sites that are not accessible in predominately γγpdFI-pdFN matrices.

Our studies have demonstrated that the γγ'pdFI-pdFN complex is composed exclusively of the γγ'pdFI species in a 1:1 mixture with pdFN. Assuming that the average concentrations of FI and FN in plasma are about 3 mg/ml and 0.3 mg/ml, respectively. Also, assuming that the γγ'pdFI variant represent about 10% of total plasma fibrinogen. The concentration of γγ'pdFI then becomes about 0.3 mg/ml. Since FN associate only with γγ'pdFI species, the molar ratio of γγ'FI to FN in plasma becomes 1:1. Several *in vitro* experiments indicate that the maximum cell adhesion and migration occurred at the physiologic 1:10 mass ratio of FI to FN. For example, Greiling et al reported that fibroblast migration into a fibrin clot was dependent on FN and that the optimal migration occurred at a ratio of 10:1 of FI:FN. In addition, Siobhan and colleagues reported that cell spreading and cytoskeletal organization are induced by adhesion to a three dimensional FN-fibrin matrix made from the physiologic 10:1 mass ratio of pdFI to pdFN [20]. Consequently, the FN-fibrin matrices used in these *in vitro* experiments correspond to the γγ'FI-FN complex.

Studies examining the distribution of FN on peripheral blood cells provided useful insights on how FN might function in *in vivo*. Grinnell and Feld found that FN was distributed along fibrin strands of blood clots from normal health adult donors. They concluded that blood clots formed *in vivo* are likely a fibrin-fibronectin complex and the presence of continuous layer

of FN on the clots may serve to provide mechanical stability that necessary for clot retraction [21]. Large amount of FN is covalently incorporated into fibrin clots formed *in vivo* during clotting [8]. Studies examining the distribution of FN during wound healing have shown that FN was part of the fibrin clot and distributed along fibrin strands [22]. Bound FN forms the substratum for subsequent cell migration and attachment to the clot. FN also mediates fibrin crosslinking and stabilization at the wound surfaces.

Together with the work of Bar et al [13] who showed that fibronectin was necessary for fibrin sealants binding to collagen surfaces, these studies indicate that the combination of cryo precipitation, ammonium sulfate fractionation and DEAE chromatography can be used to produce a fibrin sealant with increased clot strength, improved solubility, enhanced collagen binding and increased cell attachment for use in hemostasis and wound repair.

References

1. Mosher, D.F. and R.B. Johnson, *Specificity of fibronectin--fibrin cross-linking.* Ann N Y Acad Sci, 1983. 408: p. 583-94.
2. Wolfenstein-Todel, C. and M.W. Mosesson, *Human plasma fibrinogen heterogeneity: evidence for an extended carboxyl-terminal sequence in a normal gamma chain variant (gamma').* Proc Natl Acad Sci U S A, 1980. 77(9): p. 5069-73.
3. Chung, D.W. and E.W. Davie, *gamma and gamma' chains of human fibrinogen are produced by alternative mRNA processing.* Biochemistry, 1984. 23(18): p. 4232-6.
4. Grinnell, F., C.H. Ho, and A. Wysocki, *Degradation of fibronectin and vitronectin in chronic wound fluid: analysis by cell blotting, immunoblotting, and cell adhesion assays.* J Invest Dermatol, 1992. 98(4): p. 410-6.
5. Iida, J., et al., *Coordinate role for cell surface chondroitin sulfate proteoglycan and alpha 4 beta 1 integrin in mediating melanoma cell adhesion to fibronectin.* J Cell Biol, 1992. 118(2): p. 431-44.
6. Huebsch, J.C., et al., *Endothelial cell interactions with synthetic peptides from the carboxyl-terminal heparin-binding domains of fibronectin.* Circ Res, 1995. 77(1): p. 43-53.
7. Xu, J. and R.A. Clark, *Extracellular matrix alters PDGF regulation of fibroblast integrins.* J Cell Biol, 1996. 132(1-2): p. 239-49.

8. Greiling, D. and R.A. Clark, *Fibronectin provides a conduit for fibroblast transmigration from collagenous stroma into fibrin clot provisional matrix.* J Cell Sci, 1997. 110 (Pt 7): p. 861-70.
9. Grinnell, F. and M. Zhu, *Identification of neutrophil elastase as the proteinase in burn wound fluid responsible for degradation of fibronectin.* J Invest Dermatol, 1994. 103(2): p. 155-61.
10. McCarthy, J.B., et al., *Localization and chemical synthesis of fibronectin peptides with melanoma adhesion and heparin binding activities.* Biochemistry, 1988. 27(4): p. 1380-8.
11. Knox, P., S. Crooks, and C.S. Rimmer, *Role of fibronectin in the migration of fibroblasts into plasma clots.* J Cell Biol, 1986. 102(6): p. 2318-23.
12. Corbett, S.A., et al., *Covalent cross-linking of fibronectin to fibrin is required for maximal cell adhesion to a fibronectin-fibrin matrix.* J Biol Chem, 1997. 272(40): p. 24999-5005.
13. Bar, L., et al., *The binding of fibrin sealant to collagen is influenced by the method of purification and the cross-linked fibrinogen-fibronectin (heteronectin) content of the 'fibrinogen' component.* Blood Coagul Fibrinolysis, 2005. 16(2): p. 111-7.
14. Pearlstein, E. and M.D. Waterfield, *Metabolic studies on 125I-labeled baby hamster kidney cell plasma membranes.* Biochim Biophys Acta, 1974. 362(1): p. 1-12.
15. Pena, S.D. and R.C. Hughes, *Fibroblast to substratum contacts mediated by the different forms of fibronectin.* Cell Biol Int Rep, 1978. 2(4): p. 339-44.
16. Grinnell, F., D.G. Hays, and D. Minter, *Cell adhesion and spreading factor. Partial purification and properties.* Exp Cell Res, 1977. 110(1): p. 175-90.
17. Klebe, R.J., *Isolation of a collagen-dependent cell attachment factor.* Nature, 1974. 250(463): p. 248-51.
18. Pearlstein, E., *Plasma membrane glycoprotein which mediates adhesion of fibroblasts to collagen.* Nature, 1976. 262(5568): p. 497-500.
19. Grinnell, F., M. Feld, and D. Minter, *Fibroblast adhesion to fibrinogen and fibrin substrata: requirement for cold-insoluble globulin (plasma fibronectin).* Cell, 1980. 19(2): p. 517-25.
20. Corbett, S.A., C.L. Wilson, and J.E. Schwarzbauer, *Changes in cell spreading and cytoskeletal organization are induced by adhesion to a fibronectin-fibrin matrix.* Blood, 1996. 88(1): p. 158-66.
21. Grinnell, F. and M.K. Feld, *Distribution of fibronectin on peripheral blood cells in freshly clotted blood.* Thromb Res, 1981. 24(5-6): p. 397-404.
22. Grinnell, F., R.E. Billingham, and L. Burgess, *Distribution of fibronectin during wound healing in vivo.* J Invest Dermatol, 1981. 76(3): p. 181-9.

Chapter 6 Interaction of FN with FI by ligand blotting

Abstract

We employed ligand blotting to study the interaction of fibronectin with fibrinogen at room temperature. Results showed that FN bound to unfractionated FI, isolated complex, γγ and γγ' FI subspecies. Both α- and β-chains of fibrinogen exhibited strong signal indicating that fibronectin binding sites are localized in these two chains. The binding of FN to the α-chain of FI is in agreement with the previous observations. However, FN binding to the β-chain of FI is a novel finding. Additional experiments were carried out to test whether FN binding to immobilized FI can be inhibited by the addition of FN. Results indicated that FI in solution competed with immobilized FI for FN binding. This corroborates the DLS results that FN interacts with FI in solution.

Materials and Methods

Materials

All reagents of highest purity were purchased from Sigma Chemical Company (St. Louis, MO) unless otherwise noted. Human plasma was donated by the U.S. Army Materials Command (Fort Detrick, MD). Human plasma fibrinogen depleted of fibronectin, plasminogen, and von Willebrand Factor was purchased from Enzyme Research Laboratories (South Bend, IN). Human fibrinogen was purified from plasma by cryoprecipitation followed by two ethanol precipitation as previously described [1]. Human fibronectin was isolated from plasma on Gelatin Sepharose as previously described [2]. Plasma fibrinogen γγ variant with intact and degraded α-chains were obtained from ammonium sulfate precipitated fibrinogen fractionation on DEAE Sepharose as previously described. Plasma fibrinogen γγ' variant with intact and degraded α-chains were obtained from the disruption of the native γγ'pdFI-pdFN complex on gelatin Sepharose as described before.

Ligand blotting assay

Fibrinogen containing species were analyzed under reducing condition on 4-12% NuPAGE Bis-Tris Mini Gels (Life Technologies) as previously described. Gels were electroblotted onto polyvinylide fluoride (PVDF) membranes (Millipore, Billerica, MA) for 45 min at 25 volts. Blots were blocked in 50 ml of 5% casein in TBST (Tris-buffered Tween-20) for 30 minutes at room temperature. Blots were used in the following analysis.

Binding of FN to immobilized FI

To test whether FN interact with the various FI species, blots were incubated with 200 nm FN in TBST buffer for one hour at room temperature. To remove unbound material, blots were washed three times with TBST buffer then incubated with an anti-plasma fibronectin monoclonal antibody (Santa Cruz Biotechnology, Santa Cruz, CA) for 30 min at room temperature. Blots were washed three times with TBST then incubated with an anti-mouse IgG peroxidase conjugate (Sigma Aldrich) then developed with DAB/Metal concentrate and stable peroxide substrate buffer (Thermo Scientific, Rockford, IL).

Competitive inhibition of FN binding to immobilized FI

Blots were incubated with a mixture of plasma FN and γγ'FI for one hour at room temperature. FN (200 nm) was added with an increasing concentrations of γγ'FI. Blots were washed with TBST, incubated with an anti-plasma fibronectin monoclonal antibody, detected with an anti-mouse IgG peroxidase conjugate, and then visualized with DAB/Metal concentrate and stable peroxide substrate buffer.

Results

The interaction of fibronectin with fibrinogen species was investigated with ligand blotting assay. Unfractionated pdFI, the isolated γγ'pdFI-pdFN complex, γγ and γγ' FI subspecies with intact and degraded α-chains were analyzed under denaturing condition on 4-12%. Reduced gels were electrophoretically transferred to PVDF membrane and propped with different antibodies. Anti-FN blot (Figure 6.2) shows that the unfractionated FN-depleted pdFI (Enzyme Research), γγ and γγ' FI subspecies contain some level of FN. Anti-γγ'pdFI is shown in Figure

6.3. The unfractionated pdFI (lane 2) exhibits some level of FN consistent with the reported ~ 10 to 15% γγ' and ~ 85% γγ. As expected, the γγpdFI species (lanes 5 and 6) are devoid of γγ' whereas the isolated complex (lane 4) and γγ'pdFI species (lanes 7 and 8) display significant amount of γ'-chain.

Interaction between FI and FN

To investigate whether fibrinogen interact with fibronectin, blots were incubated with FN then detected with an anti-FN. Results are displayed in Figure 6.2. Panel shows the reduced gel analysis of the FI and FN samples. The α-chain of the isolated complex (lane 4) is severely degraded. Lanes 5 and 6 shows the severely degraded and intact α-chain γγ'pdFI, respectively. Lanes 7 and 8 display the intact and completely degraded γγ'pdFI, respectively. Panel B displays the ligand blot. It's clear from the figure that FN interacts with FN at room temperature. Both α- and β-chains of FI exhibited strong signal indicating that FN binding sites in FI are located in these chains. FN was able to bind to γγ'pdFI with completely degraded α-chain (lane 8) providing further evidence that FN interact with β-chain independent of the α-chain. The absence of signal corresponding to the γγ and γγ' suggest that FN does not interact with both chains.

Competition experiments

Additional experiments were conducted to determine whether FI in solution could interact with FN. The binding of FN to immobilized FI was competitively inhibited with by the addition of γγ'pdFI. Blots were treated with a mixture of γγ'pdFI and FN in which an increasing amount of γγ'pdFI was added to a constant level of FN. Results are shown in Figure 6.4. It is clear from the blots that the intensity of the signal decreased as more γγ'pdFI was added to FN.

This shows that the amount of FN available to bind to FI individual chains immobilized on the blot was decreased as more γγ'pdFI was added to the mixture. This demonstrates that γγ'pdFI in solution interacts with FN. The lower intensity of the β-chain compared to the α-chain suggests that the β-chain has low affinity for FN. FI in solution and FI immobilized on blot compete for binding to FN.

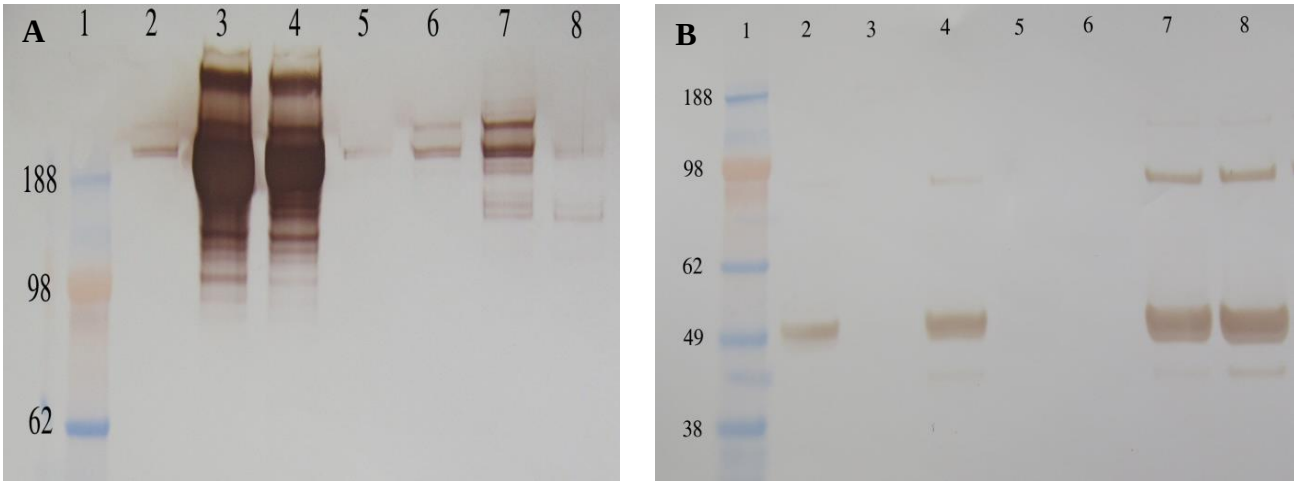

Figure 6.1 Anti-fibronectin (A) and anti-fibrinogen γ'-chain (B) Western blot analysis of fibrinogen. Samples (6 µg) were analyzed under reducing condition in 4-12% SDS-PAGE then transferred to PVDF membrane. Lane 1: molecular weight marker; Lane 2: pdFI (ER); Lane 3: pdFN; Lane 4: γγ'pdFI-pdFN; Lane 5: γγpdFI des α-chain; Lane 6: γγpdFI; Lane 7: γγ'pdFI; Lane 8: γγ'pdFI des α-chain.

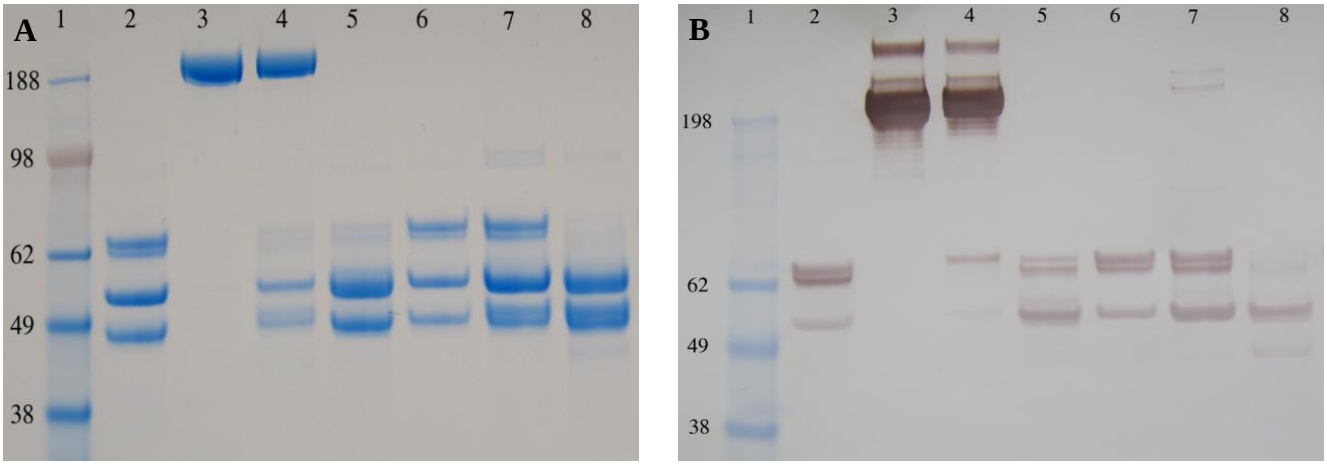

Figure 6.2 Gel electrophoresis (A) and ligand blotting analysis (B) of fibrinogen. Samples (6 µg) were analyzed under reducing condition in 4-12% SDS-PAGE and stained with colloidal blue or transferred to PVDF membrane. Blot was incubated with pdFN then an anti-plasma fibronectin monoclonal antibody and probed with an anti-mouse IgG peroxidase conjugate. Lane 1: molecular weight marker; Lane 2: pdFI (ER); Lane 3: pdFN; Lane 4: γγ'pdFI-pdFN; Lane 5: γγpdFI des α-chain; Lane 6: γγpdFI; Lane 7: γγ'pdFI; Lane 8: γγ'pdFI des α-chain.

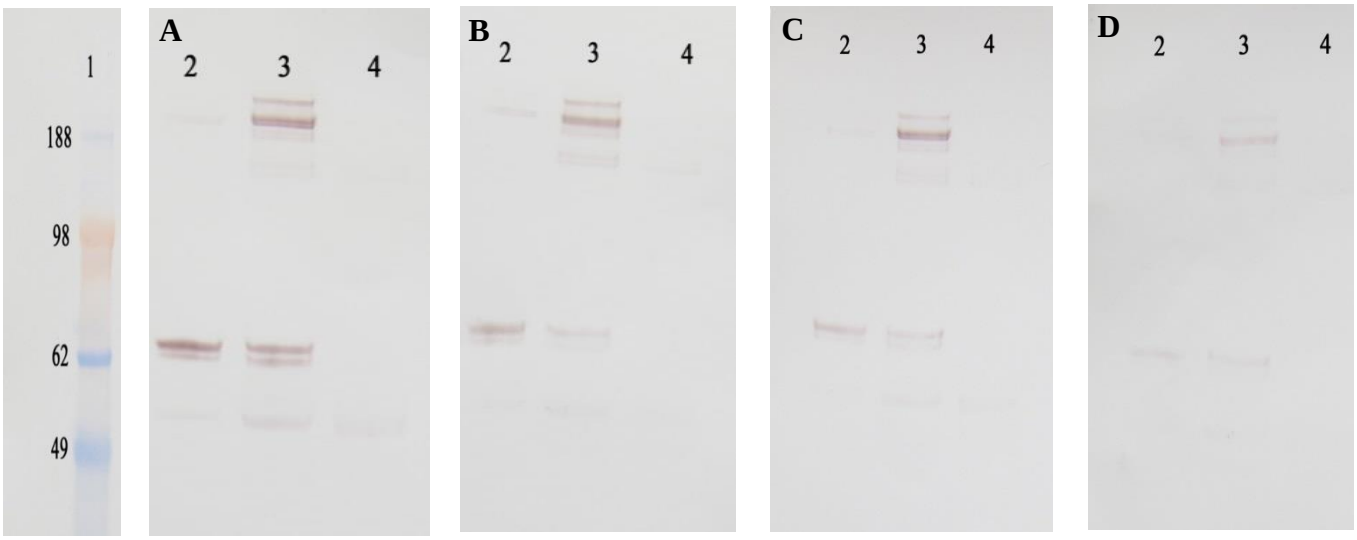

Figure 6.3 Ligand blot analysis of fibronectin binding to immobilized fibrinogen and fibrinogen in solution. Samples (3 µg) were analyzed under reducing condition in 4-12% SDS-PAGE then transferred to PVDF membrane. Blots were incubated with mixtures of pdFN and γγ'pdFI. (A) 1:0, (B) 1:20, (C) 1:30. Blots were incubated with an anti-plasma fibronectin monoclonal antibody and probed with an anti-mouse IgG peroxidase conjugate. Lane 1: molecular weight marker; Lane 2: γγpdFI; Lane 3: γγ'pdFI; Lane 4: γγ'pdFI des α-chain.

Discussion

Ligand blotting experiments revealed that FN bound to FI containing species that include unfractionated pdFI, γγpdFI, γγ'pdFI, and the isolated complex. The binding of FN to FI occurred whether FI in solution or immobilized on blot. This contradicts earlier observations that demonstrated FN interact only with fibrin. For example, Makogonenko reported that fibronectin did not bind to immobilized fibrinogen but bound fibrin with high affinity [3]. Fibronectin binding sites were thought to be cryptic in fibrinogen but become exposed when fibrinogen is converted to fibrin. Other observations have demonstrated that FN bind to fibrinogen in the cold but such binding is abolished upon warming the fibrinogen to 22 °C [4]. Other studies have shown that FN bound to fibrinogen-Sepharose at low temperature but not

The binding sites of FN are located in the α- and β-chains of FI. FN bound to the β-chain even in the absence of the α-chain .The α-chain appears to be the higher affinity binding site whereas the β-chain is the lower affinity binding site. The binding of FN to the α-chain of FI is in agreement with numerous previous studies [5-7]. The presence of additional FN binding sites in FI was suggested by others. For example, using electron microscopy, Erickson have suggested that fibronectin attachment to fibrinogen involved the g-chain [8]. Other studies have shown that FN crosslinked fibrin with degraded α-chains, indicating the presence of secondary crosslinking sites in fibrin [7]. Therefore, the binding of fibronectin to fibrinogen is complex and may involve several domains. However, no studies have reported the binding of fibronectin to the β-chain of fibrinogen.

References

1. Burnouf-Radosevich, M., T. Burnouf, and J.J. Huart, *Biochemical and physical properties of a solvent-detergent-treated fibrin glue.* Vox Sang, 1990. **58**(2): p. 77-84.
2. Brew, S.A. and K.C. Ingram, *Purification of human plasma fibronectin.* Journal of tissue culture methods. **16**(3): p. 197-199.
3. Makogonenko, E., et al., *Interaction of fibrin(ogen) with fibronectin: further characterization and localization of the fibronectin-binding site.* Biochemistry, 2002. **41**(25): p. 7907-13.
4. Rostagno, A., et al., *Further characterization of the NH2-terminal fibrin-binding site on fibronectin.* J Biol Chem, 1994. **269**(50): p. 31938-45.
5. Mosher, D.F., *Cross-linking of cold-insoluble globulin by fibrin-stabilizing factor.* J Biol Chem, 1975. **250**(16): p. 6614-21.
6. Matsuka, Y.V., M.M. Migliorini, and K.C. Ingham, *Cross-linking of fibronectin to C-terminal fragments of the fibrinogen alpha-chain by factor XIIIa.* J Protein Chem, 1997. **16**(8): p. 739-45.
7. Mosher, D.F. and R.B. Johnson, *Specificity of fibronectin--fibrin cross-linking.* Ann N Y Acad Sci, 1983. **408**: p. 583-94.
8. Erickson, H.P. and W.E. Fowler, *Electron microscopy of fibrinogen, its plasmic fragments and small polymers.* Ann N Y Acad Sci, 1983. **408**: p. 146-63.